T.R.
BOLU ABANT İZZET BAYSAL ÜNİVERSİTESİ
INSTITUTE OF GRADUATE STUDIES
Department of Chemistry

DEPENDENCE OF THE FORMATION OF LYOTROPIC UNIAXIAL AND BIAXIAL NEMATIC PHASES ON THE EXISTENCE OF HOFMEISTER IONS IN THE INTERMICELLAR REGION

MASTER OF SCIENCE

URWA SHOUKAT

THESIS SUPERVISOR
Prof. Dr. EROL AKPINAR

BOLU, JULY - 2025

APPROVAL OF THE THESIS

DEPENDENCE OF THE FORMATION OF LYOTROPIC UNIAXIAL AND BIAXIAL NEMATIC PHASES ON THE EXISTENCE OF HOFMEISTER IONS IN THE INTERMICELLAR REGION prepared and submitted by **URWA SHOUKAT** and defended before the members of the Examining Committee mentioned below, partially meeting the criteria for the degree of **Master of Science** in **Department of Chemistry, Institute of Graduate Studies of Bolu Abant İzzet Baysal University** on **25.07.2025**.

Jury Members	**Signature**
Supervisor Prof. Dr. Erol AKPINAR Bolu Abant Izzet Baysal University	.....
Prof. Dr. Öznur DEMİR ORDU Bolu Abant Izzet Baysal University	.....
Assoc. Prof. Dr. Özgür MASALCI Ege University	.....

Institute of Graduate Studies Approval

Prof. Dr. İbrahim KÜRTÜL
Director of Institute of Graduate Studies

ETHICAL DECLARATION

In this thesis, which I have prepared in according to the Thesis Writing Rules of İzzet Baysal University, Institute of Graduate Studies, I hereby declare that:

- All data, information, and documents presented in the thesis were obtained in compliance with academic and ethical rules.
- All information, documents, evaluations, and results have been presented in line with the principles of scientific ethics and integrity.
- All sources and works from which I have benefitted have been duly cited and referenced in accordance with academic standards.
- No alterations have been made to the original data used in the study.
- I declare that the work I have presented in this thesis is original.

Furthermore, I accept that in the event of any situation contrary to these declarations, I shall forfeit all rights that may otherwise be granted to me.

According to the similarity report generated through the Turnitin plagiarism detection software – with filters applied as determined by the Institute's Directorate – the similarity index of this thesis is within the limits approved by the University Senate and does not exceed 30%.

.....

URWA SHOUKAT

ÖZET

LİYOTROPİK TEK EKSENLİ VE ÇİFT EKSENLİ NEMATİK FAZLARIN OLUŞUMUNUN MİSELLER ARASI BÖLGEDEKİ HOFMEİSTER İYONLARININ VARLIĞINA BAĞIMLILIĞI

YÜKSEK LİSANS TEZİ
URWA SHOUKAT
BOLU ABANT İZZET BAYSAL ÜNİVERSİTESİ
LİSANSÜSTÜ EĞİTİM ENSTİTÜSÜ
KİMYA ANA BİLİM DALI
(TEZ DANIŞMANI: PROF. DR. EROL AKPINAR)

BOLU, TEMMUZ - 2025
XIV + 103 sayfa

Bu tez kapsamında; yüzey aktif madde, elektrolit, dekanol ve sudan oluşan bazı liyotropik karışımların fizikokimyasal özellikleri, Hofmeister serisi anyonlar ve katyonlar içeren farklı elektrolitler kullanılarak incelenmiştir. Miseller arası bölgede bulunan iyonların etkisi, misel yüzeylerinde bulunan iyonların etkisiyle karşılaştırılarak analiz edilmiştir. Numunelerin liyotropik nematik faz özelliklerini araştırmak için üç deneysel teknik uygulanmıştır. Liyotropik fazların dokuları polarize optik mikroskop kullanılarak karakterize edilmiştir. Tek eksenliden çift eksenli nematik fazlara geçişler, lazer konoskopi tekniği ile nematik fazların çift kırınımlarının sıcaklığa bağımlılıklarından belirlenmiştir. Misel çekirdeğinin ortalama boyutları, misel şekli anizotropisi ve misel yüzeyindeki yüzey aktif madde (sürfaktan) baş grubu başına düşen ortalama alan gibi bazı yapısal parametreler Küçük Açı X-ışını Saçılması verilerinin analizinden elde edilmiştir. Sonuçlar, Gouy-Chapman tabakasındaki ve/veya miseller arası bölgede bulunan iyonik türler arasındaki etkileşimlerin liyotropik nematik fazların oluşumunda önemli bir rol oynadığını ilk kez göstermektedir.

ANAHTAR KELİMELER: Liyotropik sıvı kristaller, Miseller arası bölge, Tek eksenli nematik faz, Çift eksenli nematik faz, Faz geçişleri, Misel yapısal parametreleri, Hofmeister serisi iyonlar, Çift kırınımlar, Lazer konoskopisi, Polarize optik mikroskopisi, Küçük açı X-ışını saçılması.

ABSTRACT

DEPENDENCE OF THE FORMATION OF LYOTROPIC UNIAXIAL AND BIAXIAL NEMATIC PHASES ON THE EXISTENCE OF HOFMEISTER IONS IN THE INTERMICELLAR REGION

MSC THESIS
URWA SHOUKAT
BOLU ABANT IZZET BAYSAL UNIVERSITY
INSTITUTE OF GRADUATE STUDIES
DEPARTMENT OF CHEMISTRY
(SUPERVISOR: PROF. DR. EROL AKPINAR)

BOLU, JULY 2025
XIV + 103 pages

In the frame of this thesis, the physicochemical properties of some lyotropic mixtures, composed of surfactant, electrolyte, decanol, and water, were studied using different electrolytes including Hofmeister series anions and cations. The effect of the ions present in the intermicellar region was analyzed by comparing it with the effect of the ions located at the micelle surfaces. Three experimental techniques were performed to investigate the lyotropic nematic phase properties of the samples. The textures of the lyotropic phases were characterized using a polarizing optical microscope. The transitions from the uniaxial to the biaxial nematic phases were determined from the temperature dependences of the birefringences of the nematic phases via laser conoscopy technique. Some structural parameters such as micelle' core average dimensions, micelle shape anisotropy, and average area per surfactant head group at the micelle surface were obtained from the analysis of Small-angle X-ray Scattering data. The results show for the first time that the interactions between ionic species in the Gouy-Chapman layer and/or in the intermicellar region play a crucial role in the formation of the lyotropic nematic phases.

KEYWORDS: Lyotropic liquid crystals, Intermicellar region, Uniaxial nematic phase, Biaxial nematic phase, Phase transitions, Micelle structural parameters, Hofmeister series ions, Birefringences, Laser conoscopy, Polarizing optical microscopy, Small-angle X-ray scattering.

TABLE OF CONTENTS

Page

LIST OF FIGURES

Page

LIST OF TABLES

Page

LIST OF ABBREVIATIONS AND SYMBOLS

IBM : Intrinsically Biaxial Micelles

LCs : Liquid Crystals

LCDs : Liquid Crystal Displays

LLCs : Lyotropic Liquid Crystals

LNPs : Lyotropic Nematic Phases

TLCs : Thermotropic Liquid Crystals

MCD : Mixture cylinderical and disc-like micelles

$\mathbf{N_U}$: Uniaxial Nematic Phase

$\mathbf{N_B}$: Biaxial Nematic Phase

$\mathbf{N_D}$: Discotic Nematic Phase

$\mathbf{N_C}$: Calamitic Nematic Phase

B : Magnetic field

n : Nematic phase director

POM : Polarized Optical Microscopy

SAXS : Small-Angle X-Ray Scattering

ACKNOWLEDGEMENT

First and foremost, I would like to express my deepest gratitude to my supervisor, Prof. Dr. Erol AKPINAR, for his unwavering support, guidance, and patience throughout this research journey. His invaluable insights and continuous encouragement have played a vital role in shaping the direction and outcome of this thesis.

I am also sincerely thankful to the faculty and staff of the Chemistry department at Bolu Abant Izzet Baysal University, whose expertise and dedication have provided a solid foundation for my academic and professional development.

My profound gratitude goes out to Prof. Dr. İzzet MORKAN for his insightful feedback, suggestions, and constant support.

Finally, my heartful thanks go to my beloved father, mother and my brothers for their unconditional love, sacrifices, and encouragement have been the cornerstone of my perseverance. Without their support, this accomplishment would not have been possible.

This research was supported by the Scientific and Technological Research Council of Türkiye (TÜBİTAK) under the 1001 program, Project no: 122Z515.

1. INTRODUCTION

Liquid crystals (LCs) are an intriguing phase of matter that lies between solid crystals and conventional liquids. Liquid crystals are anisotropic materials and have traits of both liquids and solids, in contrast to solids, where molecules are densely packed in a set, ordered lattice, and ordinary liquids, where molecules are arbitrarily distributed and flow freely. Essentially, they have a degree of molecular organization similar to that of solids yet flow like liquids, Figure 1.1. This intermediate state is known as mesophase.

Anisotropy is a major property of liquid crystals. It means that their physical properties vary depending on which direction they are measured. This anisotropy distinguishes the material apart from isotropic fluids like water and results from the incomplete alignment of molecules inside the substance. Liquid crystal materials are extremely sensitive to external factors including mechanical forces, temperature changes, and electric and magnetic fields (Bisoyi & Li, 2011). These stimuli can affect the molecular alignment, which can alter their mechanical, electrical, and optical characteristics. This responsiveness makes LCs particularly valuable in a variety of technical applications. The most well-known use is in the Liquid Crystal Displays (LCDs), which modulate light and create pictures. In this application, electric fields allow to control the molecular orientation (Collings & Hird, 1997). Furthermore, LCs are employed in sensors, adjustable lenses, and optical devices, and even in new fields like biomedical imaging and smart materials (Bahadur, 1990).

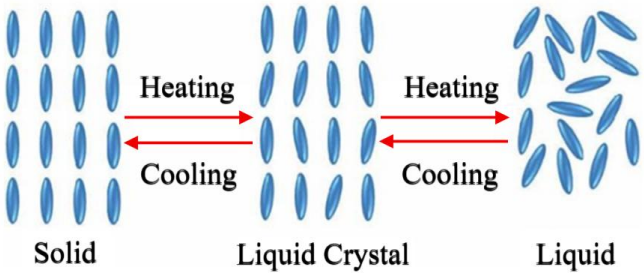

Figure 1.1. Comparison of molecular arrangement in solid, liquid crystal, and liquid. In solids, molecules are rigidly fixed in a well-defined pattern. In liquid, they are completely disordered. In liquid crystals, the molecules maintain some degree of orientation, showing intermediate order that is characteristic of mesophases.

As shown in Figure 1.1, ordinary solids and completely disordered liquids can be transformed into one another by increasing or decreasing the temperature. Molecules have positional and orientational orders in the solids. These molecules lose positional and orientational orders in the liquids and the molecules are in random motion. The liquid crystals are, in general, defined with no positional order but a certain degree of orientational order (Neto & Salinas, 2005). In the liquid crystal state, long-range molecular orientation is described by a sign-invariant unit vector, the so-called "director, $\hat{n}$" along which the molecules tend to align, and the overall degree of orientation is quantified using the scalar order parameter S with the following equation (Zografopoulos, Ferraro, & Beccherelli, 2019).

$$S = \frac{1}{2}\langle 3cos^2\theta - 1\rangle \qquad (1.1)$$

where θ is the average angle between the long axes of the molecules in the liquid crystal material and director or optical axis (Figure 1.2). The brackets denote spatial average.

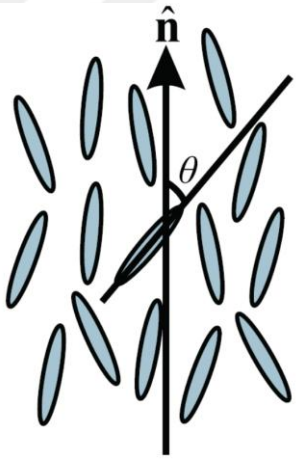

Figure 1.2. Local alignment of long axes of the molecules in a liquid crystal sample (Zografopoulos, Ferraro, & Beccherelli, 2019).

The order parameter can take a value between 0 and 1. If S=0, the molecules align in all directions in space. So, the average value of the term $\langle 3cos^2\theta - 1\rangle$ in equation 1.1 is zero and the material is called an isotropic liquid. If S=1, all molecules align parallel to the director, θ=0°, which is seen in a perfect crystal (solid). In general, the order parameter takes a value of about 0.3-0.8 for a liquid

crystal sample and it decreases with temperature. A sudden change in the S value is obtained at the "critical transition temperature, T_C". At this temperature, a relatively turbid liquid crystal phase turns into a clear isotropic liquid phase (Figure 1.3).

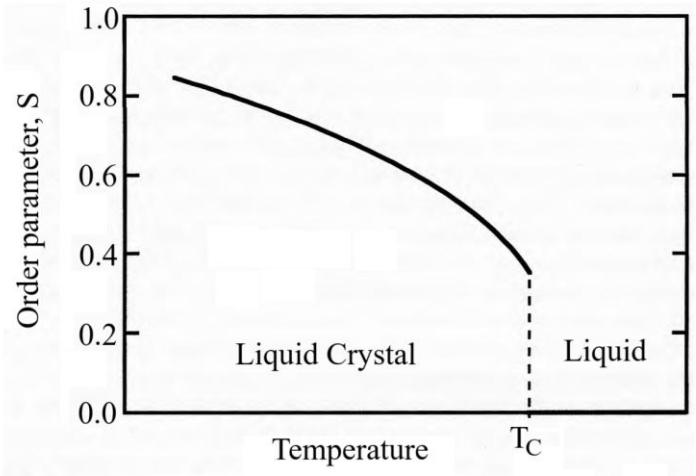

Figure 1.3. Temperature dependence of order parameter (Collings, 2002, p. 7) and (Goodby, 2014).

1.1 Types of Liquid Crystals

Considering the structural units, liquid crystals are mainly classified as "Thermotropic (TLCs)" and "Lyotropic (LLCs)" Liquid Crystals. TLCs are widely utilized in LCD technology, thermometers, and temperature sensors because they exhibit sensitivity to temperature changes (de Gennes & Prost, 1995). The phase transitions in TLCs occur by changing temperature. It means that different types of TLC structures can be obtained by changing temperature. The most common TLC structures are nematic, smectic, and cholesteric (or chiral nematic) phases. Nematic phases are characterized by the orientation of molecules along a preferred direction. This direction is called "director" or "optical axis", i.e., there is an orientational order in nematic phases. In the smectic phases, molecules form layered structures, adding positional order to the orientational order present in nematics. Cholesteric phases exhibit properties similar to nematic ones, except that the molecules form a helical structure as a result of molecular chirality.

LLCs are, in general, in close contact with biology. So, the understanding of their physicochemical properties is important for some of their technological/ biotechnological applications, for instance, soap, pharmacy, cosmetics, food, etc

(Neto & Salinas, 2005). LLCs are formed from the dissolution of amphiphilic molecules (or surfactants), which have both hydrophilic (water-loving) head and hydrophobic (water-hating) tail in a suitable solvent, mostly water, Figure 1.4 (Fairhurst et al., 1998). The head group may be ionic or polar.

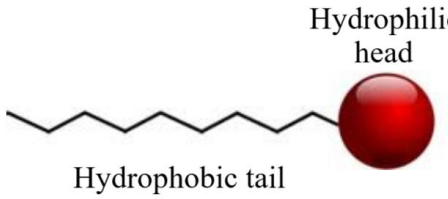

Figure 1.4. Schematic representation of an amphiphilic molecule.

Both temperature and mesogenic compound concentration affect their mesophase behaviour. In other words, LLC phases are thermodynamically stable at specified temperatures and concentrations in addition to pressure (Goodby, 2005). Surfactant molecules self-assemble in water to form a supramolecular structure, "micelles", Figure 1.5, being a structural unit of LLCs, at a certain surfactant concentration (i.e., cmc) and temperature (Krafft temperature). It means that for micelle formation there are a minimum concentration and temperature. When the free surfactant molecules present in the bulk solution aggregate to form micelles, the free energy of the whole solution above cmc is reduced (Martin et al., 2011). This phenomenon is known as the "hydrophobic effect", which is an important key factor for micelle formation. The micelles are spherical around cmc. The shape and size of micelles can change depending on the concentration of the mixture components, molecular structure of the surfactants, and some other external parameters.

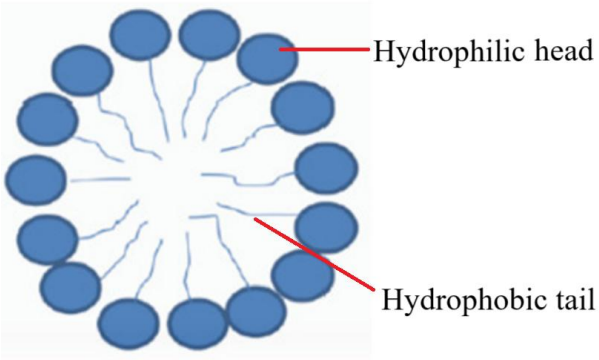

Figure 1.5. The structure of micelle formed by surfactant molecules (Alarfaj & El-Tohamy, 2015). While its inner side consists of surfactant tails, its surface is covered by surfactant head groups.

Different LLC phases can be stabilized by increasing the surfactant concentration, Figure 1.6. Main LLC structures are lamellar, hexagonal, cubic, nematic, and cholesteric (chiral nematic) phases due to the different aggregation types of surfactant in the micelles (Guo et al., 2010). Surfactant molecules form the bilayers in the lamellar phases. Polar or ionic head groups of surfactants cover both sides of the bilayers and these head groups are in contact with the aqueous phase (Yeagle, 2016). The inner of the bilayers are composed of surfactant hydrocarbon chains. The lamellar phase is two-dimensional with surfactant bilayers separated by the aqueous (or water) phase (Faergemand & Krog, 2003), however, there is a repeating order in one direction perpendicular to the bilayers. Surfactants form long rod-like (cylindrical) micelles in a hexagonal phase. Then, the cylindrical layers are organized parallel to one another in a hexagonal array. There is a two-dimensional repeating order in the hexagonal phase. Cubic phases are composed of spherical micelles where the surfaces of the spheres are covered by the surfactant head groups and their interiors are filled up by the hydrophobic chains (Israelachvili, 1991). In the cubic phases, the spherical micelles arrange to form a body-centered cubic structure (Buwalda & Engberts, 2001). In this arrangement, water molecules locate at the spaces between the structural units. In a lyotropic chiral nematic phase, micelle shapes may be disc-like or cylindrical-like with finite size. The local director of the micelles varies by a constant angle coming from one layer to the next that leads to the formation of a “helical structure”.

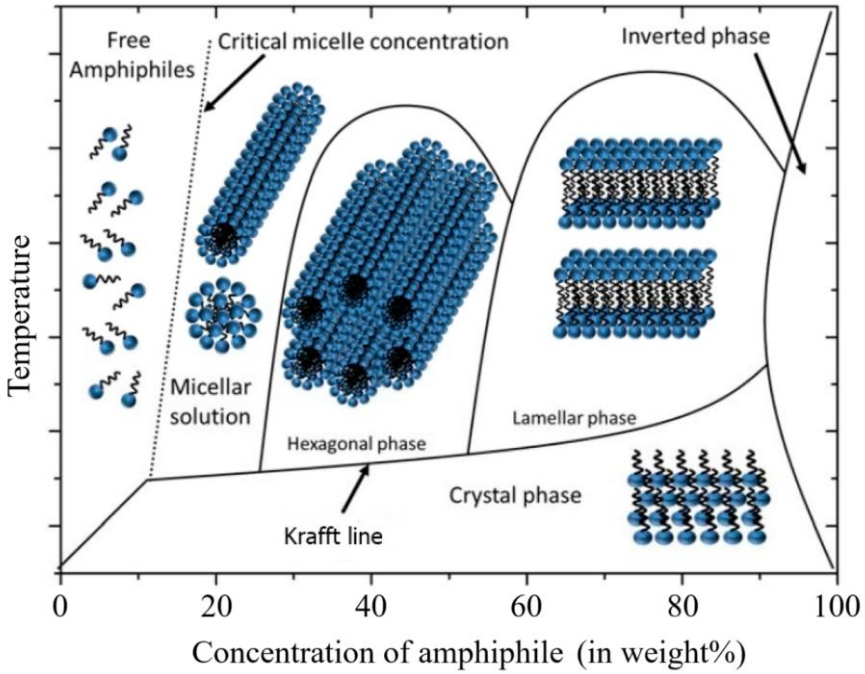

Figure 1.6. A representative partial phase diagram for a mixture composed of an amphiphilic molecule (surfactant) and water. Depending on the concentration of the amphiphilic molecule, other LLC structures may be observed at different areas in this partial phase diagram (Dierking & Martins Figueiredo Neto, 2020).

This thesis mainly concentrates on lyotropic nematic phases. So some information on these phases will be given in further parts in detail.

1.1.1 Lyotropic Nematic Phases

Nematic phases are notable structure among LLCs due to their adaptability and simplicity. Nematic phases differ from solid crystals. Although the latter ones have both orientational and positional order, in the nematic phases there is only orientational order because the local axes of the micelles orient in a preferred direction (so-called "phase director" or "optical axis").

Lawson and Flautt, in 1967, reported the first lyotropic mixture of the nematic phase in the literature (Lawson & Flautt, 1967). Lyotropic nematic phases can be divided into two primary types in terms of the existence of the number of optical axes: uniaxial (N_U) and biaxial (N_B) nematic phases (de Gennes & Prost, 1995). The uniaxial nematic phase is characterized by the preferred alignment of local optical axes of the micelles along a "**single axis**" (director, $\vec{n}$) and the rotation of those axes symmetrically around it. As seen in many liquid crystal displays, this

single-axis alignment facilitates simple molecular organization and predictable optical behaviours (Figueirinhas et al., 2005). The director $\vec{n}$ orients in the perpendicular and parallel direction to the magnetic field in the uniaxial discotic (N_D) and calamitic (N_C) nematic phases, respectively. Although both phases have a single optical axis, they differ in their formation mechanisms, molecular configurations, and optical characteristics (Bates & Luckhurst, 2002). In the case of the N_B phase, there are "**two optical axes**" and three orthogonal two-fold symmetry axes, $\vec{l}$, $\vec{m}$ and $\vec{n}$, where $\vec{n}= \vec{l} \times \vec{m}$ (Neto & Salinas, 2005),(Nasrin et al., 2016), (Kim et al., 2016a), (Kim et al., 2016b), (Akpinar & Figueiredo Neto, 2019). Figure 1.7.

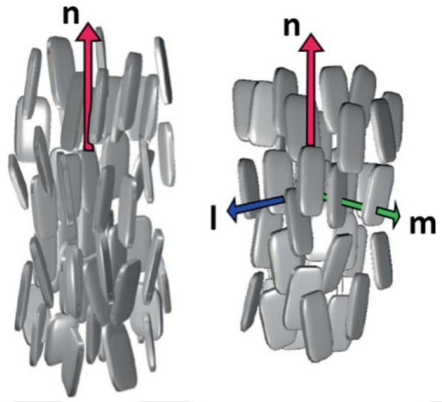

Figure 1.7. Representation of volume elements in the uniaxial nematic, N_U, (left) and orthorhombic biaxial nematic phases, N_B, (right). The N_U and N_B phases have $D_{\infty h}$ and D_{2h} symmetries, respectively; each volume element is composed of parallelepiped statistical mesogens (Samulski, 2010).

The calamitic nematic phase is composed of cylindrical-like or elongated micelles, which orient parallel to one another, preserving long-range orientational order.

1.2 Optical and Magnetic Properties of Liquid Crystals

Liquid crystals (LCs) have distinct optical and magnetic characteristics due to their anisotropic molecular organization, making them vital in current technology and scientific study. These features are a direct result of their incomplete molecular order, which causes direction-dependent (anisotropic) behaviour when interacting with light and magnetic fields.

Due to the anisotropic character of liquid crystals, their physical properties are different when those properties are measured in parallel or perpendicular direction to the average alignment of the structural units with the phase director. If a polarized light beam is passed into the anisotropic LC sample, it travels in the medium by splitting into two plane-polarized rays (ordinary and extraordinary rays) having different velocities and exhibiting two different refractive indices. The electric field vectors of these rays vibrate in perpendicular directions to each other, Figure 1.8. This phenomenon is known as "birefringence" or "double refraction" or "optical anisotropy". The electrical vectors of the ordinary (n_o) and extraordinary (n_e) rays vibrate perpendicular and parallel to the director of the liquid crystal, respectively. The birefringence (Δn) is given by the equation,

$$\Delta n = n_e - n_o = n_{//} - n_{\perp} \qquad (1.2)$$

If $n_e > n_o$ ($n_e < n_o$), Δn is positive (negative).

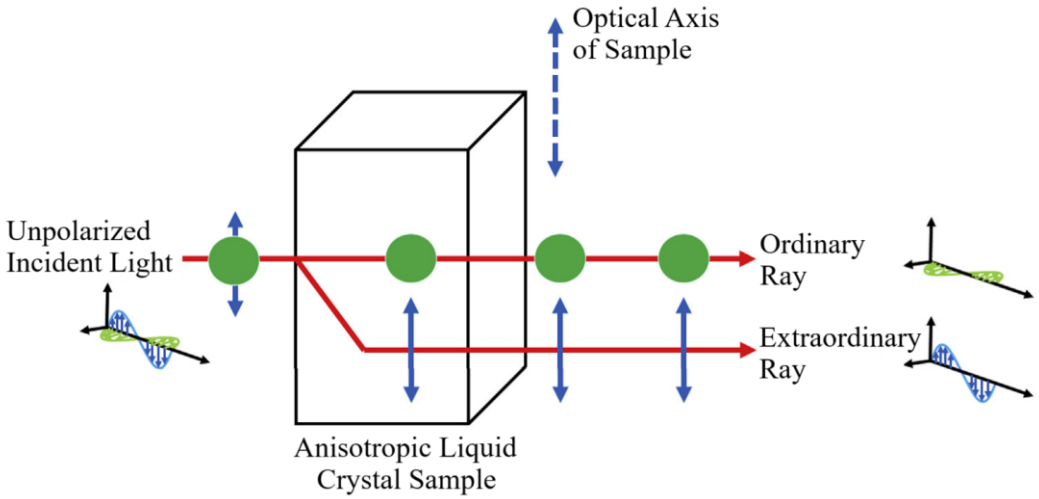

Figure 1.8. Schematic representation of birefringence occurring in an LC sample (Adopted from [Mohan et al., 2019]).

For the nematic phases, the sign of the optical anisotropy can be determined from conoscopic investigations using a polarizing optical microscope. When the nematic phase director aligns perpendicular (parallel) to the applied magnetic field direction and a large surface of the flat capillary, it gives a homeotropic (planar) texture (Figure 1.9). The homeotropic and planar alignments correspond to positive and negative optical anisotropy (Δn), respectively. The observed characteristic

interference colors along the ¼ λ-retardation plate direction are shown in Figure 1.10, which represent that Δn>0 or Δn<0.

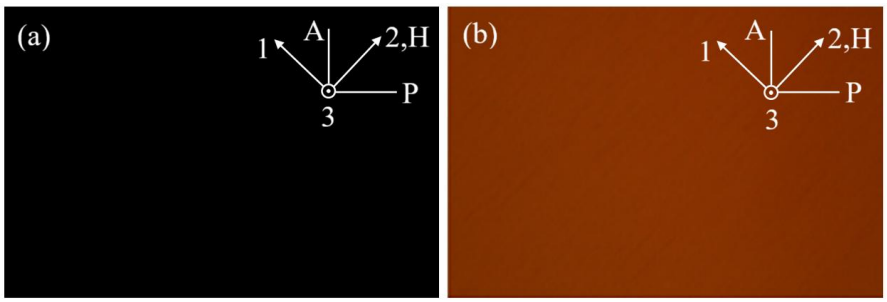

Figure 1.9. Homeotropic and planar alignments in the uniaxial (a) N_D and (b) N_C phases. A and P represent the directions of the analyzer and polarizer, respectively. H: magnetic field direction; 1, 2, and 3 are the laboratory frame axes.

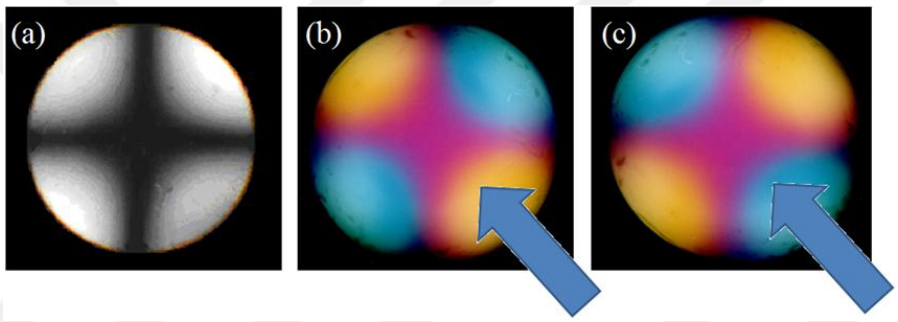

Figure 1.10. (a) Characteristic crossed-dark brushes obtained from the conoscopic investigations of well-aligned textures of uniaxial nematic phases. Interference colors of nematic phases for (b) Δn >0 and (c) Δn <0 when a ¼ λ-retardation plate (its direction is shown by blue arrow) is placed in the light path of the polarizing optical microscope.

Two different refractive indices are involved in the uniaxial nematic phases. If the laboratory frame axes are selected along 1, 2, and 3 directions, which are orthogonal with one another and axis-3 is perpendicular to the 1-2 plane, three refractive indices can be written as n_1, n_2, and n_3, respectively. Then, $\Delta n = n_2 - n_1$, where $n_1 \neq n_2 = n_3$ (Figure 1.11). Thus, the uniaxial nematics are described with only one birefringence (Δn). However, the biaxial nematics have two different birefringences: $\Delta n = n_2 - n_1$ and $\Delta\delta = n_3 - n_2$ (Figure 1.11), where $n_1 \neq n_2 \neq n_3$. If $n_3 - n_2 > n_2 - n_1$ ($n_3 - n_2 < n_2 - n_1$), the biaxial nematic phase has positive (negative) birefringence (Santos et al., 2021).

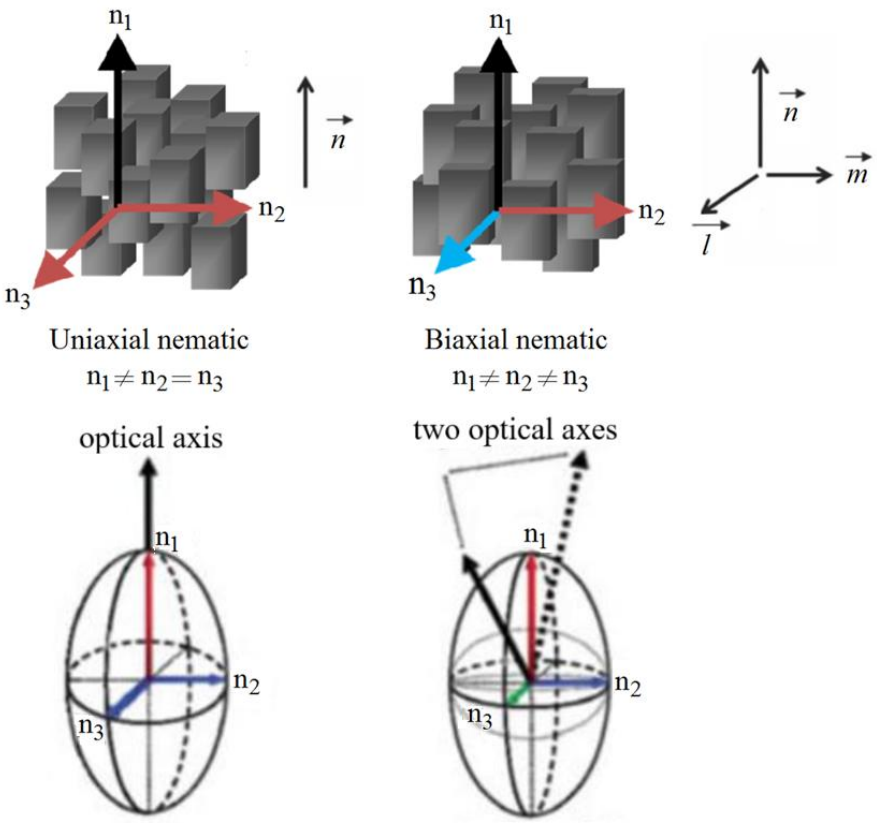

Figure 1.11. Schematic representations of the molecular/micellar orientation (top) and the optical axis (axes) (bottom) in uniaxial nematic and biaxial nematic phases (the magnetic field is omitted in this representation). Adopted from the Refs. (Yang & Lee, 2016) and (Qing et al., 2024). n_1, n_2 and n_3 are the refractive indices along three orthogonal axes.

Figure 1.12, shows how the optical sign of the biaxial nematic phases can be determined by conoscopy under the polarizing optical microscope. When the lyotropic biaxial nematic sample is investigated without the inserting retardation plate into the light path, the crossed-dark brushes (also known as 'Maltese cross'), is seen as shown in Figure 1.12a (the center of the Maltese cross is open). If the retardation plate is put into the light path, the optical anisotropy (birefringence) may be positive (Figure 1.12b) or negative (Figure 1.12c).

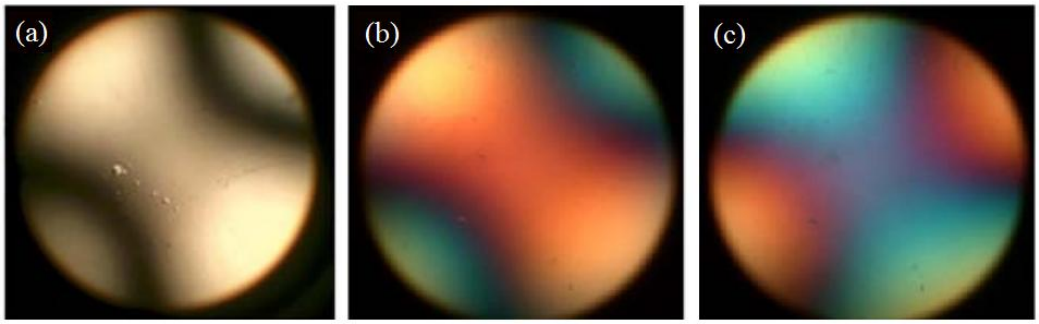

Figure 1.12. Conoscopic images of a well-aligned lyotropic biaxial nematic phase: (a) no retardation plate; after inserting the retardation plate, exhibiting (b) positive and (c) negative birefringences (Santos et al., 2021).

Magnetic materials are classified as diamagnetic, paramagnetic, and ferromagnetic, and investigation of their properties under the effect of magnetic field may be important for their potential applications. Liquid crystals are diamagnetic materials (Kurilov et al., 2021). The magnetization, M, for diamagnetic materials is proportional to the magnetic field strength H (Stannarius, 2014).

$$M=\chi H \qquad (1.3)$$

Here, χ is the magnetic susceptibility. χ is always negative for diamagnetic materials.

If the direction of the applied magnetic field is parallel (perpendicular) to that of the optical axis of the phase, the resultant magnetic susceptibility is indicated as $\chi_{//}$ ($\chi_{\perp}$). Thus, the diamagnetic susceptibility anisotropy $\Delta\chi$ of a liquid crystal sample is

$$\Delta\chi = \chi_{//} - \chi_{\perp} \qquad (1.4)$$

When a liquid crystalline sample has a positive (negative) diamagnetic susceptibility anisotropy, $\Delta\chi>0$ ($\Delta\chi<0$), the optical axis of the liquid crystal aligns parallel (perpendicular) to the applied magnetic field direction. When it equals zero, the system is isotropic.

The biaxial nematic phases are characterized by three two-fold magnetic susceptibilities. The diamagnetic susceptibility anisotropy of the biaxial nematic phase is

$$\Delta\chi = \chi_{33} - \frac{1}{2}(\chi_{11} + \chi_{22}) \qquad (1.5)$$

where the subscripts 11, 22, and 33 correspond to the three orthogonal directions. If a biaxial phase aligns with the axis of the largest (smallest) diamagnetic

susceptibility parallel (perpendicular) to the magnetic field direction, $\Delta\chi>0$ ($\Delta\chi<0$) (Neto & Salinas, 2005).

1.3 Intrinsically Biaxial Micelles Model of Lyotropic Nematic Phases

The two types of nematic phases were identified as Type I and Type II in early studies, considering different orientations of the nematic phase director in the magnetic field (Radley & Reeves, 1975), (Radley & Reeves, 1976), (Forrest et al., 1981). The director of the Type I (Type II) nematic phase orients parallel (perpendicular) to the magnetic field direction. As a result of the studies carried out in the following years, the Type I (Type II) phase was named N_C (N_D) (Charvolin et al., 1979), considering that the Type I and Type II phases were composed of cylindrical-like and disc-like micelles, respectively (Charvolin et al., 1979); (Radley & Saupe, 1978); (Amaral et al., 1979); (Amaral & Tavares, 1980); (Yu & Saupe, 1980). However, the micelle shapes in those phases were hypothetical because there was no experimental evidence for the presence of those kinds of micelles.

Over the following years, especially after the experimental discovery of the biaxial nematic phase in 1980 (Yu & Saupe, 1980b), researchers concentrated on understanding the formation mechanisms of lyotropic nematic phases (Bartolino et al., 1982); (Galerne & Liébert, 1985); (Oliveira et al., 1989); (Vasilevskaya et al., 1990); (Ho et al., 1991); (Quist, 1995); & (Filho el al., 2003). Some models were proposed to explain all three nematic phases. In 1984, Stroobants and Lekkerkerker proposed a model (Stroobants & Lekkerker, 1984). In this model, the N_D and N_C phases were composed of disc-like and rod-like (cylindrical-like) micelles, and the coexistence of those micelles gave rise to the formation N_B phase. Because of the assumption of this model, it was called the “mixture of disc-like and cylindrical-like micelles, MCD model”. However, some theoretical and experimental studies showed that MCD-type models had problems in explaining the formation of the N_B Phase (Kooji & Lekkerker, 2000); (Neto & Galerne, 2015); (Varga et al., 2002); (Galindo et al., 2003); (Kooji, Vogel, & Lekkerkerker, 2000); (Wensink et al., 2002). In 1985, Neto and co-workers proposed a useful model, the so-called “intrinsically biaxial micelles model, IBM”, (Galerne, Neto, & Liebert, 1987) & (Neto et al., 1985a). They assumed that the micelles in all three lyotropic nematic phases exhibit orthorhombic symmetry. In other words, the micelles of the three

nematic phases are analogous from the local symmetry point of view. The IBM model considers two assumptions: (a) the micelles have orthorhombic symmetry in all three different nematic phases with typical dimensions (A', B', and C') and the axes of the local coordinate system α, β, and γ fixed in the micelle (Figure 1.13a); (b) different orientational fluctuations are responsible for the stabilization of the three nematic phases (N_D, N_B, or N_C). The orientational fluctuations around the axis perpendicular to the largest micelle surface (along axis y) give rise to the N_D phase, as shown in Figure 1.13b. By changing the temperature to reach the transition from N_D to N_B, the small-amplitude orientational fluctuations along the three axes (x, y, and z) lead to the N_B phase (Figure 1.13c). If the temperature is changed until obtaining the N_C phase, the orientational fluctuations around the long micellar axis (along the z-axis) are dominant, Figure 1.13d.

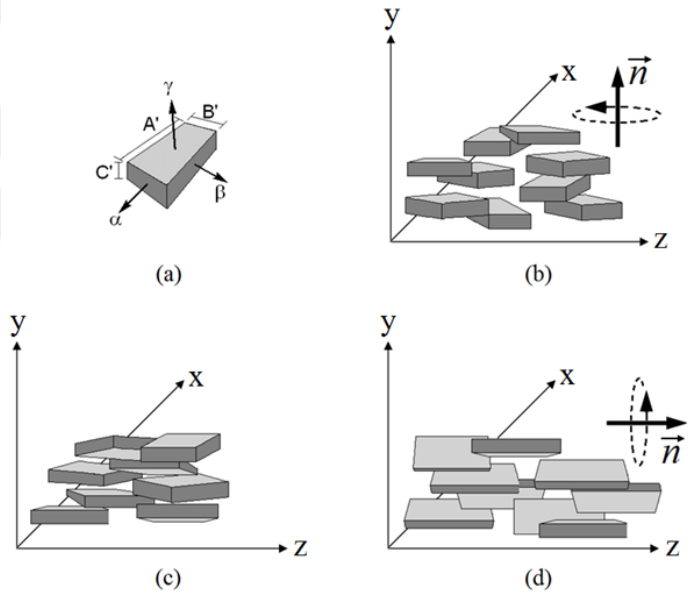

Figure 1.13. (a) Sketch of the orthorhombic micelle in the framework of the IBM model. The detergent amphiphilic bilayer is represented by C'. (b), (c), and (d) show schematically the formation of N_D, N_B, and N_C phases, respectively, from the different orientational fluctuations point of view.

In this thesis, the experimental results of the lyotropic mixtures will be discussed considering the IBM model.

1.4 Role of Components of Lyotropic Nematic Mixtures

Lyotropic systems are micellar solutions at relatively high surfactant concentrations. Similar to the micellar solutions at low surfactant concentrations (hereafter, we will call them “isotropic micellar solutions”), the additional components to the solution cause similar modifications in lyotropic mixtures. Another important point is that scientific information obtained from isotropic micellar solutions may help to understand the properties of lyotropic nematic phases.

Mainly, electrolytes and cosurfactants (oppositely charged surfactants or long-chain alcohols) are added to the lyotropic mixtures as additives to obtain different lyotropic structures. Thus, lyotropic mixtures may have two components (surfactant and solvent), three components (surfactant, electrolyte or cosurfactant, water), or four components (surfactant, electrolyte, cosurfactant, water) systems.

When surfactant molecules form micelles, three different regions may be defined in the micellar systems: core, micelle surface, and aqueous bulk solution or intermicellar aqueous region, Figure 1.14. The micelle core is composed of the surfactant hydrocarbon chain. There is an electrical double layer between the core and the aqueous bulk solution. The Stern and Gouy-Chapman layers form an electrical double layer (Chakraborty et al., 2011) around the micelle surface by covering the micelle core. Thus, it can be said that an electric double layer mainly consists of three parts (Park & Seo, 2011):

(a) Surface charge: it arises from charged ions adsorbed on the ionic micelle surface.

(b) Stern layer: it includes counterions with oppositely charged to the surface charge formed by surfactant head groups. Those counterions are attracted to the micelle surface and closely attached to the surface by the electrostatic force.

(c) Gouy-Chapman or Diffuse layer (Jin et al., 2020): a film of the dispersion medium (solvent) adjacent to the Stern layer of the micelle. This layer contains free ions with a higher concentration of the counterions. The electrostatic force between the charged particles affects the ions of the diffuse layer.

The electrical potential within the electric double layer has its maximum value on the micelle surface (Stern layer). The potential decreases with the increase of distance from the micelle surface and reaches zero at the boundary of the electric double layer (Park & Seo, 2011). The Stern layer is an immobile layer and ions are

closest to the charged micelle surface in this layer. However, ions are looser and relatively mobile in the Gouy-Chapman (diffuse) layer (Ugochukwu, 2019). Furthermore, the electrical double layer is compressed in the presence of electrolyte or increased electrolyte concentration due to the reduction of the electrostatic attractions between ions and the micelles (Xu et al., 2007); (Yang et al., 2005); (Demissie & Duraisamy, 2016).

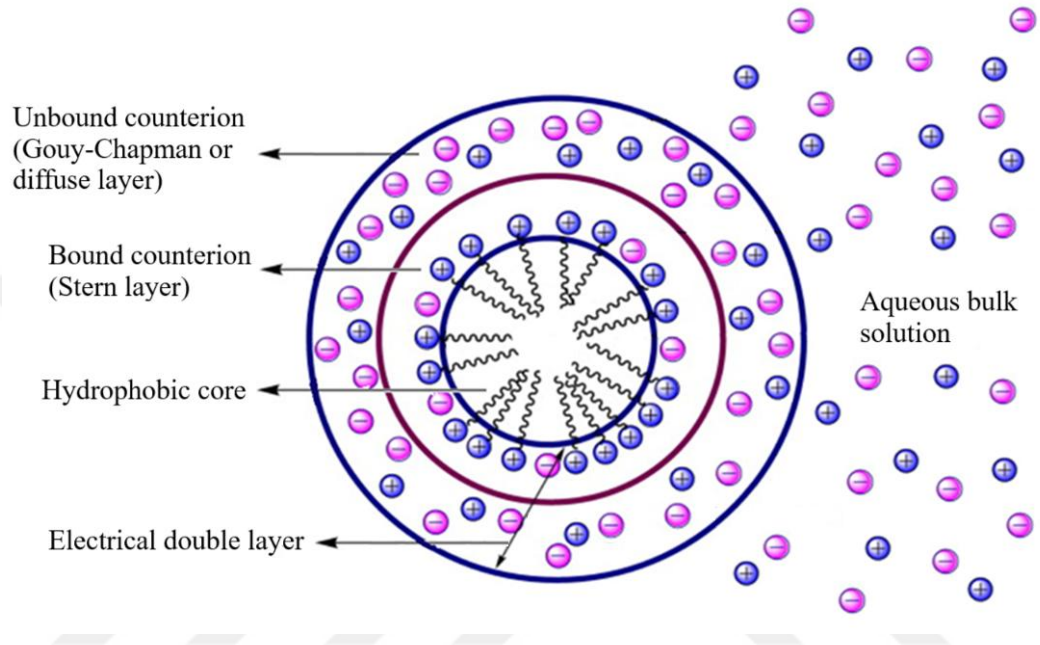

Figure 1.14. Schematic representation of the micellar microstructure of ionic surfactant (here, for example, cationic surfactant) showing the electrical double layer (Modified from [Yadav et al., 2015]).

Mainly, two important driving forces play a role in the micelle formation. When the surfactant molecules come together to form a micelle, there are electrostatic repulsive forces between similarly charged ionic surfactant head groups at the micelle surface (Mozrzymas, 2019). Furthermore, variations in the surfactants' head group structure influence the micelle formation (Das et al., 2005) & (Schnee et al., 2008). Then, some parts of the surfactant counterions are bound to the surfactant head groups to reduce those repulsions. At the same time, there are van der Waals attractions between the surfactant tails (alkyl chains) in the micelle core (Lei et al., 2025) & (Centeno et al., 2017). These two forces (reducing the repulsions at the micelle surface and favoring the attractions between the surfactant tails) result in the formation of a thermodynamically stable micelle structure.

The types of counterions/ions, coming from electrolytes, added to the micellar solutions are important parameters for the micellization because the interactions between these ionic species and the surfactant head groups affect the reduction of repulsions between surfactant head groups at the micelle surfaces differently, and consequently micelle formation. So, the presence of the electrolyte ions results in the growth in the micelle size (Sein & Engberts, 1995) & (Oelschlaeger et al., 2010). The electrolyte ions also lead to the packing of a larger amount of the surfactant molecules in the micelles, in the dilute isotropic (Neto & Salinas, 2005); (Aswal & Goyal, 2000); & (Israelachvili, 1991) and lyotropic (Dawin et al., 2009); (Leaver & Holmes, 1993); & (Holmes et al., 1995) solutions of surfactants. The change in micelle shape anisotropy, especially for the lyotropic nematic phases, is observed due to the interactions between ionic species (surfactant head groups, and ions of the electrolytes. Experimental studies indicated that the extent of those interactions is governed by the "kosmotropic" and "chaotropic" behaviour of the ionic species (Akpinar et al., 2019); (Akpinar et al., 2015); (Akpinar et al., 2016a); (Akpinar et al., 2016b). Collins et al. summarily defined these two characteristic properties of the ionic species depending on their hydration degree of the ions (Collins, 2004) & (Collins, 2007), i.e., they may be surrounded by a larger (for kosmotropic ions) or less (for chaotropic ions) amount of free water molecules. Comparing kosmotropic and chaotropic ions with different ionic radii and the same electrostatic charge, as expected, smaller ions are surrounded by a larger amount of structured water molecules if compared with the bigger ions, Figure 1.15. The ionic species with similar (different) extent of the kosmotropic/chaotropic characters leads to the formation of close contact (loosely bound) ion pairs (Conway, 1981); (Marcus, 1985); (Collins, 1997); (Moreira & Firoozabadi, 2010), Figure 1.16. Furthermore, the kosmotrope and chaotrope ions are ordered in the Hofmeister series of ions, which are, in general, given in Figure 1.17.

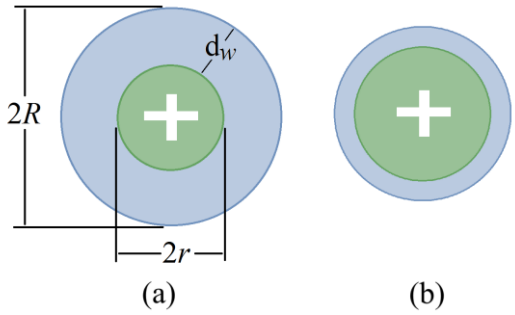

Figure 1.15. Comparison of (a) small kosmotropic and (b) the bigger chaotropic ions with the same electrostatic charge. 2r: ionic diameter; 2R: hydrodynamic diameter; d_w is the thickness of the water layer (Adopted from [Akpinar et al., 2019]).

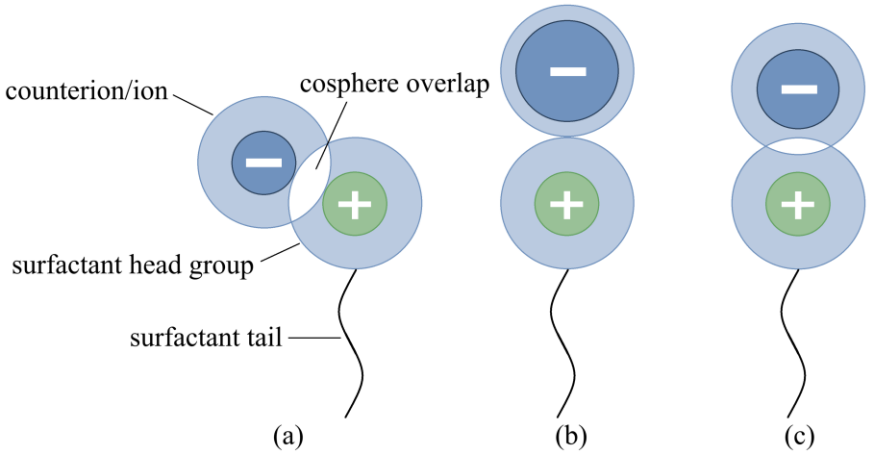

Figure 1.16. Formation of the different ion pairs, considering the interactions between, for example, the positively charged kosmotropic surfactant head group and (a) strongly kosmotropic, (b) strongly chaotropic, (c) weakly chaotropic or kosmotropic counterion/ion (Moreira & Firoozabadi, 2010). While a tightly bound ion pair is produced in (a), a loosely bound ion pair is produced in (b) (Adopted from [Akpinar et al, 2019]).

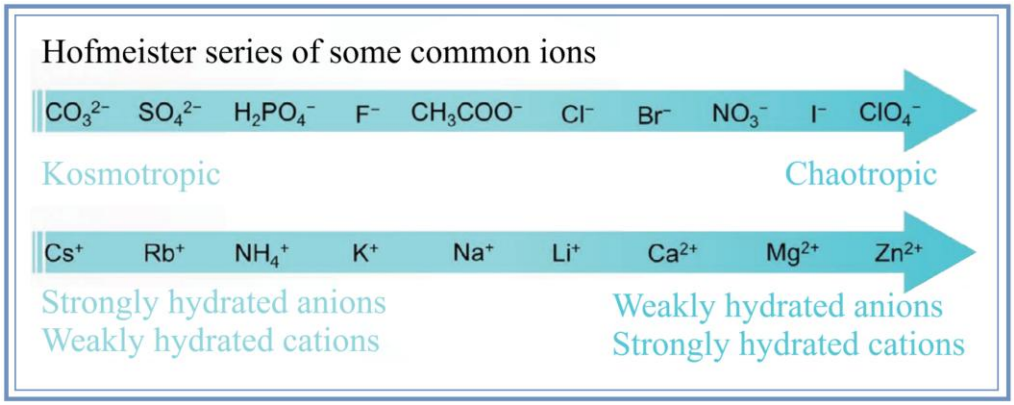

Figure 1.17. General order of kosmotropic and chaotropic anions/cations in the Hofmeister series (Adopted from [Mao et al., 2024]).

Akpinar and Neto investigated the effect of the interactions between the conventional inorganic salt (electrolyte) ions of some Hofmeister series anions and surfactant head groups (Akpinar et al., 2019) & (Akpinar et al., 2021). Their results indicated that those interactions are one of the important effect to stabilize different lyotropic nematic phases by changing micelle surface curvature, Figure 1.18.

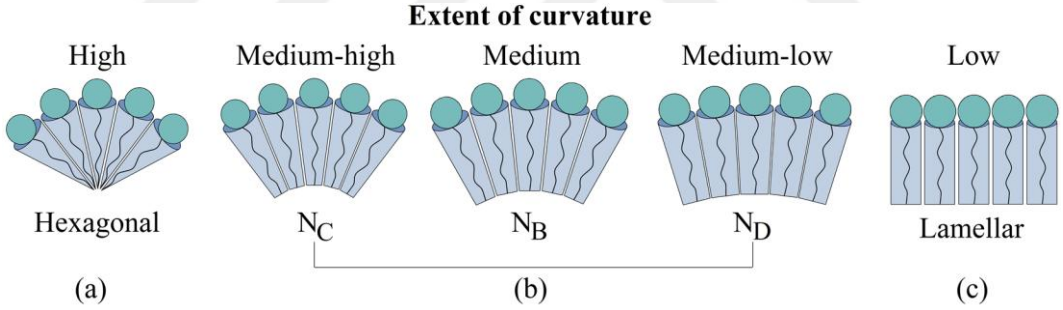

Figure 1.18. Relationship between the micelle surface curvature and the expected lyotropic structures as a result of the interactions between ionic species at the micelle surfaces [Adopted from (Akpinar et al., 2021)].

Similar to the effect of electrolytes, cosurfactants such as long-chain alcohols screen the repulsions between the surfactant head groups at the micelle surfaces, and, at the same time, their alkyl chains fill the interior (core) of the micelles, both favoring the micellization. In general, in lyotropic mixtures, alcohol molecules concentrate in the flattest surface of the micelle, rather than in its curved borders (Hendrikx et al., 1986). It means that there is segregation on the partitions of the surfactant and alcohol molecules in the less curved areas and rims of the micelles. From an experimental point of view, the increase in the relative

concentration of alcohol and water in the mixture enlarges the N_D phase domain (Figueiredo, 1985b). In other words, considering the IBM model of the lyotropic nematic phases, there is an increase in the dimensions of the micelles in the plane $\alpha - \beta$ of the orthorhombic micelles by favoring the orientational fluctuation that degenerates axis 3 to stabilize the N_D phase. However, it is also possible that alcohol molecules with relatively longer alkyl chains compared to the alkyl chain of surfactant molecules may tend to locate preferentially in the curved surfaces of the micelle, which favors the formation of the N_C phase by passing through the N_B phase (Akpinar et al., 2012a).

Consequently, the selection of suitable additives (electrolytes, cosurfactants) is an important parameter to obtain different lyotropic structures, especially nematic phases.

1.5 Objective and Hypothesis

In the literature, in general, the effect of modifications in the lyotropic mixtures has been investigated by researchers to form different lyotropic phases, especially biaxial nematic ones. These modifications were mainly based on the specific interactions (a) between surfactant head groups and oppositely charged counterions/ions of strong electrolytes (Akpinar et al., 2016b) & (Akpinar et al., 2015) and of weak electrolytes (Akpinar et al., 2016a) at the micelle surfaces, and (b) between surfactant and alcohol chains in the micelle (Akpinar et al., 2017) & (Akpinar et al., 2012a). However, the effect of the electrolyte ions, which have the same charge with the surfactant head groups, has not been investigated yet. As expected, those ions cannot penetrate the Stern layer (micelle surface) but can be located in the Gouy-Chapman layer and/or the intermicellar region (aqueous bulk phase).

The study's main goal is to find out how Hofmeister ions, present in the intermicellar region or Gouy-Chapman layer but not in the Stern layer (micelle surface), especially affect the stabilization of uniaxial and biaxial nematic phases. To do so, a surfactant molecule with a negatively charged kosmotropic head group (potassium dodecanoate, KDD) was chosen and electrolytes of different Hofmeister series anions were investigated in the KDD-lyotropic mixtures.

2. MATERIALS and METHODOLOGY

2.1 Materials

The surfactant molecule KDD, Figure 2.1, was widely used to prepare lyotropic mixtures, since the first lyotropic mixture of the biaxial nematic phases was reported in the literature in 1980 (Yu & Saupe, 1980b). So, its simple synthesis procedure, including neutralization reaction of dodecanoic acid (Merck) with KOH (Merck) and purification 3 times with absolute ethanol, was well-defined in the literature to have KDD with a purity of >99%.

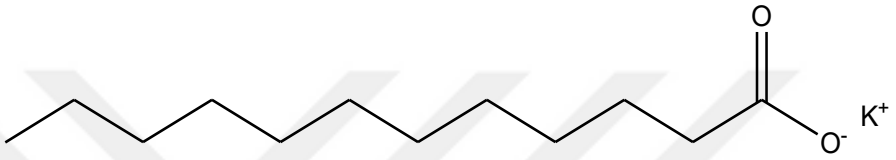

Figure 2.1. Molecular structure of KDD.

The electrolytes (KF, KCl, KBr, KI, KSCN, NaF, NaCl, NaBr, RbBr, and CsBr) were purchased from Merck and Sigma-Aldrich (purity >99%). The cosurfactant DeOH was provided commercially with a purity of 99% (Merck). Ultrapure water was obtained from the Millipore Direct-Q3 UV purification system with a resistivity of 18.2 MΩ.cm at 25ºC.

2.2 Sample Preparation

Lyotropic liquid crystal mixtures were prepared by weighing the required amounts of each component in capped glass test tubes at appropriate concentrations using a precision balance (Radwag AS82/220.R2, ±0.00001 g). After the weighing process was completed, mixing with a vortex (Ika MS 3 Basic) and centrifugation (Hettich EBA20) processes were performed several times for the homogenization process of the lyotropic mixtures. Because highly oriented nematic phases are necessary for laser conoscopy, polarized optical microscopy, and small-angle X-ray scattering measurements, a water-based ferrofluid (Ferrotec, EMG-607) was added at 1 μL per 1 g of lyotropic mixtures in the presence of the magnetic field (~2.0, ~1.0 and ~1.0 kG, respectively). In the previous experiments, it was proved that the addition of ferrofluid in this concentration does not cause any modification in the transition temperatures and shape anisotropy of the micelles (Neto & Salinas,

2005), (Akpinar, Reis, & Figueiredo Neto, 2012b), (Akpinar, Reis, & Figueiredo Neto, 2014). The compositions of lyotropic mixtures are given in Table 2.1.

Table 2.1. Compositions of lyotropic phase types of KDD/Electrolyte/DeOH/water mixtures. X corresponds to the percent mole fraction of each component.

Mixture	Electrolyte	X_{KDD}	$X_{electrolyte}$	X_{DeOH}	X_{water}
s0	---	3.317	0.000	1.212	95.471
s1	KF	3.308	0.275	1.209	95.209
s2	KCl	3.308	0.273	1.209	95.210
s3	KBr	3.307	0.276	1.209	95.208
s4	KI	3.308	0.275	1.209	95.209
s5	KSCN	3.307	0.274	1.209	95.210
s6	NaBr	3.308	0.277	1.209	95.206
s7	RbBr	3.308	0.276	1.209	95.208
s8	CsBr	3.307	0.275	1.209	95.209
s9	NaF	3.308	0.278	1.209	95.205
s10	NaCl	3.307	0.273	1.209	95.211

2.3 Experimental Techniques

2.3.1 Polarising optical microscopy

Lyotropic nematic phase textures were analyzed in a Nikon Eclipse Ci-POL (Nikon, Japan) polarized optical microscope. In these measurements, some parts of nematic samples were transferred into a microslide (Vitrocom, Japan) of 0.2, 0.3, and/or 0.4 mm thicknesses. The ends of the microslides were closed with a special fluidic nanocomposite (DLine, Lithuania) and then UV light was applied to prevent water loss. Microslides were placed in a Linkam LTS120E temperature control unit (0.1°C precision), to which a Polyscience SD07R circulating water bath, which controls the temperature with an accuracy of ±0.04 ◦C, was connected to provide homogeneous heat distribution. The phase textures were recorded with a digital microscope camera (DFK41AU02, The Imaging Source, Germany) and characterized with special software (NIS-Element-D computer software, Nikon).

The samples were placed in the temperature control unit in a position where the magnetic field was oriented at 45° with respect to the optical analyzer and polarizer.

2.3.2 Laser conoscopy

Laser conoscopy technique was used to determine the second-order nematic-nematic phase transition temperatures. Lyotropic nematic samples were sandwiched between two circular optical glasses (Helma) with a diameter of 2.5 cm, using a 2.5 mm thick glass ring. Then, the sample were placed in a sample holder. A temperature controller (Lakeshore 335) and Pt102 sensor with 0.001°C sensitivity was used to control the temperature in the system. The homogeneous heat temperature in the sample was provided by a circulating water bath (Polyscience AD07R), with accuracy of 0.01°C. For the nematic phase director alignment in each nematic phases, a magnetic field was applied to the system by using neodymium magnets (NdFeB) and its strength (~2.3 kG) was measured with a Gaussmeter (Lakeshore, Model 455) during the measurements.

2.3.3 Small-angle X-ray scattering

The SAXS measurements in transmission geometry were carried out in a Xeuss 2.0 laboratory-based system (Xenocs, France). The measurements' details and the analysis of SAXS results were also given in (Akpinar et al., 2020). Briefly, the monochromatic and collimated incident X-ray beam has a wavelength of 1.5419 Å and a square cross-section of 0.7 mm side in the sample position. A Pilatus 300K detector (Dectris, Switzerland) recorded the two-dimensional X-ray scattering patterns. The sample-to-detector distance was 937 mm. The samples were transferred into cylindrical Mark-tube capillaries of 1.5 mm diameter (Hilgenberg, Germany), and closed with UV-sensitive photopolymer to prevent water evaporation. A sufficient homogeneous static magnetic field was generated with NdFeB magnets (~1 kG). From the 2D anisotropic scattering patterns, frame integrations were performed along the directions parallel and perpendicular to the magnetic field direction. The frame integrations of 2D SAXS were obtained in circular sectors of 20° around the vertical (VRT) and horizontal (HRZ) directions of the images (Akpinar et al., 2023), Figure 2.2. These operations resulted in curves of X-ray scattering intensity as a function of the momentum transfer modulus, q =

$(4\pi/\lambda)\sin\theta$, where 2θ is the scattering angle. A representative frame integrations is shown in Figure 2.3.

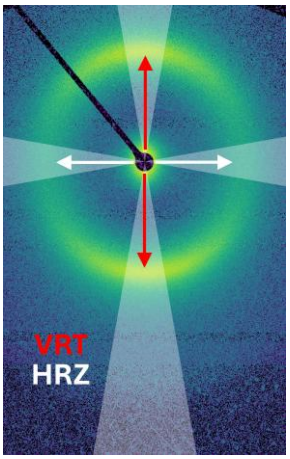

Figure 2.2. An example for frame integrations of a 2D anisotropic SAXS pattern in circular sectors of 20° around the vertical (VRT) and horizontal (HRZ) directions of the images (Akpinar et al., 2025).

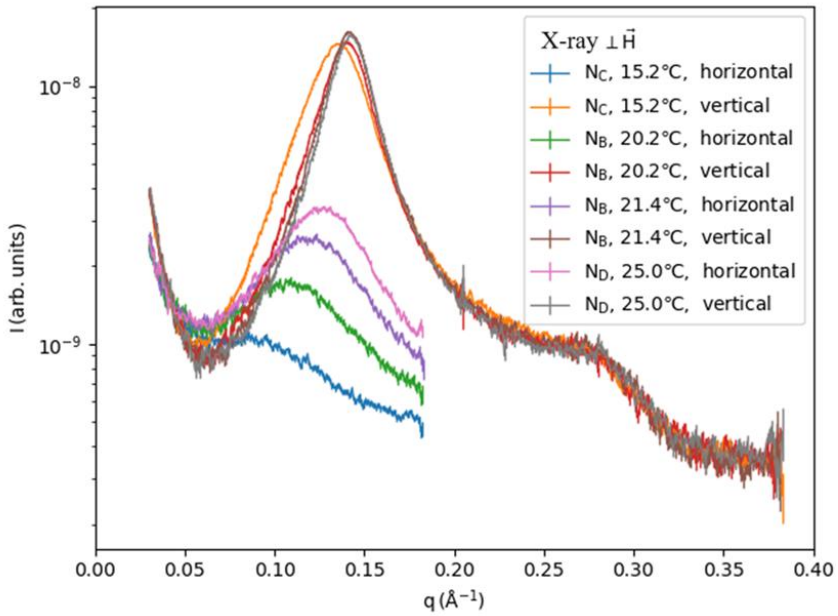

Figure 2.3. An example from the literature for frame integration of the 2D SAXS patterns of the aligned nematic phases. Only for the X-ray beam perpendicular to the magnetic field direction, The nematic phase, temperature and integration direction of each curve are indicated in the figure (Akpinar et al., 2023).

3. RESULTS

3.1 Characterization of Lyotropic Liquid Crystal Samples

The textures of lyotropic nematic samples were characterized by polarizing optical microscopy. The following figures show the textures of the samples given in Table 2.1.

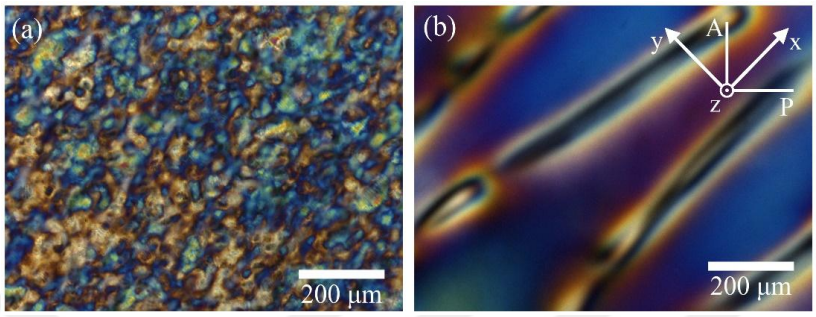

Figure 3.1. Phase textures observed under a polarized optical microscope for s0 mixture: (a) Non-nematic or crystalline-like phase at 15.0°C and (b) partly aligned N_C at 25.0°C, after 24 h in the presence of a magnetic field (0.9 kG). Objective: 10x. Sample thickness: 0.200 mm. A and P are the directions of analyzer and polarizer, respectively. X, y and z are the laboratory frame axes. The direction of the magnetic field and the long capillary axis were along x-axis and y-axis, respectively. Similar measurement configuration was applied to other samples.

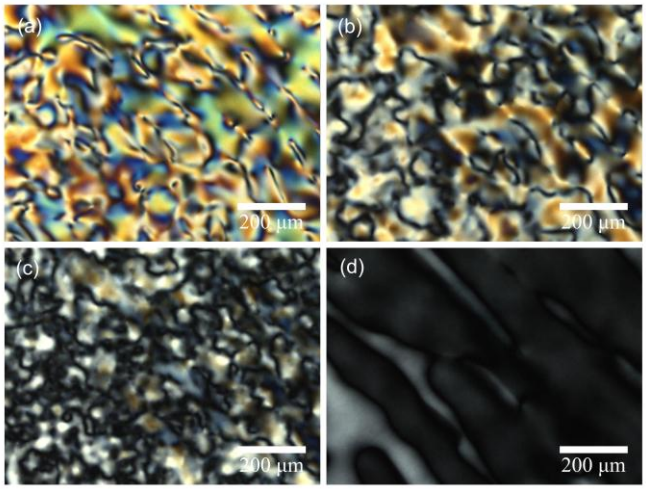

Figure 3.2. Phase textures observed under a polarized optical microscope for s1 mixture: (a) N_C at 20.0°C, (b) N_B at 29.0°C, (c) N_B at 30.0°C, and (b) N_D at 40.0°C. Objective: 10x. Sample thickness: 0.300 mm. No magnetic field was applied.

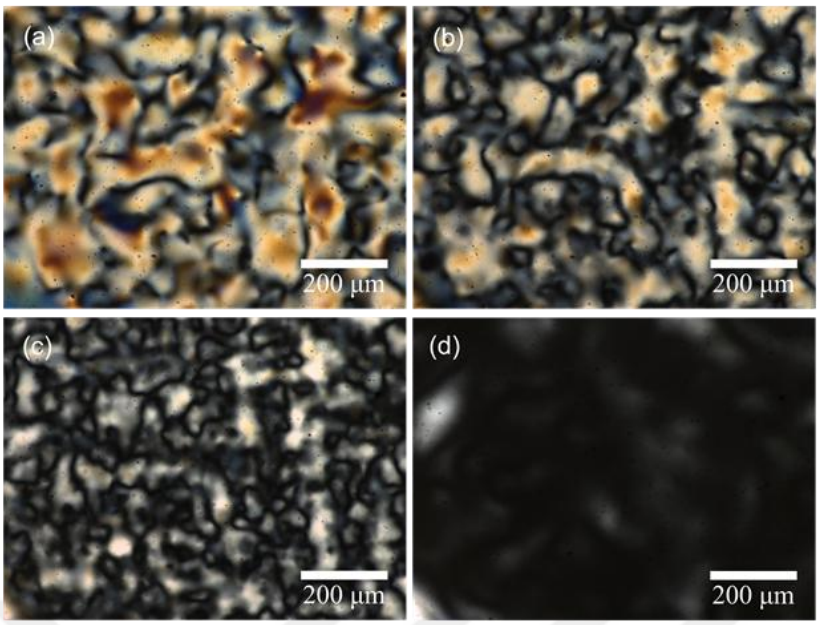

Figure 3.3. Phase textures observed under a polarized optical microscope for s2 mixture: (a) N_C at 20.0°C, (b) N_B at 29.0°C, (c) N_B at 31.0°C, and (b) N_D at 40.0°C. Objective: 10x. Sample thickness: 0.300 mm. No magnetic field was applied.

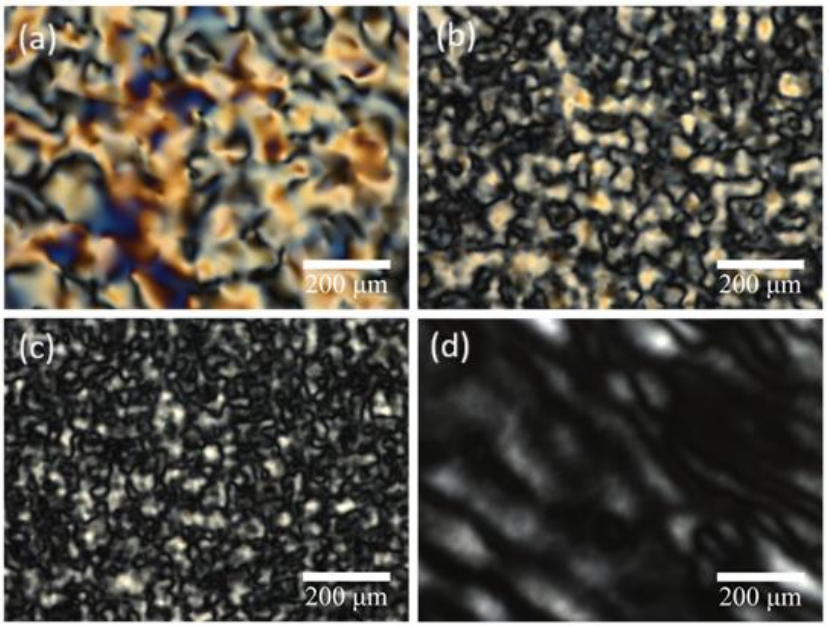

Figure 3.4. Phase textures observed under a polarized optical microscope for s3 mixture: (a) N_C at 20.0°C, (b) N_B at 29.0°C, (c) N_B at 30.0°C, and (d) N_D at 40.0°C. Objective: 10x. Sample thickness: 0.300 mm. No magnetic field was applied.

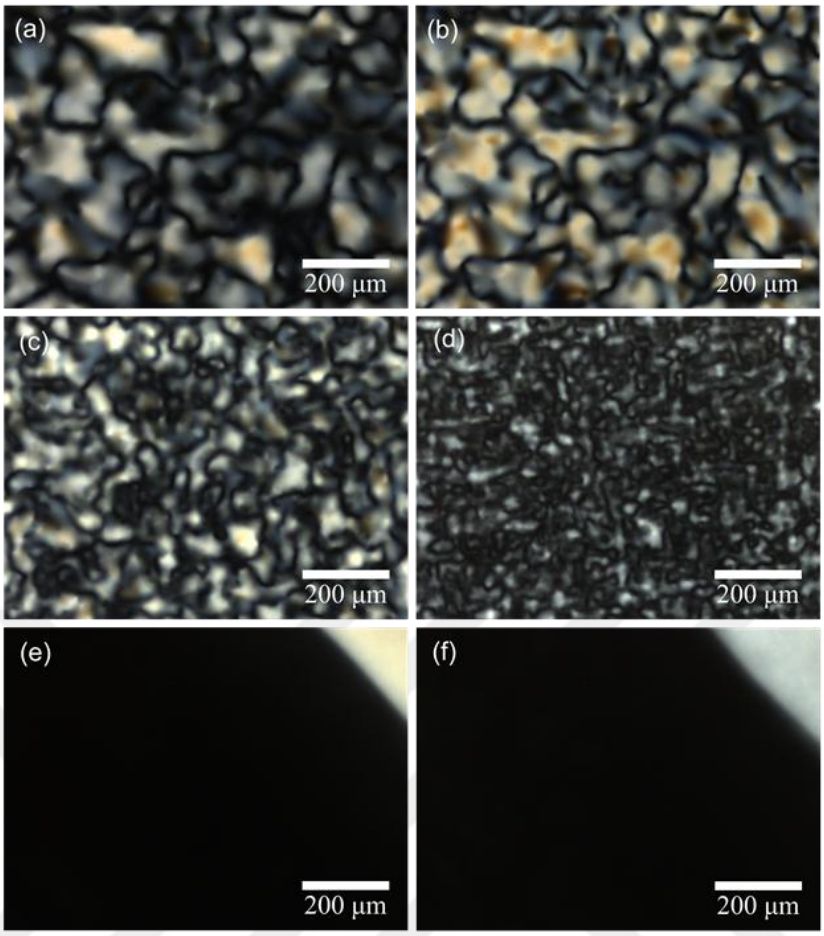

Figure 3.5. Phase textures observed under a polarized optical microscope for s4 mixture: (a) N_B at 15.0°C, (b) N_B at 20.0°C, (c) N_B at 25.0°C, (d) N_B at 27.0°C, (e) N_D at 29.0°C and (f) N_D at 40.0°C. Objective: 10x. Sample thickness: 0.300 mm. No magnetic field was applied.

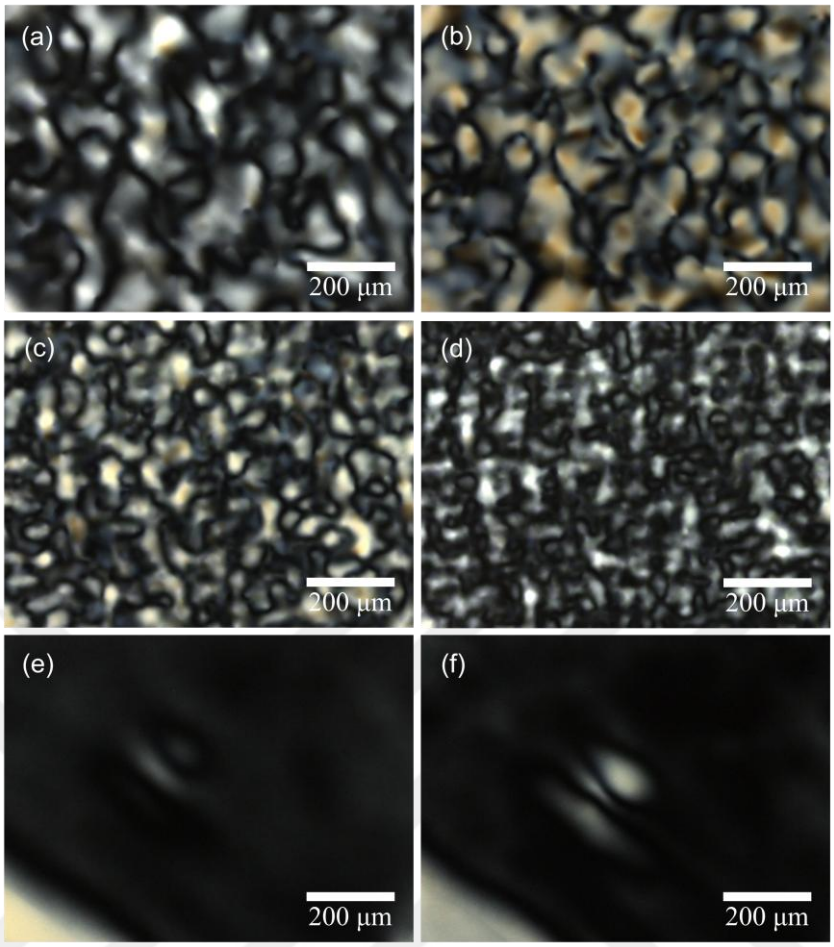

Figure 3.6. Phase textures observed under a polarized optical microscope for s5 mixture: (a) N_c at 15.0°C, (b) N_c at 20.0°C, (c) N_B at 26.0°C, (d) N_B at 28.0°C, (e) N_D at 32.0°C and (f) N_D at 40.0°C. Objective: 10x. Sample thickness: 0.300 mm. No magnetic field was applied.

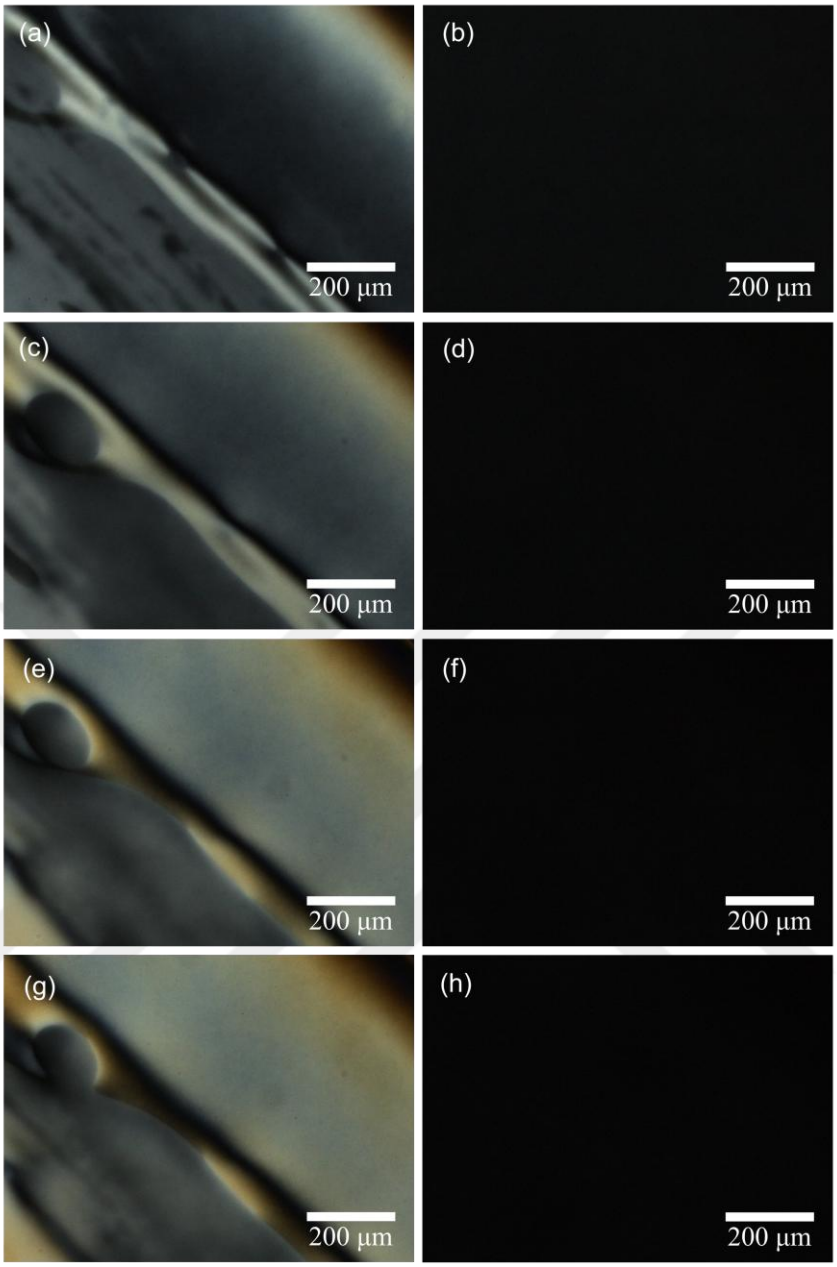

Figure 3.7. Phase textures observed under a polarized optical microscope for s6 mixture: (a) N_D at 40.0°C, (b) N_D at 40.0°C aligned with a magnetic field of 0.9 kG, (c) N_D at 30.0°C, (d) N_D at 30.0°C aligned with a magnetic field of 0.9 kG, (e) N_D at 20.0°C, (f) N_D at 20.0°C aligned with a magnetic field of 0.9 kG, (g) N_D at 15.0°C, (h) N_D at 15.0°C aligned with a magnetic field of 0.9 kG. Objective: 10x. Sample thickness: 0.300 mm.

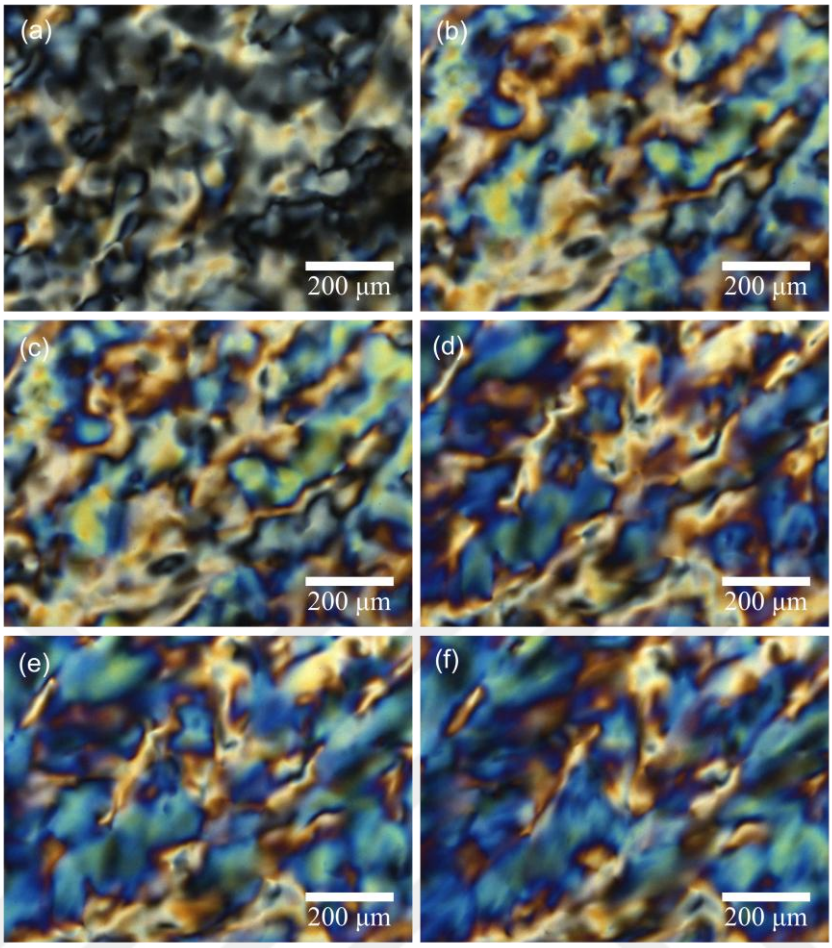

Figure 3.8. Phase textures observed under a polarized optical microscope for s7 mixture: (a) N_D at 40.0°C, (b) N_B at 29.0°C, (c) N_c at 27.0°C, (d) N_C at 25.0°C, (e) N_C at 20.0°C and (f) N_C at 15.0°C. Objective: 10x. Sample thickness: 0.300 mm. No magnetic field was applied.

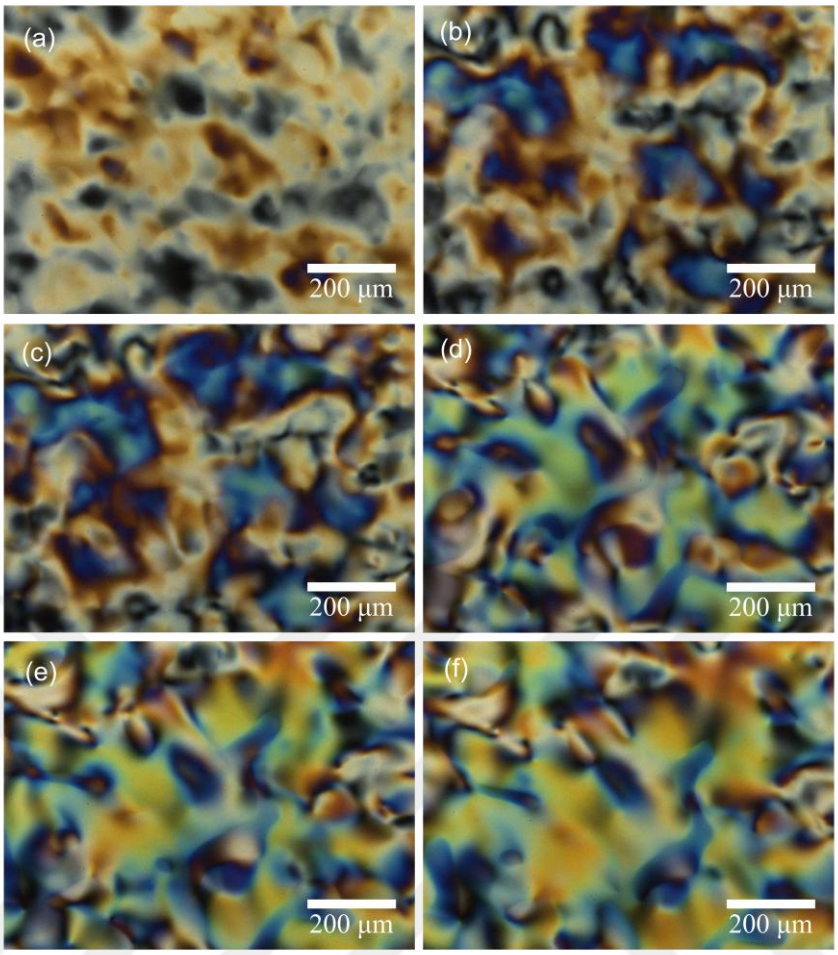

Figure 3.9. Phase textures observed under a polarized optical microscope for s8 mixture: (a) N_D at 40.0°C, (b) N_B at 34.0°C, (c) N_c at 32.0°C, (d) N_C at 25.0°C, (e) N_C at 20.0°C and (f) N_C at 15.0°C. Objective: 10x. Sample thickness: 0.300 mm. No magnetic field was applied.

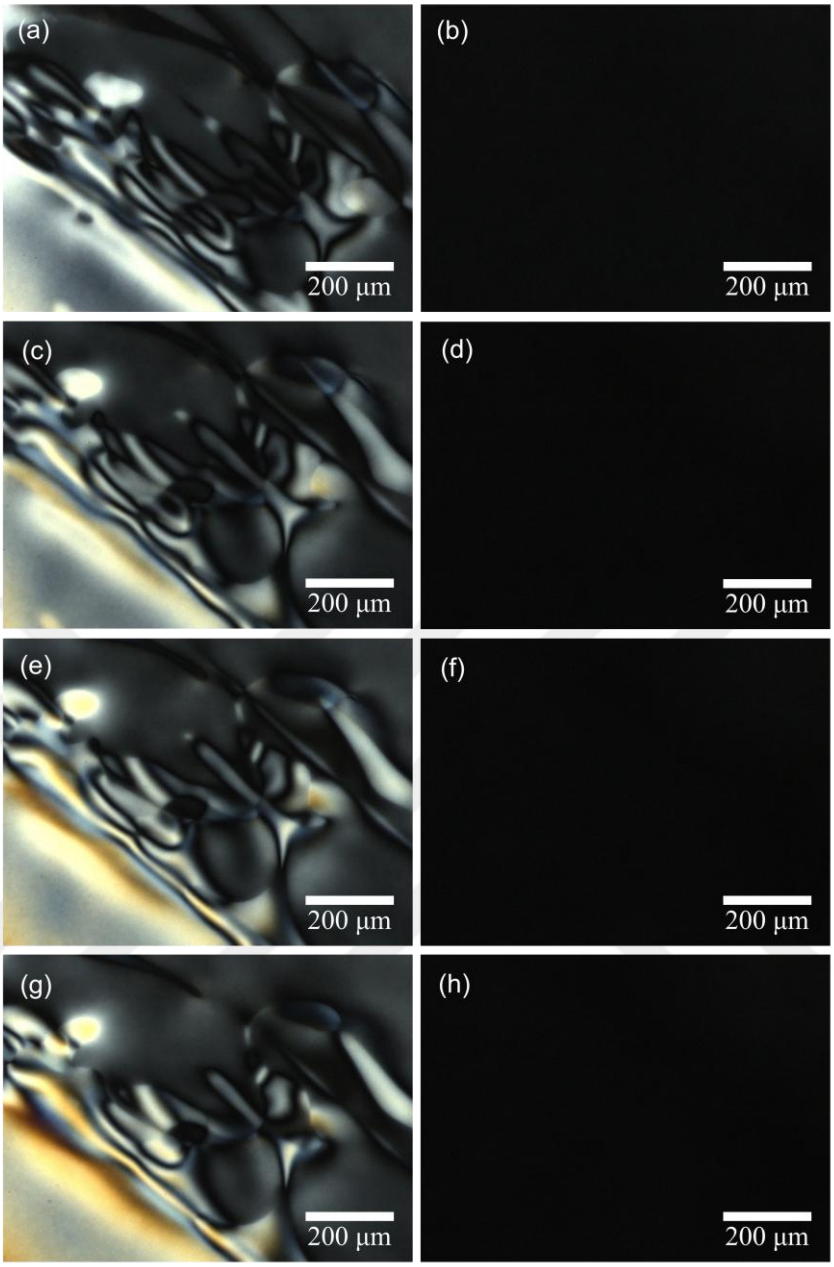

Figure 3.10. Phase textures observed under a polarized optical microscope for s9 mixture: (a) N_D at 40.0°C, (b) N_D at 40.0°C aligned with a magnetic field of 0.9 kG, (c) N_D at 30.0°C, (d) N_D at 30.0°C aligned with a magnetic field of 0.9 kG, (e) N_D at 20.0°C, (f) N_D at 20.0°C aligned with a magnetic field of 0.9 kG, (g) N_D at 15.0°C, (h) N_D at 15.0°C aligned with a magnetic field of 0.9 kG. Objective: 10x. Sample thickness: 0.300 mm.

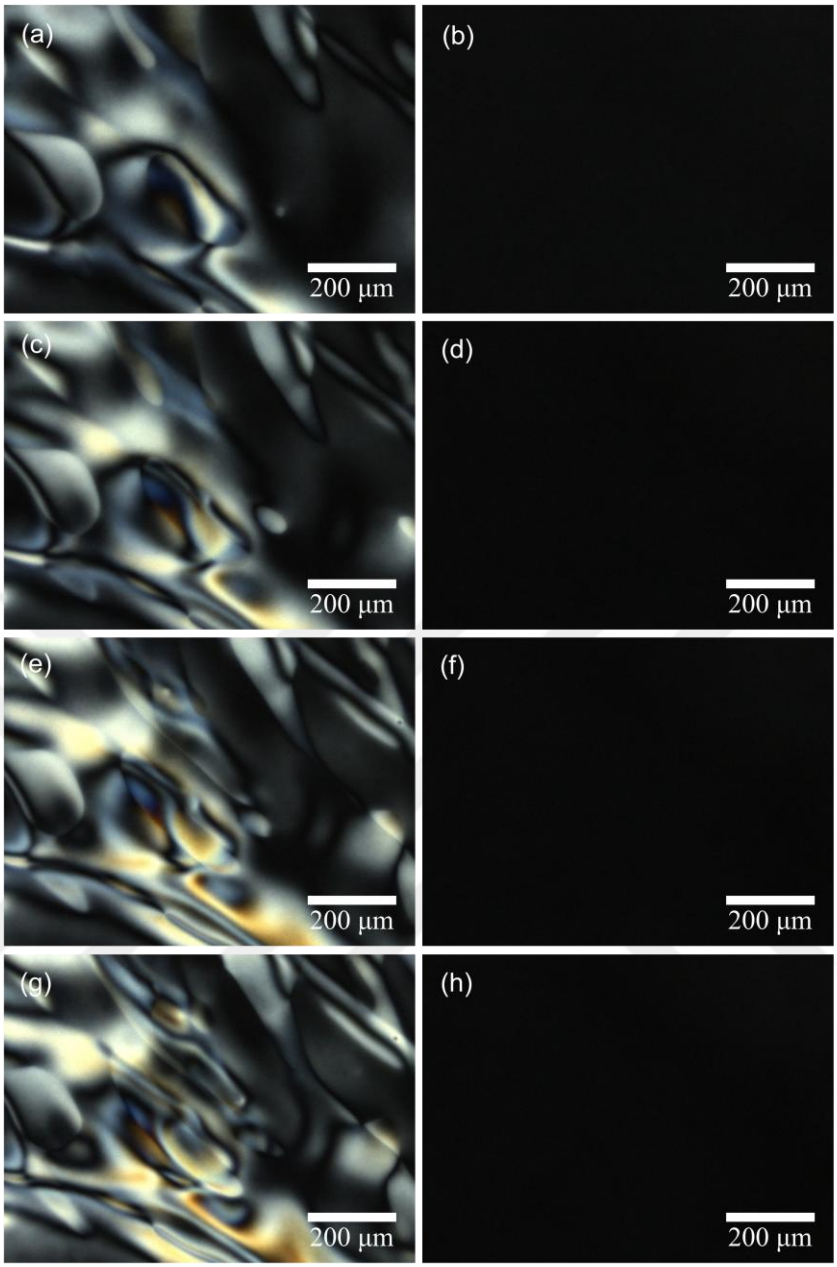

Figure 3.11. Phase textures observed under a polarized optical microscope for s10 mixture: (a) N_D at 40.0°C, (b) N_D at 40.0°C aligned with a magnetic field of 0.9 kG, (c) N_D at 30.0°C, (d) N_D at 30.0°C aligned with a magnetic field of 0.9 kG, (e) N_D at 20.0°C, (f) N_D at 20.0°C aligned with a magnetic field of 0.9 kG, (g) N_D at 15.0°C, (h) N_D at 15.0°C aligned with a magnetic field of 0.9 kG. Objective: 10x. Sample thickness: 0.300 mm.

3.2 Birefringences Measurements of Lyotropic Liquid Crystal Samples

Temperature dependences of the birefringences of the lyotropic nematic phases were evaluated from the laser conoscopy, which also enables us to determine the symmmetric tensor invariants. Lyotropic nematic phases are characterized by a second-rank, traceless, symmetric tensor order parameter (Freiser, 1970) & (Shih & Alben, 1972). The optical dielectric tensor $\overleftrightarrow{\varepsilon}$, which has the same symmetry as the nematic phases, can be assumed as the order parameter (de Gennes & Prost, 1995, p. 58). The diagonal elements of the anisotropic part of the dielectric tensor are written in terms of the optical birefringences (Galerne & Marcerou, 1985), & (Galerne & Marcerou, 1983),

$$\varepsilon_{a,1} = -\frac{4\langle n\rangle}{3}\left(\Delta n + \frac{\delta n}{2}\right)$$

$$\varepsilon_{a,2} = \frac{2\langle n\rangle}{3}(\Delta n - \delta n)$$

$$\varepsilon_{a,3} = \frac{4\langle n\rangle}{3}\left(\frac{\Delta n}{2} - \delta n\right)$$

where $\langle n\rangle$ is the average refractive index of the nematic phase. Then, the symmetric invariants of the tensor order parameter, σ_1, σ_2 and σ_3 (Freiser, 1970) are

$$\sigma_1 = \varepsilon_{a,1} + \varepsilon_{a,2} + \varepsilon_{a,3}$$

$$\sigma_2 = \frac{2}{3}\left(\varepsilon_{a,1}^2 + \varepsilon_{a,2}^2 + \varepsilon_{a,3}^2\right)$$

$$\sigma_3 = 4\varepsilon_{a,1}\varepsilon_{a,2}\varepsilon_{a,3}$$

where σ_1 is zero. In the uniaxial phases, σ_3 is related to σ_2 by $\sigma_3 = \pm\sigma_2^{3/2}$ (Galerne & Marcerou, 1985) Figure 3.12. The sign + (−) refers to the N_D (N_C) phase. In the biaxial phase, σ_3 takes values in the range of $-\sigma_2^{3/2}$ and $+\sigma_2^{3/2}$, which is evidence of the location of the N_B phase between the two uniaxial nematic phases in the partial phase diagrams.

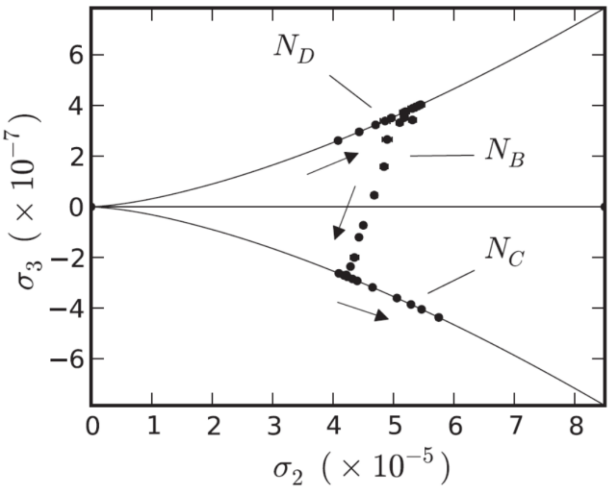

Figure 3.12. A representative example for the dependence of σ_3 on σ_2 obtained from KL/undecanol/K_2SO_4/water lyotropic mixture from the literature. The arrows shows the direction of the cooling process applied to measure the birefringences (Akpinar, Reis, & Figueiredo Neto, 2012b).

The temperature dependences of the birefringences (Δn and δn) and the symmetric invariants of the tensor order parameter (σ_2 and σ_3), and also the dependence of σ_3 on σ_2 were determined from the laser conoscopy measurements. The data were given in Tables 3.1-3.22.

Table 3.1. The change in the Δn and δn values with temperature for sample s0. This sample gives only N_C phase in the temperature range studied.

T/°C	δn	Δn	T/°C	δn	Δn
45.00	0.00	2.13	31.00	0.00	2.60
43.00	0.00	2.22	29.00	0.00	2.65
41.00	0.00	2.31	27.00	0.00	2.68
39.00	0.00	2.34	25.00	0.00	2.73
37.00	0.00	2.45	23.00	0.00	2.77
35.00	0.00	2.49	22.00	0.00	2.81
33.00	0.00	2.56			

Table 3.2. The change in the σ_2 and σ_3 values with temperature for sample s0.

T/°C	$\sigma_2/10^{-5}$	$\sigma_3/10^{-7}$	T/°C	$\sigma_2/10^{-5}$	$\sigma_3/10^{-7}$
45.00	1.54	-0.61	31.00	2.31	-1.11
43.00	1.68	-0.69	29.00	2.39	-1.17
41.00	1.81	-0.77	27.00	2.44	-1.21
39.00	1.90	-0.82	25.00	2.55	-1.29
37.00	2.04	-0.92	23.00	2.62	-1.34
35.00	2.11	-0.97	22.00	2.68	-1.39
33.00	2.23	-1.05			

Table 3.3. The change in the Δn and δn values with temperature for sample s1. This sample gives three nematic phases in the temperature range studied.

T/°C	δn	Δn	T/°C	δn	Δn
45.00	1.51	0.00	26.80	1.34	1.46
43.50	1.61	0.01	26.30	1.25	1.57
42.00	1.70	0.00	25.80	1.16	1.64
40.50	1.82	0.00	25.30	1.03	1.74
39.00	1.88	0.00	24.80	0.89	1.84
37.50	1.97	0.00	24.30	0.75	1.92
36.25	2.04	0.00	23.80	0.64	2.02
35.00	2.11	0.00	23.30	0.51	2.11
34.00	2.22	0.01	22.80	0.36	2.23
33.00	2.31	0.01	22.50	0.24	2.30
32.00	2.34	0.00	22.30	0.16	2.35
31.00	2.33	0.01	22.20	0.12	2.37
30.70	2.35	0.00	22.10	0.06	2.40
30.60	2.35	0.02	22.00	0.00	2.44
30.50	2.26	0.11	21.80	0.01	2.52
30.40	2.23	0.24	21.50	0.00	2.56
30.30	2.16	0.33	20.75	0.01	2.61
30.10	2.10	0.48	20.00	0.01	2.64
29.80	2.01	0.63	19.00	0.01	2.66
29.30	1.88	0.82	18.00	0.01	2.69
28.80	1.75	0.94	17.00	0.00	2.70
28.30	1.65	1.11	16.00	0.00	2.75
27.80	1.58	1.22	15.00	0.00	2.77
27.30	1.45	1.37			

Table 3.4. The change in the σ_2 and σ_3 values with temperature for sample s1.

T/°C	$\sigma_2/10^{-5}$	$\sigma_3/10^{-7}$	T/°C	$\sigma_2/10^{-5}$	$\sigma_3/10^{-7}$
45.00	0.78	0.22	26.80	2.02	-0.07
43.50	0.88	0.26	26.30	2.05	-0.18
42.00	0.99	0.31	25.80	2.03	-0.26
40.50	1.13	0.38	25.30	2.00	-0.38
39.00	1.20	0.42	24.80	1.97	-0.49
37.50	1.33	0.48	24.30	1.94	-0.58
36.25	1.41	0.53	23.80	1.96	-0.67
35.00	1.52	0.59	23.30	1.98	-0.75
34.00	1.68	0.69	22.80	2.01	-0.84
33.00	1.81	0.77	22.50	2.01	-0.87
32.00	1.87	0.81	22.30	2.02	-0.89
31.00	1.86	0,80	22.20	2.01	-0.90
30.70	1.88	0.81	22.10	2.00	-0.89
30.60	1.91	0.83	22.00	2.03	-0.91
30.50	1.83	0.78	21.80	2.16	-1.01
30.40	1.89	0.79	21.50	2.24	-1.06
30.30	1.87	0.76	20.75	2.31	-1.11
30.10	1.92	0.72	20.00	2.37	-1.16
29.80	1.94	0.66	19.00	2.40	-1.17
29.30	1.96	0.54	18.00	2.48	-1.23
28.80	1.91	0.41	17.00	2.48	-1.23
28.30	1.97	0.29	16.00	2.57	-1.30
27.80	2.01	0.20	15.00	2.61	-1.33
27.30	2.03	0.05			

Table 3.5. The change in the Δn and δn values with temperature for sample s2. This sample gives three nematic phases in the temperature range studied.

T/°C	δn	Δn	T/°C	δn	Δn
45.00	1.43	0.00	30.70	1.18	1.30
44.00	1.50	0.00	30.20	1.01	1.44
43.00	1.54	0.00	29.70	0.86	1.59
42.00	1.61	0.00	29.20	0.67	1.75
41.00	1.70	0.00	28.70	0.49	1.88
40.00	1.75	0.00	28.50	0.30	1.99
39.00	1.82	0.00	28.40	0.21	2.07
38.00	1.88	0.00	28.30	0.13	2.13
37.00	1.91	0.00	28.20	0.00	2.24
36.00	1.95	0.00	28.00	0.00	2.32
35.00	2.00	0.00	27.50	0.00	2.36
34.25	2.03	0.00	26.75	0.00	2.42
33.90	2.05	0.00	26,00	0.00	2.48
33.80	2.06	0.00	25.00	0.00	2.53
33.70	2.06	0.00	24.00	0.00	2.57
33.60	2.05	0.00	23.00	0.00	2.62
33.50	2.06	0.06	22.00	0.00	2.67
33.40	2.03	0.14	21.00	0.00	2.72
33.30	1.97	0.31	20.00	0.00	2.75
33.20	1.96	0.38	19.00	0.00	2.78
33.00	1.83	0.53	18.00	0.00	2.80
32.70	1.67	0.67	17.00	0.00	2.81
32.20	1.55	0.84	16.00	0.00	2.83
31.70	1.42	1.02	15.00	0.00	2.84
31.20	1.31	1.16			

Table 3.6. The change in the σ_2 and σ_3 values with temperature for sample s2.

T/°C	$\sigma_2/10^{-5}$	$\sigma_3/10^{-7}$	T/°C	$\sigma_2/10^{-5}$	$\sigma_3/10^{-7}$
45.00	0.70	0.18	30.70	1.57	-0.05
44.00	0.77	0.21	30.20	1.55	-0.18
43.00	0.81	0.23	29.70	1.59	-0.31
42.00	0.88	0.26	29.20	1.60	-0.44
41.00	0.99	0.31	28.70	1.60	-0.54
40.00	1.05	0.34	28.50	1.58	-0.59
39.00	1.13	0.38	28.40	1.62	-0.63
38.00	1.21	0.42	28.30	1.64	-0.66
37.00	1.24	0.44	28.20	1.71	-0.71
36.00	1.30	0.47	28.00	1.84	-0.79
35.00	1.36	0.50	27.50	1.91	-0.83
34.25	1.41	0.53	26.75	2.01	-0.90
33.90	1.43	0.54	26.00	2.10	-0.96
33.80	1.44	0.55	25.00	2.18	-1.02
33.70	1.45	0.55	24.00	2.26	-1.07
33.60	1.45	0.55	23.00	2.35	-1.14
33.50	1.49	0.57	22.00	2.41	-1.19
33.40	1.50	0.57	21.00	2.51	-1.26
33.30	1.57	0.58	20.00	2.58	-1.31
33.20	1.61	0.58	19.00	2.65	-1.36
33.00	1.56	0.50	18.00	2.69	-1.39
32.70	1.48	0.38	17.00	2.70	-1.40
32.20	1.51	0.28	16.00	2.73	-1.43
31.70	1.54	0.17	15.00	2.74	-1.43
31.20	1.56	0.07			

Table 3.7. The change in the Δn and δn values with temperature for sample s3. This sample gives three nematic phases in the temperature range studied.

T/°C	δn	Δn	T/°C	δn	Δn
45.00	1.35	0.00	30.50	1.20	1.23
44.00	1.41	0.00	30.00	1.00	1.38
43.00	1.48	0.00	29.50	0.90	1.54
42.00	1.53	0.00	29.00	0.67	1.69
41.00	1.58	0.00	28.60	0.57	1.82
40.00	1.65	0.00	28.40	0.48	1.89
39.00	1.72	0.00	28.30	0.38	1.95
38.00	1.79	0.00	28.20	0.19	2.03
37.25	1.84	0.00	28.10	0.15	2.08
36.50	1.89	0.00	28.00	0.00	2.19
35.75	1.91	0.00	27.90	0.00	2.28
35.25	1.93	0.01	27.70	0.00	2.30
34.75	1.93	0.00	27.00	0.00	2.34
34.25	1.94	0.00	26.00	0.00	2.41
33.75	1.96	0.00	25.00	0.00	2.47
33.25	1.95	0.00	24.00	0.00	2.53
33.00	1.96	0.00	23.00	0.00	2.58
32.80	1.97	0.00	22.00	0.00	2.63
32.70	1.88	0.10	21.00	0.00	2.66
32.60	1.82	0.24	20.00	0.00	2.70
32.50	1.90	0.35	19.00	0.00	2.73
32.30	1.75	0.51	18.00	0.00	2.75
32.00	1.66	0.67	17.00	0.00	2.77
31.50	1.53	0.89	16.00	0.00	2.78
31.00	1.39	1.07	15.00	0.00	2.78

Table 3.8. The change in the σ_2 and σ_3 values with temperature for sample s3.

T/°C	$\sigma_2/10^{-5}$	$\sigma_3/10^{-7}$	T/°C	$\sigma_2/10^{-5}$	$\sigma_3/10^{-7}$
45.00	0.62	0.15	30.50	1.51	-0.02
44.00	0.68	0.18	30.00	1.46	-0.15
43.00	0.74	0.20	29.50	1.56	-0.27
42.00	0.79	0.22	29.00	1.52	-0.39
41.00	0.85	0.25	28.60	1.60	-0.49
40.00	0.93	0.28	28.40	1.61	-0.54
39.00	1.00	0.32	28.30	1.60	-0.58
38.00	1.10	0.36	28.20	1.56	-0.60
37.25	1.15	0.39	28.10	1.60	-0.63
36.50	1.21	0.42	28.00	1.65	-0.67
35.75	1.24	0.44	27.90	1.76	-0.74
35.25	1.27	0.45	27.70	1.79	-0.76
34.75	1.28	0.46	27.00	1.86	-0.80
34.25	1.28	0.46	26.00	1.98	-0.88
33.75	1.31	0.47	25.00	2.08	-0.95
33.25	1.30	0.47	24.00	2.18	-1.02
33.00	1.31	0.47	23.00	2.27	-1.08
32.80	1.33	0.49	22.00	2.34	-1.14
32.70	1.27	0.45	21.00	2.39	-1.17
32.60	1.31	0.45	20.00	2.48	-1.24
32.50	1.50	0.53	19.00	2.54	-1.28
32.30	1.43	0.43	18.00	2.58	-1.31
32.00	1.47	0.37	17.00	2.62	-1.34
31.50	1.53	0.26	16.00	2.62	-1.34
31.00	1.56	0.14	15.00	2.63	-1.35

Table 3.9. The change in the Δn and δn values with temperature for sample s4. This sample gives three nematic phases in the temperature range studied.

T/°C	δn	Δn	T/°C	δn	Δn
45.00	1.43	0.00	27.30	1.74	0.84
43.50	1.46	0.00	26.80	1.61	0.98
42.00	1.56	0.00	26.30	1.53	1.16
40.50	1.74	0.00	25.80	1.44	1.27
39.00	1.78	0.00	25.30	1.31	1.37
37.75	1.86	0.00	24.80	1.22	1.50
36.50	1.96	0.00	24.30	1.12	1.60
35.25	1.95	0.00	23.80	0.99	1.69
34.00	2.05	0.00	23.30	0.90	1.81
33.00	2.13	0.00	22.80	0.79	1.88
32.00	2,17	0.00	22.30	0.69	1.93
31.00	2.23	0.00	21.80	0.55	2.05
30.00	2.22	0.00	21.30	0.55	2.11
29.25	2.24	0.00	20.80	0.56	2.13
28.70	2.24	0.00	20.30	0.50	2.20
28.60	2.29	0.06	19.70	0.51	2.22
28.50	2.23	0.09	19.00	0.48	2.24
28.40	2.07	0.24	18.00	0.44	2.25
28.30	2.01	0.33	17.00	0.43	2.27
28.10	1.98	0.48	16.00	0.49	2.24
27.80	1.88	0.67	15.00	0.47	2.25

Table 3.10. The change in the σ_2 and σ_3 values with temperature for sample s4.

T/°C	$\sigma_2/10^{-5}$	$\sigma_3/10^{-7}$	T/°C	$\sigma_2/10^{-5}$	$\sigma_3/10^{-7}$
45.00	0.70	0.18	27.30	1.77	0.42
43.50	0.73	0.20	26.80	1.75	0.30
42.00	0.82	0.24	26.30	1.87	0.19
40.50	1.04	0.34	25.80	1.89	0.09
39.00	1.08	0.36	25.30	1.83	-0.03
37.75	1.18	0.41	24.80	1.90	-0.15
36.50	1.32	0.48	24.30	1.92	-0.25
35.25	1.30	0.47	23.80	1.88	-0.36
34.00	1.43	0.54	23.30	1.95	-0.47
33.00	1.54	0.61	22.80	1.92	-0.54
32.00	1.60	0.64	22.30	1.90	-0.59
31.00	1.69	0.69	21.80	1.92	-0.69
30.00	1.68	0.69	21.30	2.02	-0.76
29.25	1.71	0.71	20.80	2.06	-0.78
28.70	1.71	0.71	20.30	2.12	-0.84
28.60	1.84	0.79	19.70	2.16	-0.87
28.50	1.77	0.74	19.00	2.17	-0.88
28.40	1.65	0.64	18.00	2.14	-0.88
28.30	1.64	0.62	17.00	2.15	-0.90
28.10	1.74	0.62	16.00	2.17	-0.88
27.80	1.79	0.54	15.00	2.17	-0.90

Table 3.11. The change in the Δn and δn values with temperature for sample s5. This sample gives three nematic phases in the temperature range studied.

T/°C	δn	Δn	T/°C	δn	Δn
45.00	1.10	0.00	28.20	1.35	1.06
43.50	1.28	0.00	27.70	1.20	1.19
42.00	1.39	0.00	27.20	1.05	1.35
40.50	1.51	0.00	26.70	0.90	1.49
39.00	1.57	0.00	26.20	0.69	1.63
37.50	1.70	0.00	25.70	0.53	1.78
36.00	1.76	0.00	25.20	0.37	1.92
34.50	1.86	0.00	24.90	0.22	2.03
33.00	1.90	0.00	24.80	0.11	2.08
31.75	1.97	0.00	24.70	0.00	2.19
30.75	2.04	0.00	24.50	0.00	2.26
30.20	2.05	0.00	24.00	0.00	2.31
30.10	2.06	0.00	23.25	0.00	2.37
30.00	1.99	0.00	22.25	0.00	2.40
29.90	1.91	0.13	21.00	0.00	2.46
29.80	1.87	0.24	19.500	0.00	2.52
29.70	1.80	0.37	18.000	0.00	2.53
29.50	1.72	0.53	16.500	0.00	2.58
29.20	1.63	0.69	15.000	0.00	2.63
28.70	1.45	0.89			

Table 3.12. The change in the σ_2 and σ_3 values with temperature for sample s5.

T/°C	$\sigma_2/10^{-5}$	$\sigma_3/10^{-7}$	T/°C	$\sigma_2/10^{-5}$	$\sigma_3/10^{-7}$
45.00	0.41	0.08	28.20	1.49	0.12
43.50	0.56	0.13	27.70	1.45	0.01
42.00	0.66	0.17	27.20	1.48	-0.12
40.50	0.77	0.21	26.70	1.49	-0.24
39.00	0.83	0.24	26.20	1.46	-0.35
37.50	0.98	0.31	25.70	1.50	-0.46
36.00	1.06	0.35	25.20	1.55	-0.55
34.50	1.180	0.41	24.90	1.57	-0.60
33.00	1.23	0.43	24.80	1.56	-0.61
31.75	1.32	0.48	24.70	1.63	-0.66
30.75	1.41	0.53	24.50	1.76	-0.74
30.20	1.42	0.54	24.00	1.83	-0.78
30.10	1.44	0.55	23.25	1.92	-0.84
30.00	1.37	0.51	22.25	1.98	-0.88
29.90	1.34	0.48	21.00	2.07	-0.94
29.80	1.36	0.48	19.500	2.16	-1.00
29.70	1.39	0.46	18.000	2.19	-1.02
29.50	1.42	0.41	16.500	2.29	-1.09
29.20	1.46	0.36	15.000	2.36	-1.15
28.70	1.49	0.24			

Table 3.13. The change in the Δn and δn values with temperature for sample s6. This sample only N_D phase in the temperature range studied.

T/°C	δn	Δn	T/°C	δn	Δn
45.00	1.55	0.00	28.50	2.50	0.00
43.50	1.66	0.00	27.00	2.57	0.00
42.00	1.80	0.00	25.50	2.60	0.00
40.50	1.90	0.00	24.00	2.68	0.00
39.00	2.02	0.00	22.50	2.69	0.00
37.50	2.09	0.00	21.00	2.77	0.00
36.00	2.19	0.00	19.50	2.81	0.00
34.50	2.25	0.00	18.00	2.85	0.00
33.00	2.31	0.00	16.50	2.92	0.00
31.50	2.41	0.00	15.00	2.95	0.00
30.00	2.46	0.00			

Table 3.14. The change in the σ_2 and σ_3 values with temperature for sample s6.

T/°C	$\sigma_2/10^{-5}$	$\sigma_3/10^{-7}$	T/°C	$\sigma_2/10^{-5}$	$\sigma_3/10^{-7}$
45.00	0.82	2.14	28.50	0.24	0.99
43.50	0.94	2.26	27.00	0.29	1.08
42.00	1.11	2.31	25.50	0.37	1.11
40.50	1.24	2.46	24.00	0.44	1.22
39.00	1.40	2.47	22.50	0.52	1.23
37.50	1.49	2.61	21.00	0.58	1.33
36.00	1.63	2.69	19.50	0.66	1.39
34.50	1.72	2.75	18.00	0.71	1.44
33.00	1.81	2.90	16.50	0.77	1.56
31.50	1.99	2.95	15.00	0.89	1.60
30.00	2.06	2.14			

Table 3.15. The change in the Δn and δn values with temperature for sample s7. This sample gives three nematic phases in the temperature range studied.

T/°C	δn	Δn	T/°C	δn	Δn
45.00	1.47	0.00	31.00	0.79	1.67
43.50	1.53	0.00	30.50	0.54	1.86
42.00	1.60	0.00	30.30	0.29	1.98
40.75	1.65	0.00	30.20	0.17	2.06
39.50	1.72	0.00	30.10	0.10	2.11
38.25	1.83	0.00	30.00	0.00	2.21
37.00	1.93	0.00	29.80	0.00	2.26
36.00	1.94	0.00	29.30	0.00	2.29
35.30	1.93	0.00	28.50	0.00	2.35
35.00	1.99	0.00	27.75	0.00	2.41
34.80	1.97	0.00	27.00	0.00	2.46
34.60	1.97	0.00	26.00	0.00	2.52
34.50	1.93	0.07	24.75	0.00	2.58
34.40	1.91	0.20	23.50	0.00	2.64
34.20	1.83	0.40	22.25	0.00	2.71
33.90	1.76	0.60	21.00	0.00	2.76
33.50	1.60	0.81	19.50	0.00	2.81
33.00	1.42	0.99	18.00	0.00	2.85
32.50	1.37	1.16	16.50	0.00	2.87
32.00	1.21	1.32	15.00	0.00	2.88
31.50	1.04	1.49			

Table 3.16. The change in the σ_2 and σ_3 values with temperature for sample s7.

T/°C	$\sigma_2/10^{-5}$	$\sigma_3/10^{-7}$	T/°C	δn	Δn
45.00	0.73	0.20	31.00	1.61	-0.37
43.50	0.79	0.22	30.50	1.62	-0.52
42.00	0.87	0.26	30.30	1.56	-0.58
40.75	0.92	0.28	30.20	1.57	-0.61
39.50	1.00	0.32	30.10	1.60	-0.63
38.25	1.15	0.39	30.00	1.67	-0.68
37.00	1.27	0.45	29.80	1.73	-0.72
36.00	1.29	0.46	29.30	1.78	-0.75
35.30	1.28	0.46	28.50	1.88	-0.81
35.00	1.36	0.50	27.75	1.98	-0.88
34.80	1.31	0.48	27.00	2.08	-0.95
34.60	1.33	0.48	26.00	2.18	-1.02
34.50	1.32	0.48	24.75	2.26	-1.08
34.40	1.39	0.50	23.50	2.37	-1.16
34.20	1.45	0.48	22.25	2.51	-1.26
33.90	1.53	0.44	21.00	2.61	-1.33
33.50	1.55	0.32	19.50	2.69	-1.40
33.00	1.50	0.17	18.00	2.76	-1.45
32.50	1.64	0.10	16.50	2.82	-1.50
32.00	1.64	-0.05	15.00	2.84	-1.51
31.50	1.65	-0.21			

Table 3.17. The change in the Δn and δn values with temperature for sample s8. This sample gives three nematic phases in the temperature range studied.

T/°C	δn	Δn	T/°C	δn	Δn
45.00	1.28	0.00	35.60	0.63	1.55
43.50	1.40	0.0	35.30	0.56	1.67
42.00	1.53	0.00	35.00	0.38	1.81
40.75	1.59	0.00	34.70	0.22	1.98
39.75	1.64	0.00	34.60	0.02	2.15
39.00	1.66	0.00	34.40	0.00	2.19
38.70	1.70	0.00	34.00	0.00	2.27
38.60	1.68	0.00	33.00	0.00	2.34
38.50	1.75	0.00	32.00	0.00	2.46
38.40	1.72	0.06	30.50	0.00	2.56
38.30	1.69	0.10	29.00	0.00	2.64
38.00	1.47	0.36	27.00	0.00	2.77
37.70	1.29	0.59	25.00	0.00	2.89
37.40	1.19	0.71	23.00	0.00	2.97
37.00	1.07	0.89	21.00	0.00	3.07
36.60	0.94	1.10	19.00	0.00	3.13
36.20	0.82	1.30	17.00	0.00	3.17
35.90	0.76	1.44	15.00	0.00	3.21

Table 3.18. The change in the σ_2 and σ_3 values with temperature for sample s8.

T/°C	$\sigma_2/10^{-5}$	$\sigma_3/10^{-7}$	T/°C	$\sigma_2/10^{-5}$	$\sigma_3/10^{-7}$
45.00	0.56	0.13	35.60	1.29	-0.31
43.50	0.66	0.17	35.30	1.38	-0.38
42.00	0.80	0.22	35.00	1.40	-0.46
40.75	0.86	0.25	34.70	1.51	-0.56
39.75	0.91	0.27	34.60	1.60	-0.64
39.00	0.94	0.29	34.40	1.63	-0.66
38.70	0.98	0.31	34.00	1.750	-0.73
38.60	0.96	0.30	33.00	1.87	-0.81
38.50	1.05	0.34	32.00	2.05	-0.93
38.40	1.04	0.33	30.50	2.24	-1.06
38.30	1.04	0.33	29.00	2.39	-1.17
38.000	0.96	0.25	27.00	2.63	-1.35
37.70	0.94	0.17	25.00	2.84	-1.52
37.40	0.95	0.12	23.00	3.02	-1.66
37.00	0.99	0.05	21.00	3.22	-1.83
36.60	1.07	-0.05	19.00	3.33	-1.92
36.20	1.17	-0.15	17.00	3.43	-2.01
35.90	1.27	-0.23	15.00	3.51	-2.08

Table 3.19. The change in the Δn and δn values with temperature for sample s9. This sample only N_D phase in the temperature range studied.

T/°C	δn	Δn	T/°C	δn	Δn
45.00	1.46	0.00	29.00	2.05	0.00
43.00	1.53	0.00	27.00	2.10	0.00
41.00	1.60	0.00	25.00	2.15	0.00
39.00	1.68	0.00	23.00	2.17	0.00
37.00	1.75	0.00	21.00	2.24	0.00
35.00	1.87	0.00	19.00	2.26	0.00
33.00	1.96	0.00	17.00	2.33	0.00
31.00	1.99	0.00	15.00	2.36	0.00

Table 3.20. The change in the σ_2 and σ_3 values with temperature for sample s9.

T/°C	$\sigma_2/10^{-5}$	$\sigma_3/10^{-7}$	T/°C	$\sigma_2/10^{-5}$	$\sigma_3/10^{-7}$
45.00	0.73	0.20	29.00	1.44	0.55
43.00	0.79	0.22	27.00	1.51	0.59
41.00	0.88	0.26	25.00	1.58	0.63
39.00	0.96	0.30	23.00	1.61	0.65
37.00	1.04	0.34	21.00	1.71	0.71
35.00	1.20	0.41	19.00	1.74	0.73
33.00	1.31	0.48	17.00	1.84	0.79
31.00	1.35	0.49	15.00	1.90	0.83

Table 3.21. The change in the Δn and δn values with temperature for sample s10. This sample only N_D phase in the temperature range studied.

T/°C	δn	Δn	T/°C	δn	Δn
45.00	1.79	0.00	29.00	2.45	0.00
43.00	1.92	0.00	27.00	2.48	0.00
41.00	2.04	0.00	25.00	2.51	0.00
39.00	2.14	0.00	23.00	2.58	0.00
37.00	2.22	0.00	21.00	2.63	0.00
35.00	2.26	0.00	19.00	2.70	0.00
33.00	2.31	0.00	17.00	2.73	0.00
31.00	2.38	0.00	15.00	2.77	0.00

Table 3.22. The change in the σ_2 and σ_3 values with temperature for sample s10.

T/°C	$\sigma_2/10^{-5}$	$\sigma_3/10^{-7}$	T/°C	$\sigma_2/10^{-5}$	$\sigma_3/10^{-7}$
45.00	1.10	0.36	29.00	2.03	0.92
43.00	1.25	0.44	27.00	2.10	0.96
41.00	1.42	0.54	25.00	2.15	1.00
39.00	1.56	0.62	23.00	2.26	1.07
37.00	1.69	0.70	21.00	2.35	1.14
35.00	1.75	0.73	19.00	2.47	1.23
33.00	1.82	0.78	17.00	2.54	1.28
31.00	1.92	0.84	15.00	2.59	1.32

4. DISCUSSION

4.1 Interpretation of POM and Laser Conoscopy Results

The lyotropic samples s0-s10 were well-characterized by polarizing optical microscopy (POM) and it was shown that all samples exhibited “schlieren textures”, which are very characteristic of the nematic phases (Figure 3.1-3.11). The unaligned discotic nematic textures were aligned in the presence of a magnetic field to give homeotropic texture, i.e., the textures were turned from colored texture to completely homogeneous dark textures because the optical axis of the nematic phase is parallel to that of the incident polarized light and perpendicular to the direction of the magnetic field. When the temperature was decreased to obtain the biaxial nematic phase starting from the uniaxial discotic one, the uniaxial character of the latter one started to disappear due to the presence of two optical axes in the case of the biaxial nematic phase. A further decrease in the temperature caused the appearance of the completely “planarly aligned” uniaxial calamitic nematic phase where the optical axis is now perpendicular to the propagation direction of the polarized light and parallel to the magnetic field direction.

The data obtained from the laser conoscopy and the small-angle X-ray scattering measurements also supported the formation of different nematic phases as a function of temperature in the studied temperature range (15-45°C). In other words, the POM, laser conoscopy and SAXS measurements are within the experimental error limit, in good agreement with each other.

In this thesis, we concentrated on the investigation of the Hofmeister series ions of strong electrolytes existing in the intermicellar region. To do so, we chose some Hofmeister series anions of potassium salts (KF, KCl, KBr, KI, and KSCN). We also studied some Hofmeister series cations of bromines (NaBr, KBr, RbBr, and CsBr), which are located at the micelle surfaces by interacting with the surfactant head groups, for a better understanding of the role of the ions present in the intermicellar region. Furthermore, the effect of the presence of NaF and NaCl in the mixtures was investigated for comparison.

The uniaxial-to-biaxial nematic phase transitions can be precisely determined from the temperature dependence of the birefringences of the nematic phases via laser conoscopy. The results of the birefringences measurements (Table 3.1-3.22) are graphically shown in Figures 4.1-4.11, and summarized in Table 4.1.

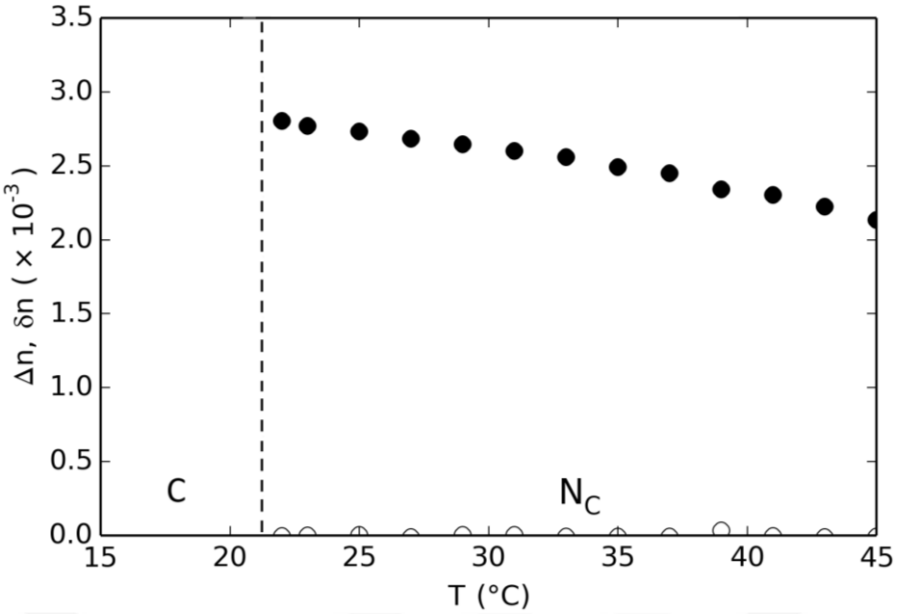

Figure 4.1. Birefringences of the nematic phase as a function of temperature for sample s0 without doping electrolyte.

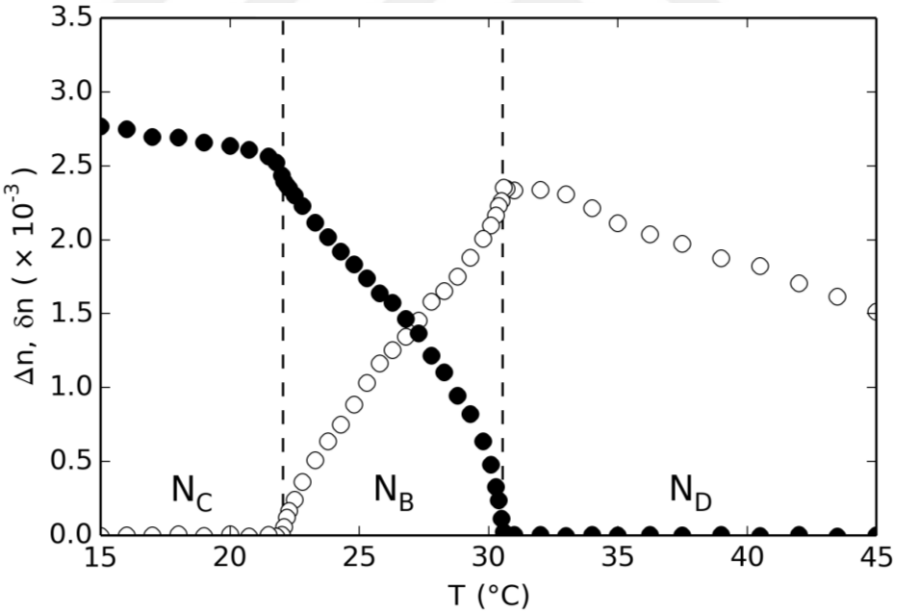

Figure 4.2. Birefringences of the nematic phases as a function of temperature for sample s1 with doping electrolyte, KF.

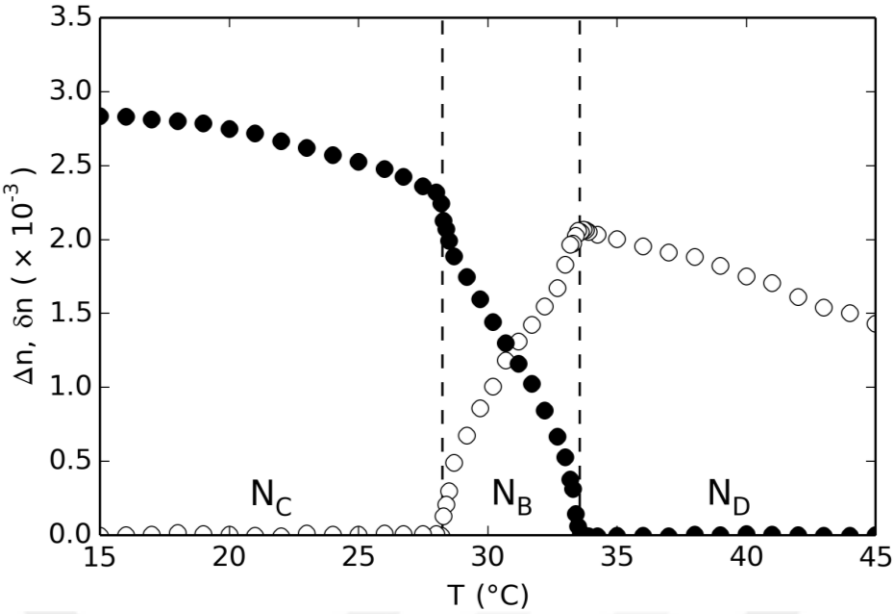

Figure 4.3. Birefringences of the nematic phases as a function of temperature for sample s2 with doping electrolyte, KCl.

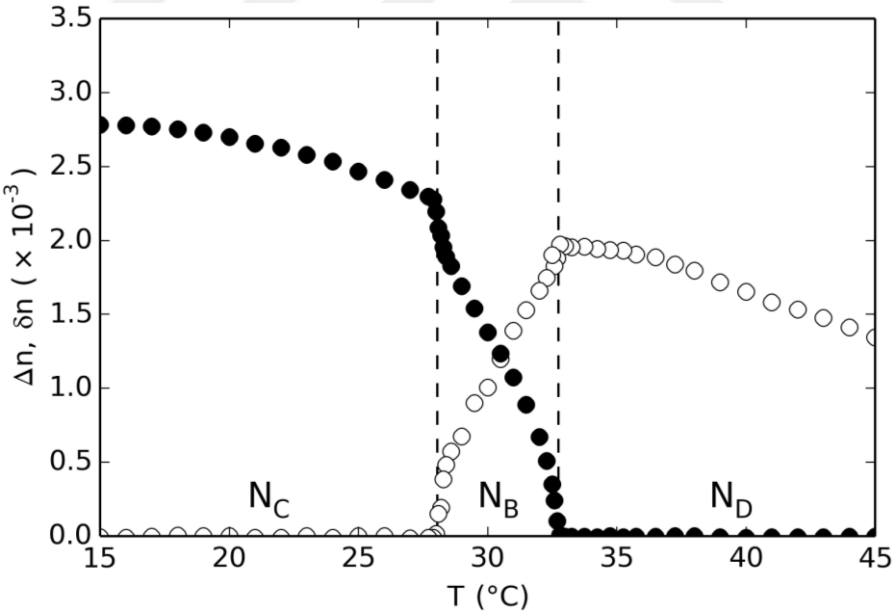

Figure 4.4. Birefringences of the nematic phases as a function of temperature for sample s3 with doping electrolyte, KBr.

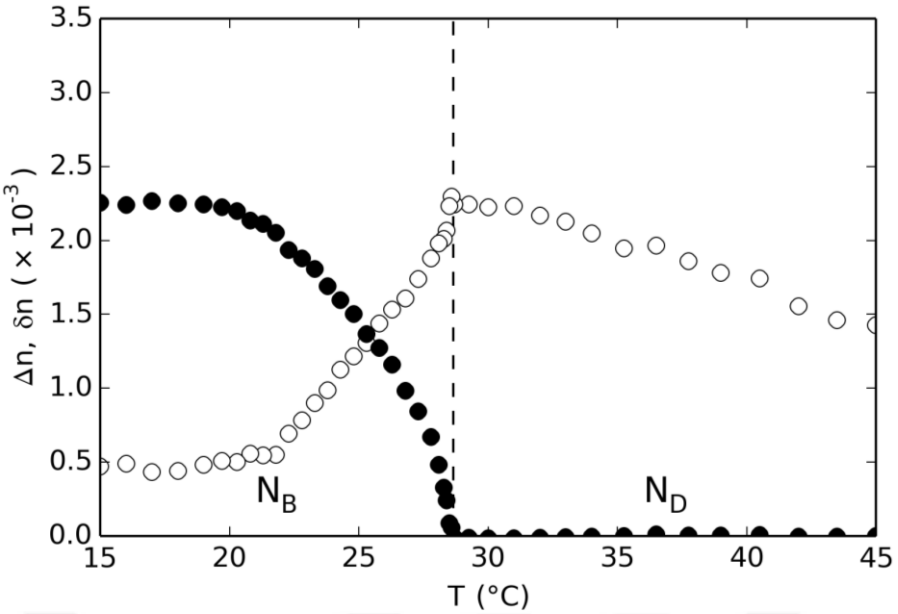

Figure 4.5. Birefringences of the nematic phases as a function of temperature for sample s4 with doping electrolyte, KI.

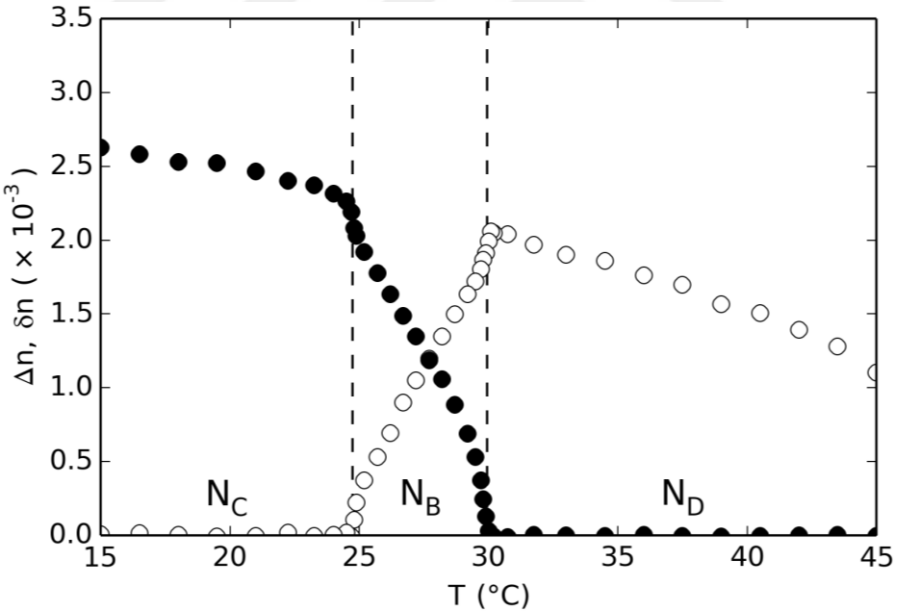

Figure 4.6. Birefringences of the nematic phases as a function of temperature for sample s5 with doping electrolyte, KSCN.

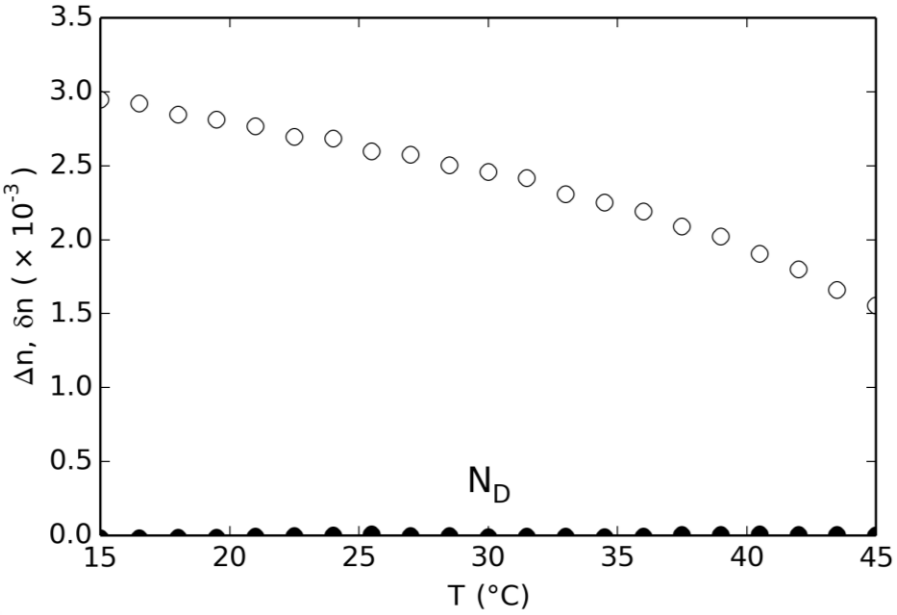

Figure 4.7. Birefringences of the nematic phase as a function of temperature for sample s6 with doping electrolyte, NaBr.

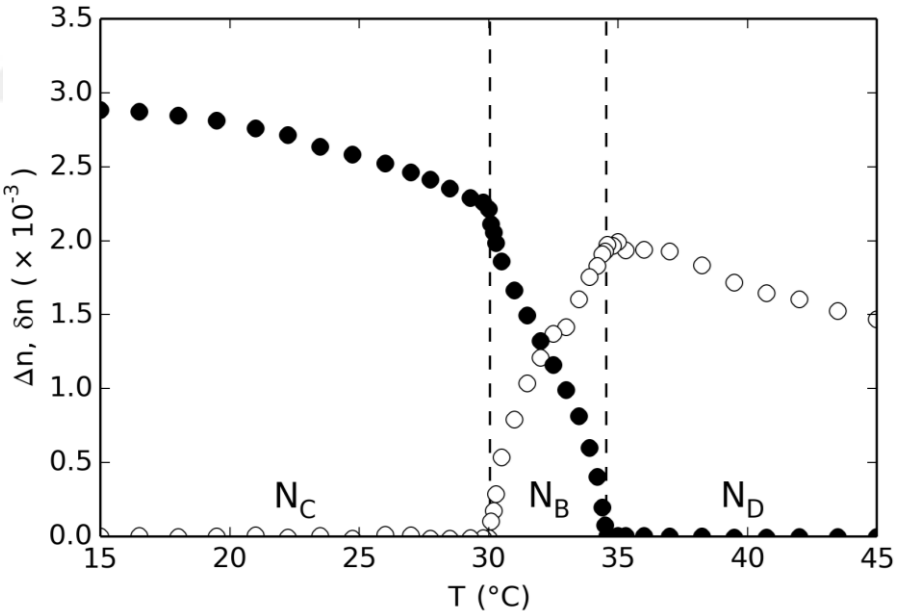

Figure 4.8. Birefringences of the nematic phases as a function of temperature for sample s7 with doping electrolyte, RbBr.

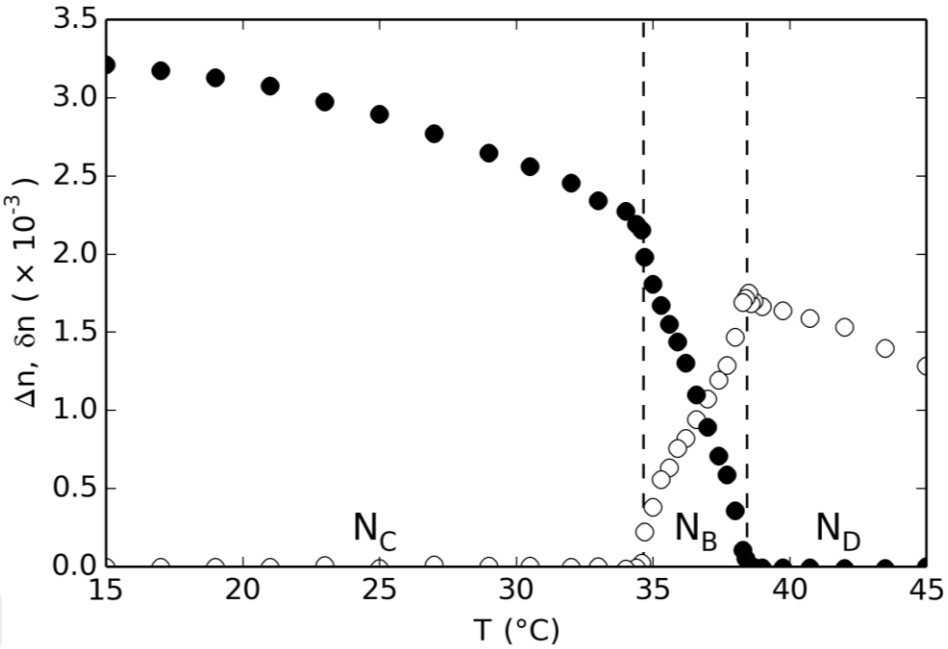

Figure 4.9. Birefringences of the nematic phases as a function of temperature for sample s8 with doping electrolyte, CsBr.

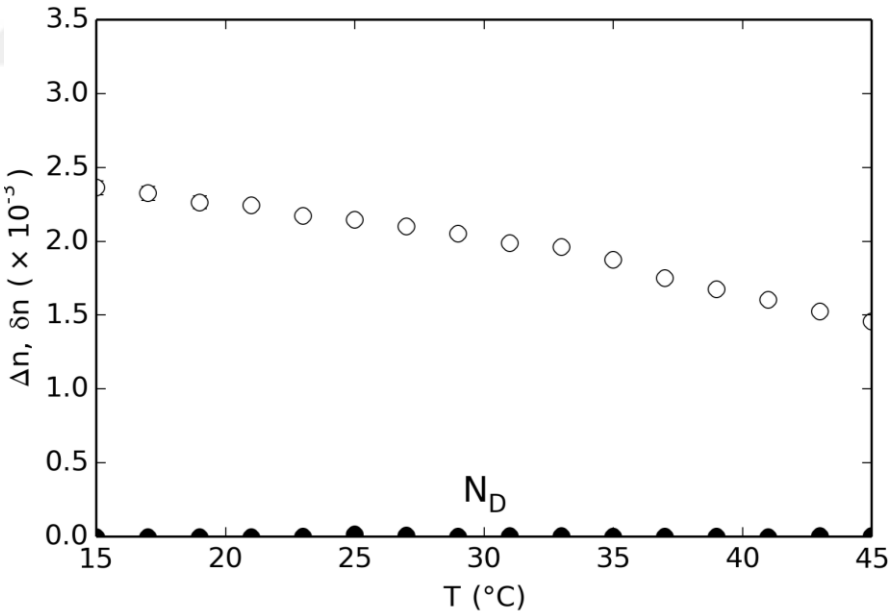

Figure 4.10. Birefringences of the nematic phase as a function of temperature for sample s9 with doping electrolyte, NaF.

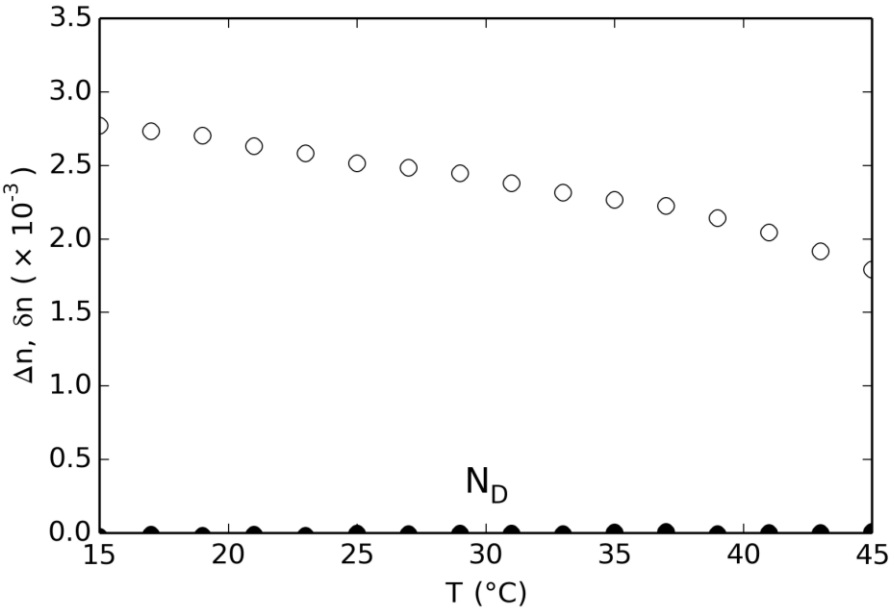

Figure 4.11. Birefringences of the nematic phase as a function of temperature for sample s10 with doping electrolyte, NaCl.

Table 4.1. Nematic phase types, uniaxial-to-biaxial nematic phase transition temperatures*, and temperature range of biaxial nematic phase domain, $\Delta T(N_B)$, in partial phase diagrams for KDD/Electrolyte/DeOH/water mixtures.

Mixture	Electrolyte	Nematic phase type	$N_D \rightarrow N_B$	$N_B \rightarrow N_C$	$\Delta T(N_B)/°C$
s0	---	N_C	---	---	---
s1	KF	N_C, N_B, N_D	30.65	22.05	8.60
s2	KCl	N_C, N_B, N_D	33.65	28.20	5.45
s3	KBr	N_C, N_B, N_D	32.75	28.00	4.75
s4	KI	N_B, N_D	28.65	---	≥13.65
s5	KSCN	N_C, N_B, N_D	30.05	24.75	5.30
s6	NaBr	N_D	---	---	---
s7	RbBr	N_C, N_B, N_D	34.55	30.05	4.50
s8	CsBr	N_C, N_B, N_D	38.45	34.55	3.90
s9	NaF	N_D	---	---	---
s10	NaCl	N_D	---	---	---

**Differences in nematic-nematic phase transition temperatures (if any) for the mixtures studied with the three different techniques (polarizing optical microscopy, laser conoscopy, and SAXS) are likely due to differences in the temperature control units of the devices. However, no differences in the phase topologies were identified.*

The interactions between ionic species at micelle surfaces play an important role in preparing lyotropic mixtures presenting different lyotropic nematic phases. Experimental results indicated that if those interactions are strong (weak) enough, it is highly possible to obtain a lyotropic N_D (N_C) phase (Akpinar, Reis, & Figueiredo Neto, 2015), (Akpinar et al., 2016b), (Akpinar et al., 2020). If there exists a moderate level of those interactions, the formation of the N_B phase is favored. The aforementioned interactions can be mainly modified in two ways: (i) the addition of electrolytes to the lyotropic mixture and (ii) considering the kosmotropic/chaotropic character of ionic surfactant heads/counterions/ions of electrolytes added. For the case (i), the existence of electrolyte ions in the lyotropic mixture causes the increase in the concentration of ions bound to the surfactant head groups and leads to the screening of the repulsions between similarly charged surfactant head groups at the micelle surfaces more effectively. Then, highly possibly N_B and/or N_D phases can be obtained. It is well-known from the literature that if two ionic species have similar (opposite) kosmotrope or chaotrope properties, they form tightly (loosley) bound ion pairs (Moreira & Firoozabadi, 2010), (Conway, 1981), (Marcus, 1985). So, in the case of (ii), by controlling the degree of kosmotropic-kosmotropic, kosmotropic-chaotropic, and chaotropic-chaotropic interactions between surfactant head groups and ions (counterions or electrolyte ions), different lyotropic nematic phases can be obtained.

In the frame of this thesis, we examined the lyotropic nematic phase properties of the samples at constant total mixture compositions and electrolyte concentrations by modifying the interactions in terms of the kosmotropic/chaotropic nature of ionic species. In this way, keeping the concentrations of ions of electrolytes in the mixtures constant, we had a chance to discuss the interactions between ionic species, located in the intermicellar region and at the micelle surfaces. Considering the Hofmeister series of ions, only F^- anion is identified as kosmotropic. Cl^-, Br^-, I^-, and SCN^- are chaotropic anions and the order of their chaotropicity is $SCN^- > I^- > Br^- > Cl^-$. In the same way, while Na^+ is classified as kosmotropic cations, K^+, Rb^+, and Cs^+ exhibit chaotropic character with their chaotropic order $Cs^+ > Rb^+ > K^+$. Furthermore, the head group KDD surfactant (carboxylate, $-COO^-$) is also identified as kosmotrope (Vlachy et al., 2009).

The mixture of KDD/DeOH/H_2O has no electrolyte (sample, s0) and it gives only the N_C phase, Figure 4.1. When the selected electrolytes were added to this sample, only N_D or N_D and N_B or three nematic phases was/were obtained, Figure 4.2-4.11, due to the increase in the concentrations of counterions bound to the surfactant head groups at the micelle surfaces and change in the strength of the interactions between ionic species. It means that, as expected, the cations coming from the added electrolytes are bound to micelle surfaces by diffusing to electric double layer to form N_D and/or N_B phases, and decrease the micelle surface curvature if compared with the N_C phase.

Our discussions on the experimental results may be divided into two parts. In the first part, we will discuss the presence of Hofmeister series cations (Na^+, K^+, Rb^+, and Cs^+) of electrolytes with the same anion (Br^-). In this way, it is possible to investigate the interactions between kosmotropic surfactant head groups and kosmotropic and also chaotropic electrolyte ions at the micelle surfaces: kosmotrope-kosmotrope and kosmotrope-chaotrope interactions, respectively. In the second part, we will examine the effect of the ions located mainly in the intermicellar region or partly in the Gouy-Chapman layer, i.e., the ions not bound to the micelle surfaces in the Stern layer. Finally, we will compare the results of both parts to understand, especially, the effect of the ions present in the intermicellar region of the micellar system on the formation of different lyotropic nematic phases.

Samples s6, s3, s7, and s8 include NaBr, KBr, RbBr and CsBr, respectively. Na^+ ion is strongly kosmotrope and may diffuse to the electric double layer. Then, it interacts strongly with kosmotrope KDD head groups and forms tightly bound ion pairs at micelle surfaces, which leads to the formation of only the N_D phase in the studied temperature range (15-45°C), Figure 4.7. The other three electrolytes form three nematic phases (Figures 4.4, 4.8, and 4.9, respectively). They presented different (a) nematic-nematic phase transition temperatures, (b) temperature range of uniaxial phase regions, and (c) biaxial phase region, depending on the degree of kosmotrope (head groups) – chaotrope (cations) interactions. From K^+ to Cs^+, both N_D-N_B (from 32.75 to 38.45°C) and N_B-N_C (28.00-34.55°C) phase transitions shift to higher temperatures. While the N_C phase domain increases, the N_D and N_B phase domains decrease in the studied temperature range. The results indicated that kosmotrope-chaotrope interactions between surfactant head groups and the electrolyte ions at the micelle surfaces in the electric double layer get weaker as the

chaotropic character of the cations increases from K^+ to Cs^+ due to the formation of loosely bound ion pairs. This is in good agreement with the order of those ions in the Hofmeister series.

Similar results were obtained from the comparison of KF, KCl, and KBr with NaF, NaCl, and NaBr, respectively. While potassium salts of F^-, $Cl^-$and Br^- ions gave three nematic phases as a function of temperature, their sodium salts gave only the N_D phase within the same temperature range. This is another evidence of strong (weak) kosmotrope-kosmotrope (kosmotrope-chaotrope) interactions between surfactant head groups and Na^+ (K^+) ions at the micelles surfaces in the Stern layer by modifying micellar surface curvature, which yields to change in the orientational fluctuations responsible for the formation of different nematic phases, based on the IBM model of the nematic phases.

The results of lyotropic mixtures including KF, KCl, KBr, KI, and KSCN were also given in the Table 4.1. The anions of these electrolytes can be present in the intermicellar region and/or Gouy-Chapman layer, but, as expected, not in the Stern layer. Among them, only F^- is kosmotropic, and others are chaotropic. From the biaxial region observed in the birefringences-temperature partial phase diagram point of view, F^- has a significantly greater effect than chaotropic anions. Furthermore, its effect on the N_B-N_C transition is more dominant than that on the N_D-N_B transition if compared with the chaotropic anions. It means that F^- cannot effectively trigger the orientational fluctuations responsible for the formation of the N_C phase in the vicinity of the N_B-N_C transition with respect to the chaotropic ions. This may be attributed to the interactions between the free K^+ and F^- ions in the electric double layer. Because both ions have opposite characteristics they cannot form tightly bound ions pair and K^+, coming from KF, may diffuse to the Stern layer and may interact with the surfactant head groups. The last situation also explains why KF shifts both transition temperatures to lower temperatures more than KCl. In the Hofmeister series, the Cl^- is less kosmotropic (or more chaotropic) than F^-, and the former produces a more tightly bound ion pair with chaotropic K^+, thus K^+ may not diffuse to the Stern layer to interact with the surfactant head groups.

If we compare the effect of the chaotropic anions, starting from Cl^- to SCN^-, both phase transitions shift to the lower temperatures as the chaotropicity of anions increases by following the Hofmeister series, except that I^- has a higher effect than SCN^-. We observed a similar situation for tetradecyltrimethylammonium bromide

(TTMABr)/NaI/DeOH/water and TTMABr/NaSCN/DeOH/water isotropic dilute solutions and lyotropic mixtures (Akpinar et al., 2016b). In that case, TTMABr has a chaotropic cationic head group, and I^- and SCN^- ions are bound to the head groups at the micelle surfaces in the Stern layer. The results in Ref (Akpinar et al., 2016b). showed that, although the viscosity-B coefficient is an important parameter to identify the ions as kosmotrope/chaotrope, the relative effects of the Hofmeister ions are related to the surface charge density of the ionic species and the hydrodynamic radius. It means that the surface charge density of the ionic species contributes to the specific interactions between the head groups and the counterions/ions. In the present case, both anions (I^- and SCN^-) cannot be bound to the micelle surfaces by locating in the Stern layer, instead in the Gouy-Chapman layer and/or in the intermicellar region. So, the present study is different than the one in Ref. (Akpinar et al., 2016b). Consequently, the effect of the chaotropic anions present in the intermicellar region or Gouy-Chapman layer on the uniaxial-to-biaxial phase transitions, in general, follows the Hofmeister series, similar to the effect of the ions present at the micelle surfaces (in the Stern layer), and the order is F^- (0.720) > Cl^- (0.389) > Br^- (0.331) > SCN^- (0.281) > I^- (0.263) by considering the surface charge density of those ions, where the numbers in the parentheses are the surface charge densities in the unit of C/m^2 (Leontidis, 2002).

As mentioned before, the laser conoscopy allows us to evalaute the symmetric nontrivial invariants of the nematic order parameter (Galerne & Marcerou, 1983), (Neto & Salinas, 2005) σ_2 and σ_3, which are functions of the birefringences. Assuming the IBM model, the more the anisometric micelles mean the bigger the maximum optical birefringences in the nematic phases and, consequently, the bigger the invariants σ_2 and σ_3 (Neto & Salinas, 2005). The temperature dependences of σ_2 and σ_3, and also σ_2 dependence of σ_3 are graphically given below, where the latter shows the experimental evidence of the biaxial phase being an intermediate phase between other two uniaxial phases in the partial phase diagrams. All results are in good agreement with the literature (Neto & Salinas, 2005), (Akpinar et al., 2016b)

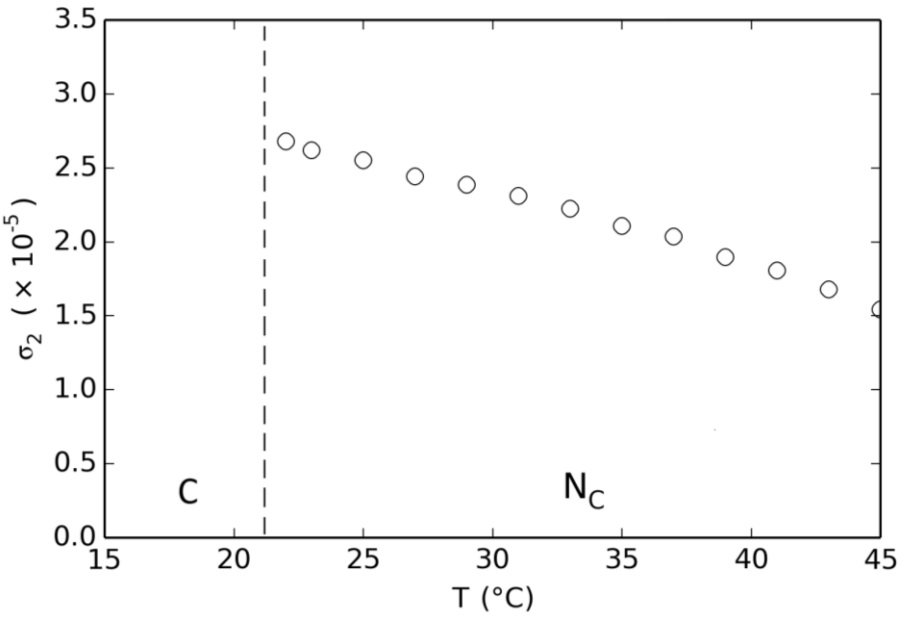

Figure 4.12. The change in the σ_2 values with temperature for sample s0. C: non-nematic or crystalline-like phase.

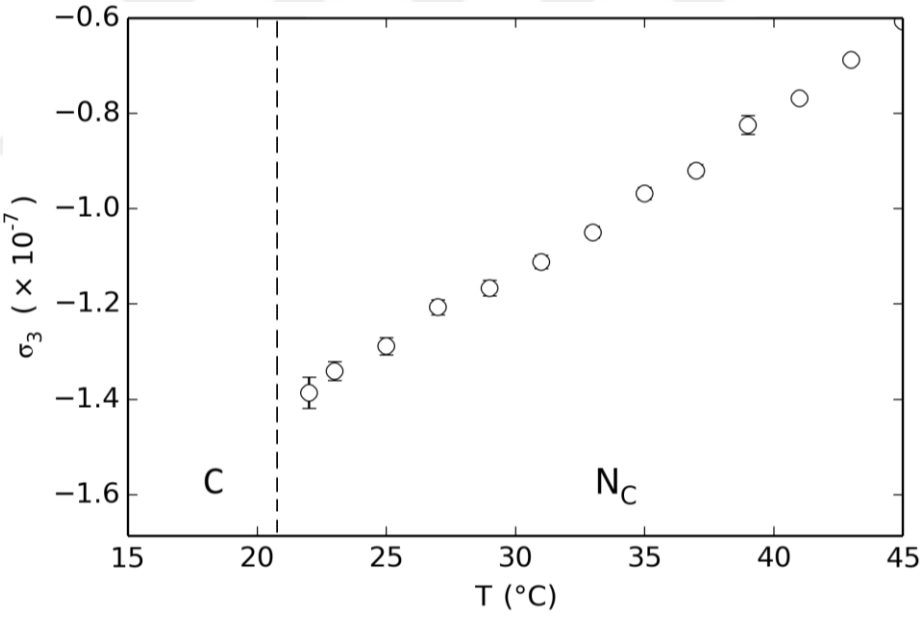

Figure 4.13. The change in the σ_3 values with temperature for sample s0.

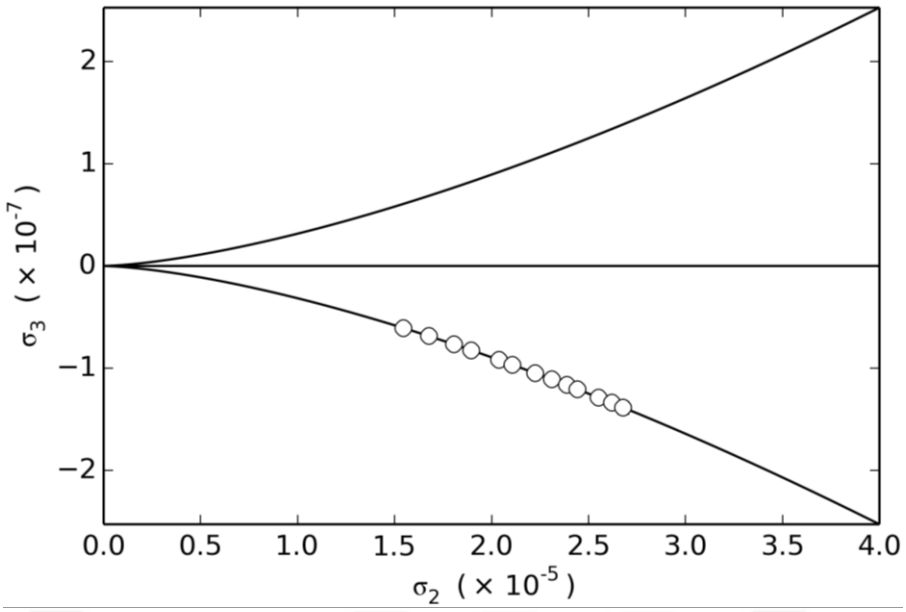

Figure 4.14. Interdependence of σ_3 and σ_2 for sample s0.

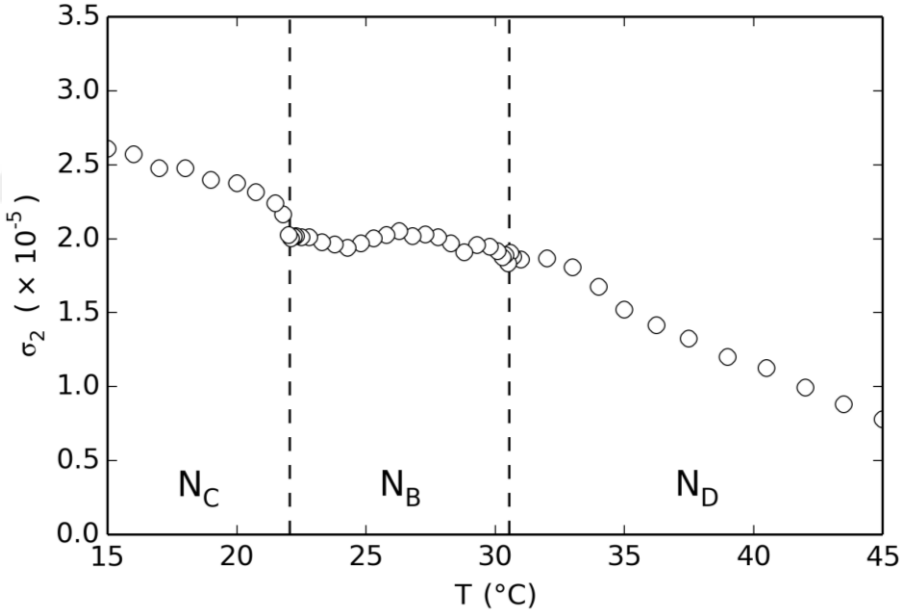

Figure 4.15. The change in the σ_2 values with temperature for sample s1.

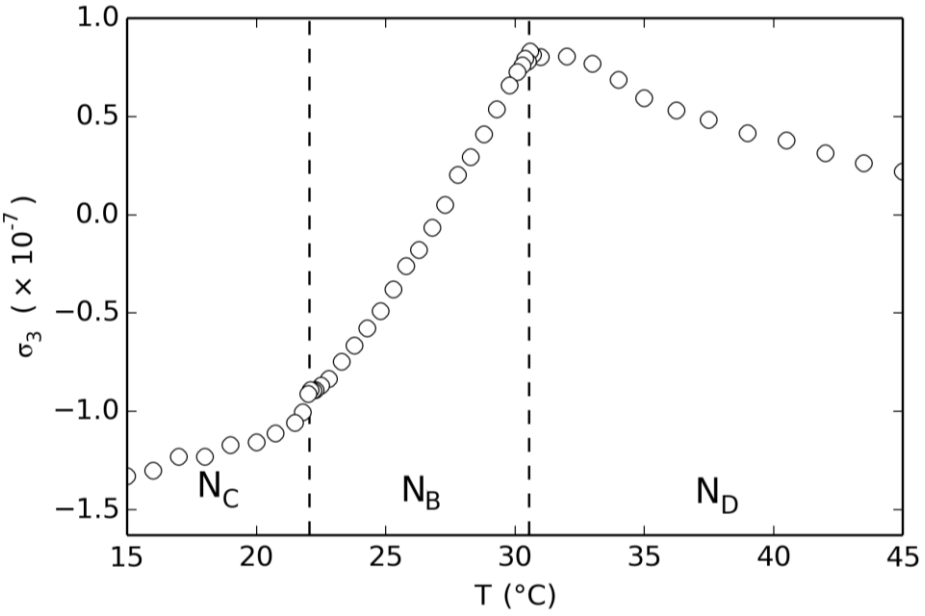

Figure 4.16. The change in the σ_3 values with temperature for sample s1.

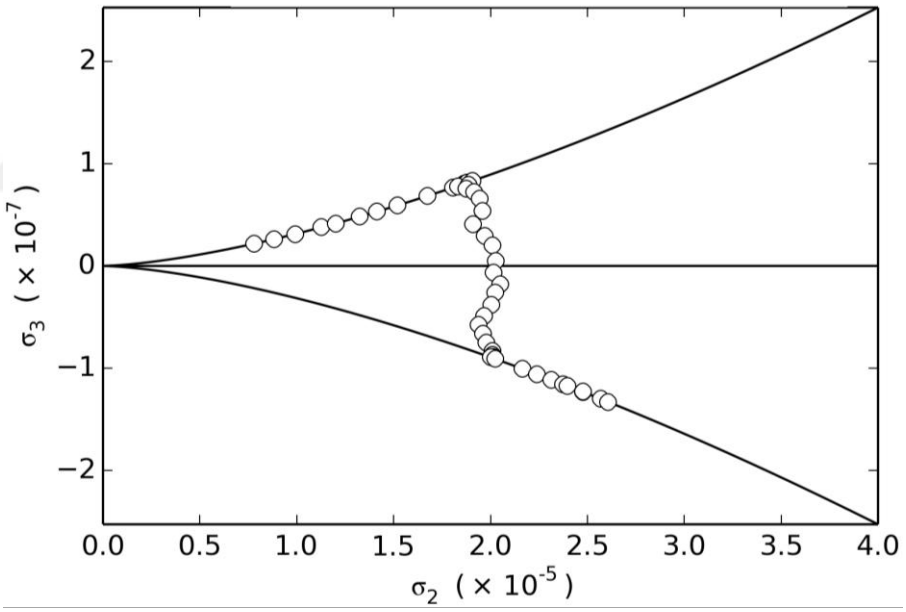

Figure 4.17. Interdependence of σ_3 and σ_2 for sample s1.

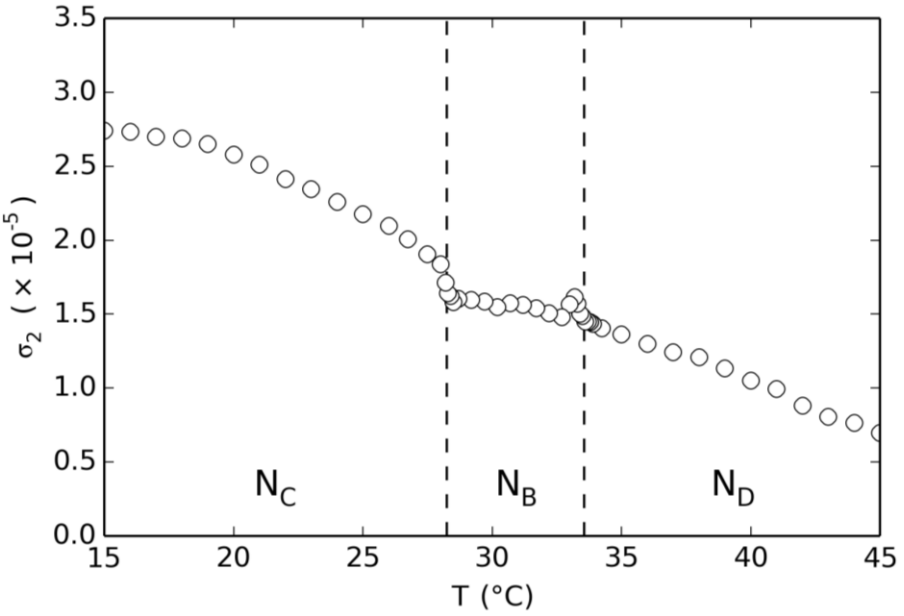

Figure 4.18. The change in the σ_2 values with temperature for sample s2.

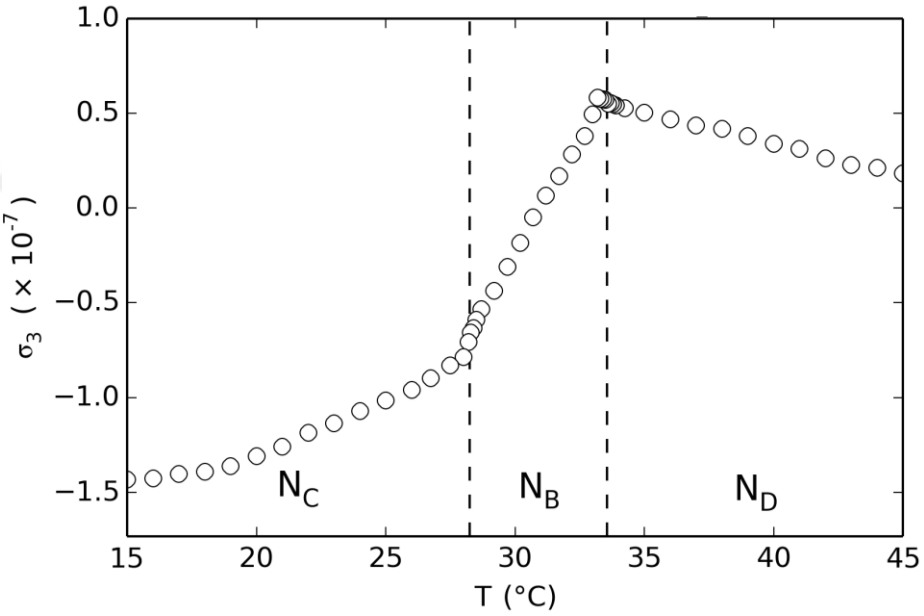

Figure 4.19. The change in the σ_3 values with temperature for sample s2.

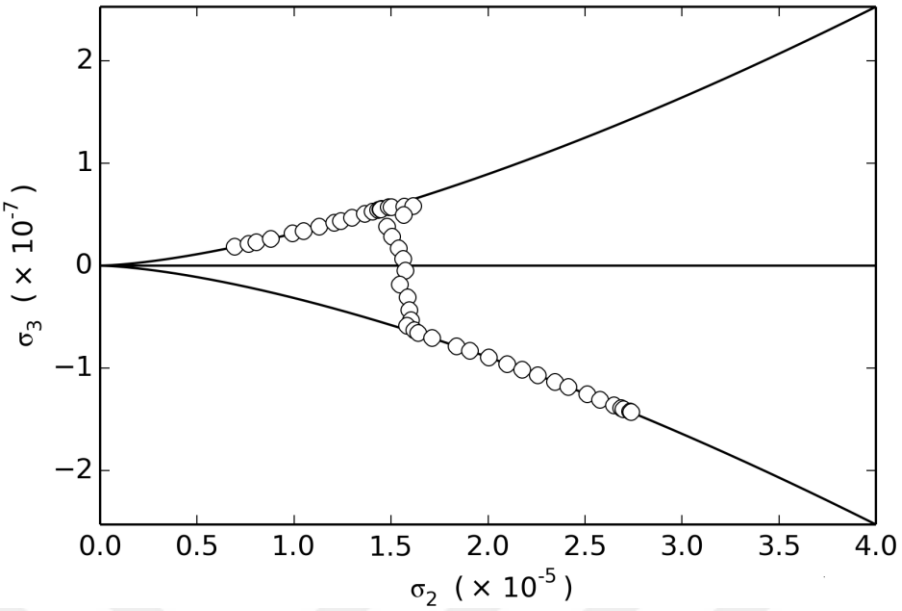

Figure 4.20. Interdependence of σ_3 and σ_2 for sample s2.

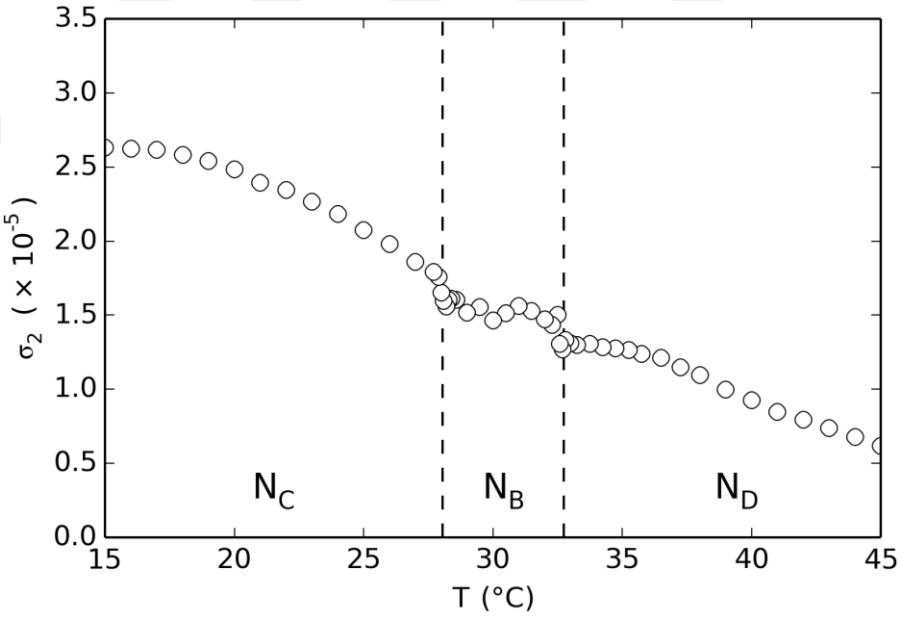

Figure 4.21. The change in the σ_2 values with temperature for sample s3.

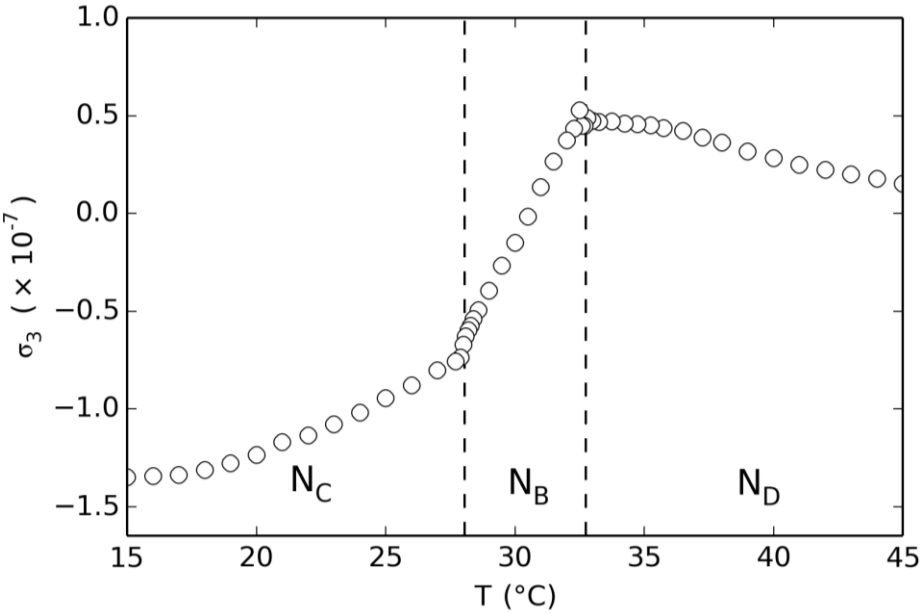

Figure 4.22. The change in the σ_3 values with temperature for sample s3.

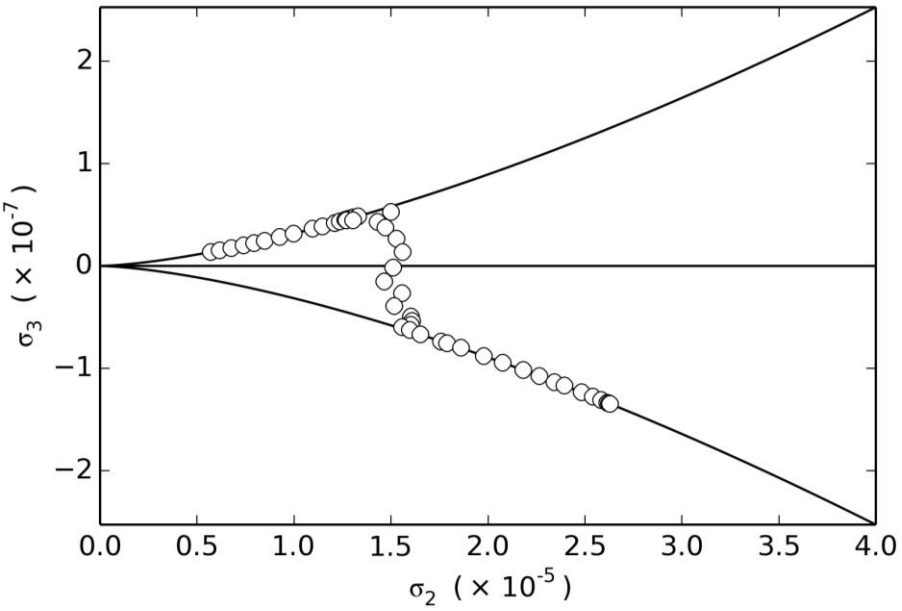

Figure 4.23. Interdependence of σ_3 and σ_2 for sample s3.

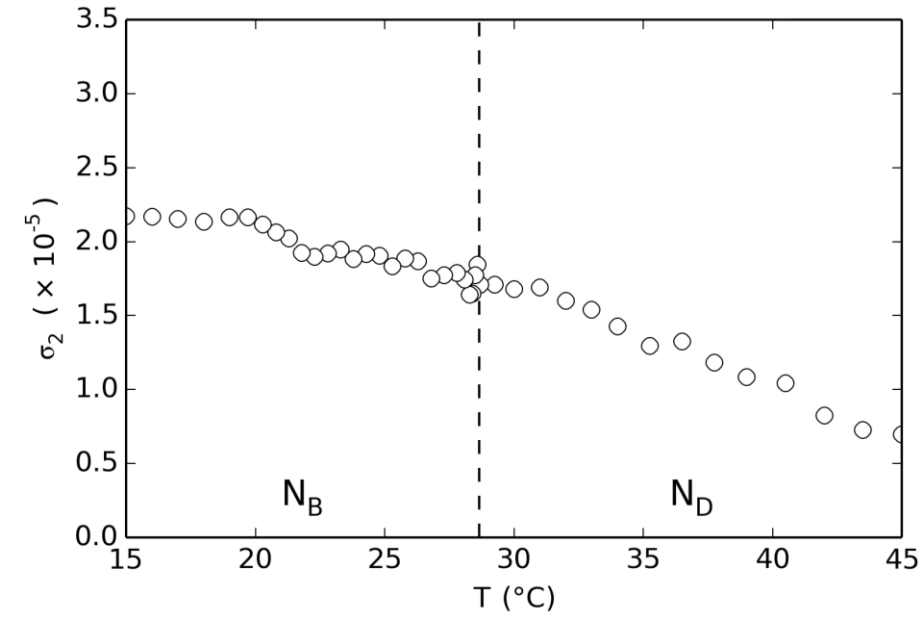

Figure 4.24. The change in the σ_2 values with temperature for sample s4.

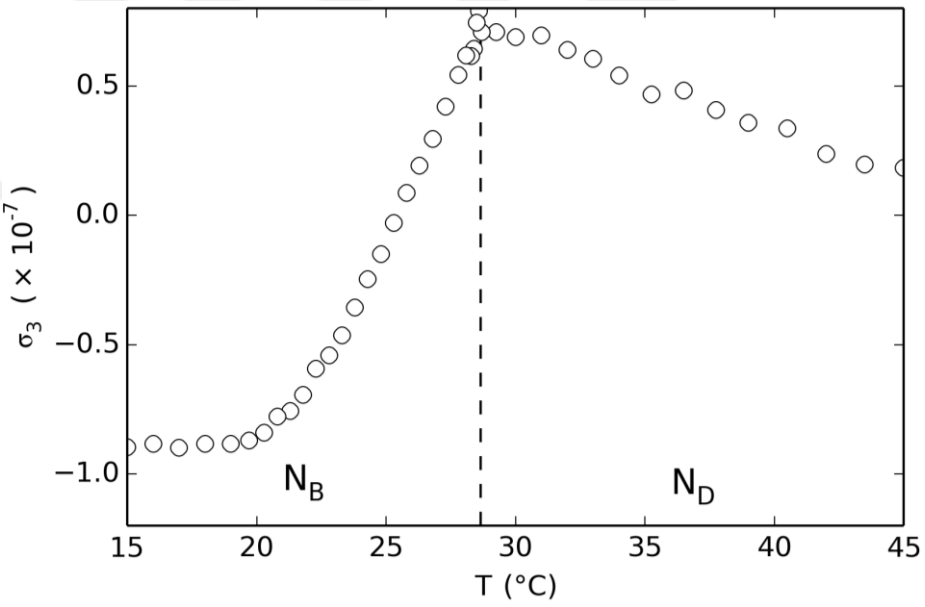

Figure 4.25. The change in the σ_3 values with temperature for sample s4.

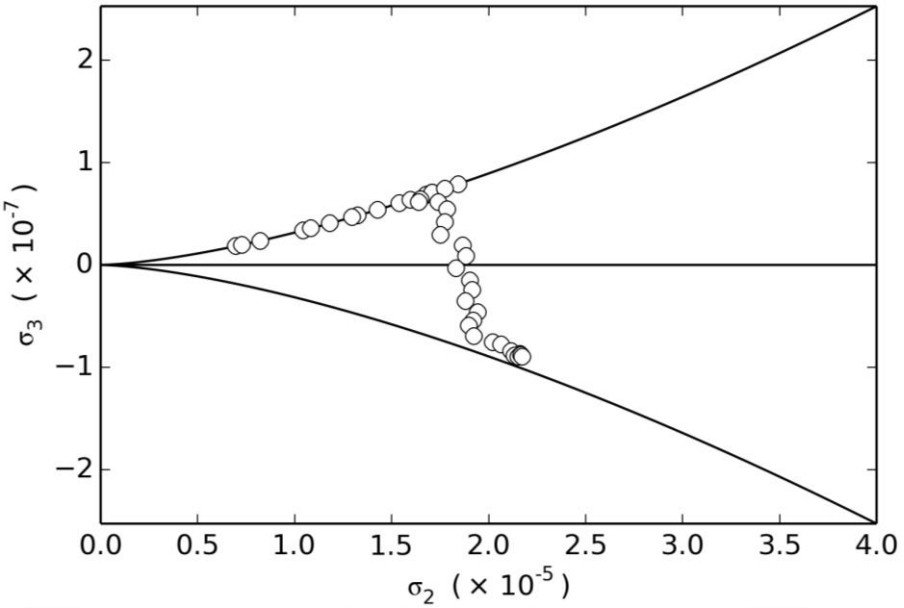

Figure 4.26. Interdependence of σ_3 and σ_2 for sample s4.

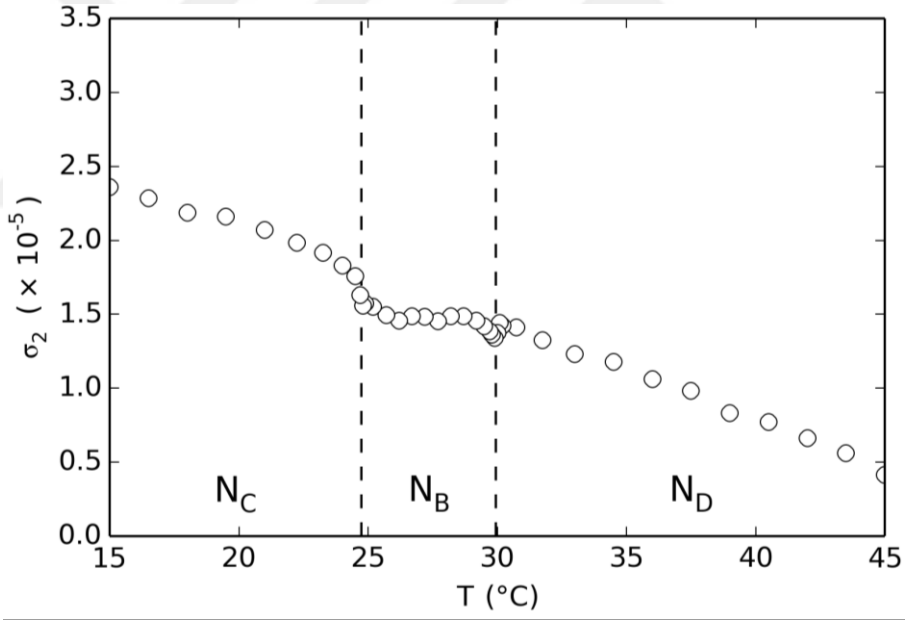

Figure 4.27. The change in the σ_2 values with temperature for sample s5.

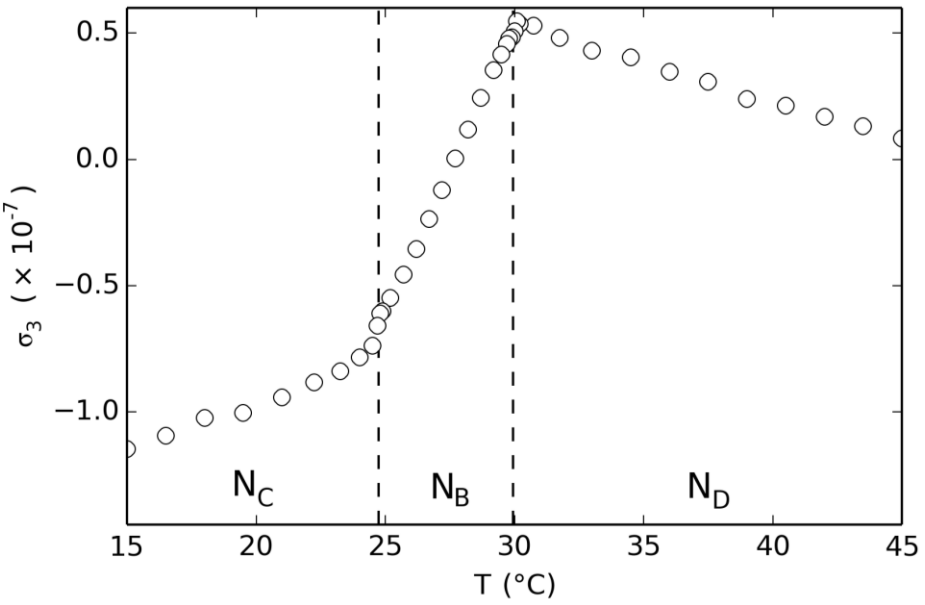

Figure 4.28. The change in the σ_3 values with temperature for sample s5.

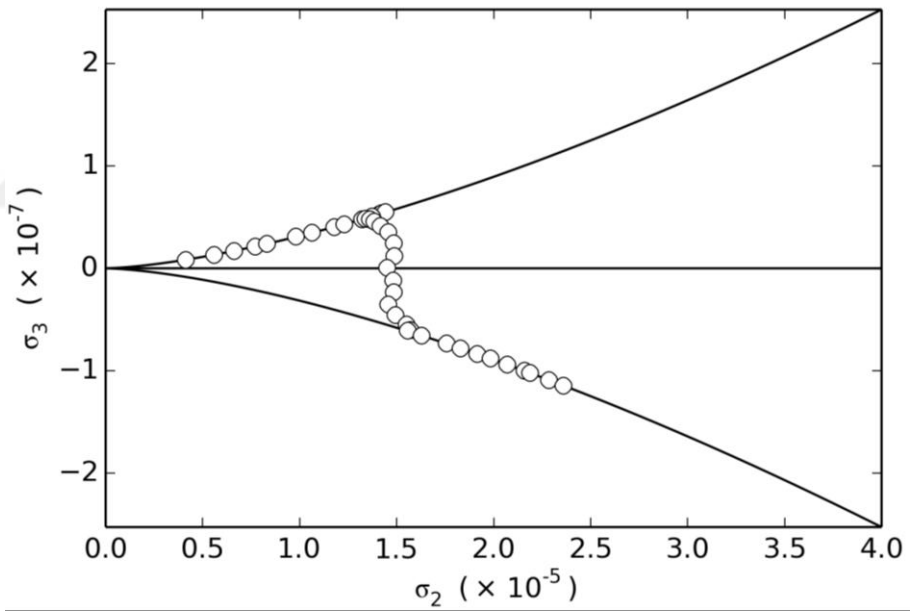

Figure 4.29. Interdependence of σ_3 and σ_2 for sample s5.

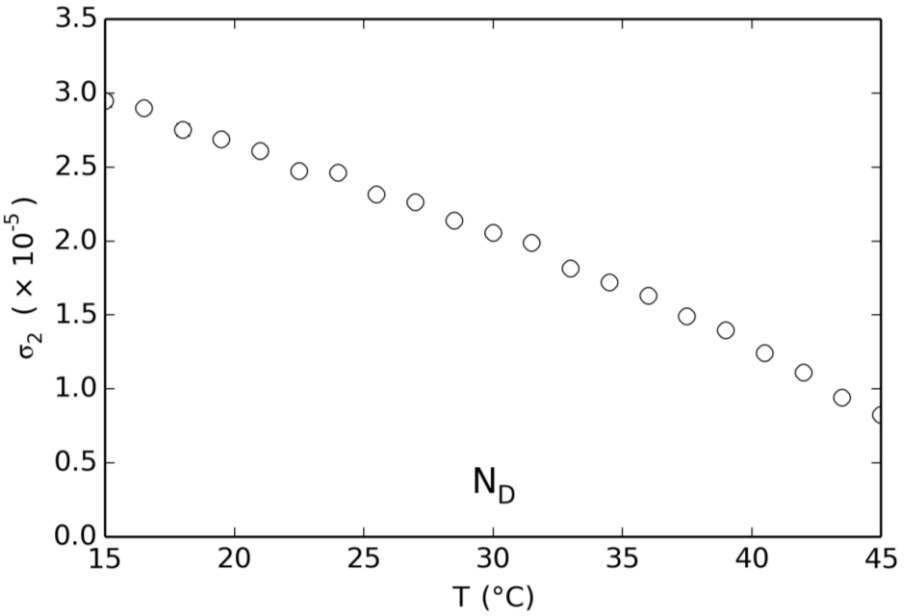

Figure 4.30. The change in the σ_2 values with temperature for sample s6.

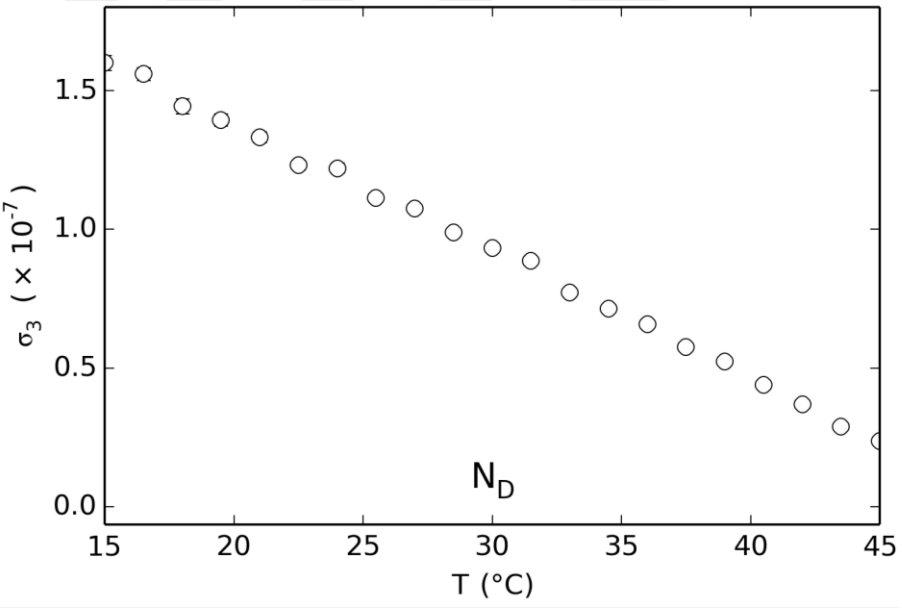

Figure 4.31. The change in the σ_3 values with temperature for sample s6.

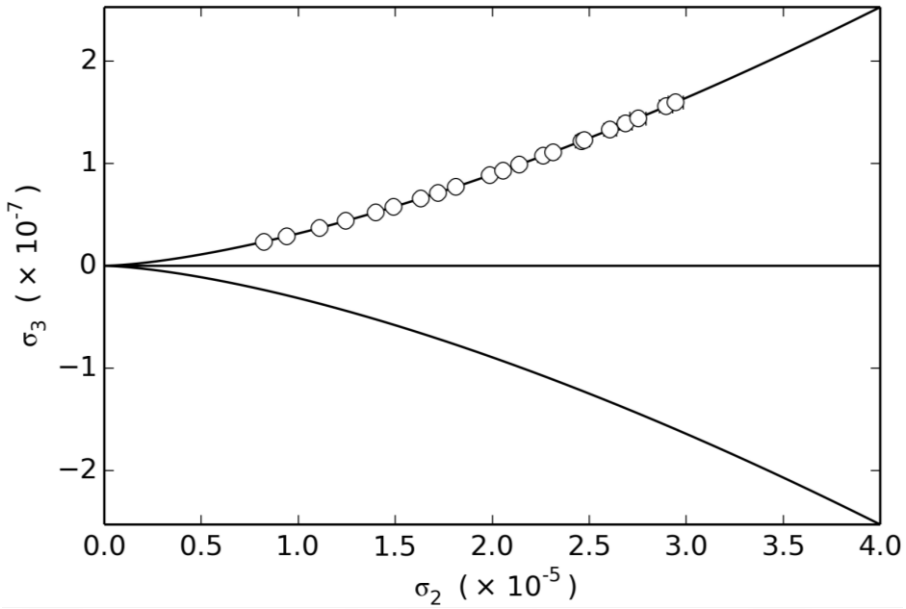

Figure 4.32. Interdependence of σ_3 and σ_2 for sample s6.

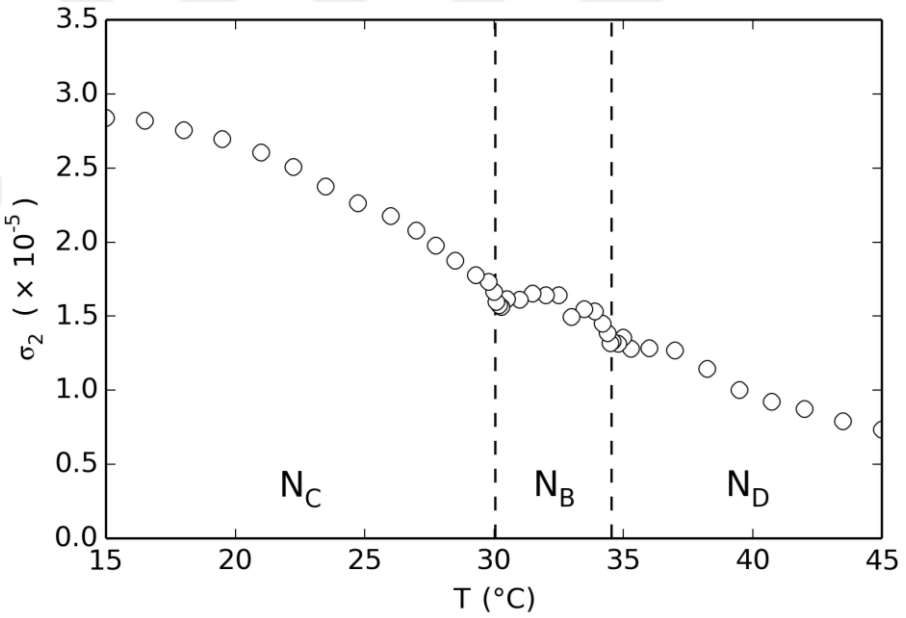

Figure 4.33. The change in the σ_2 values with temperature for sample s7.

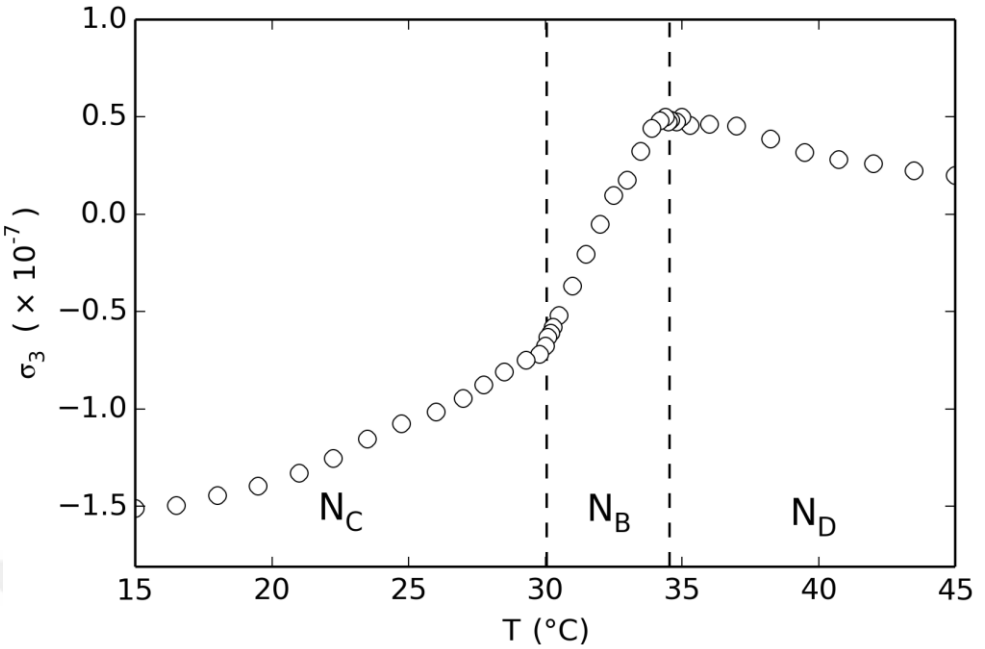

Figure 4.34. The change in the σ_3 values with temperature for sample s7.

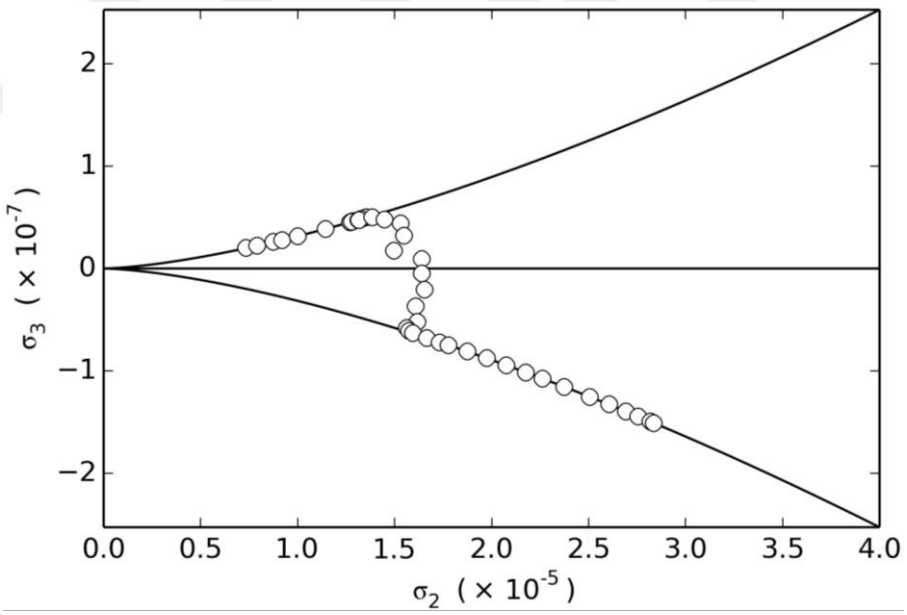

Figure 4.35. Interdependence of σ_3 and σ_2 for sample s7.

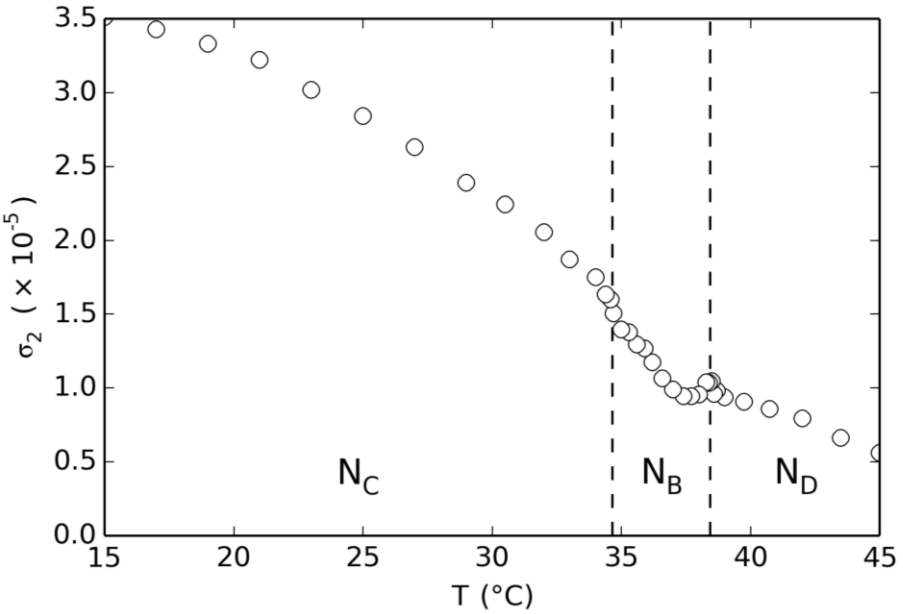

Figure 4.36. The change in the σ_2 values with temperature for sample s8.

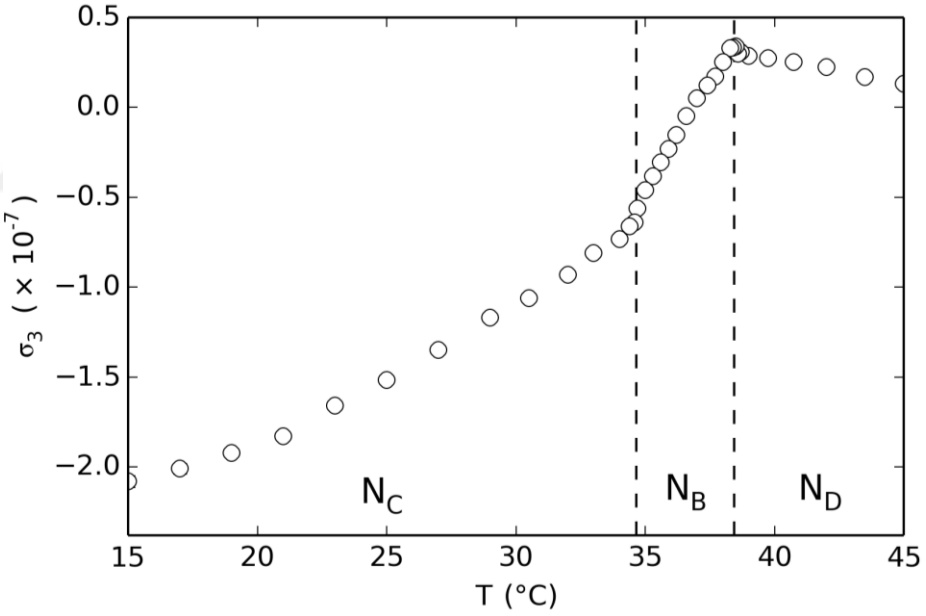

Figure 4.37. The change in the σ_3 values with temperature for sample s8.

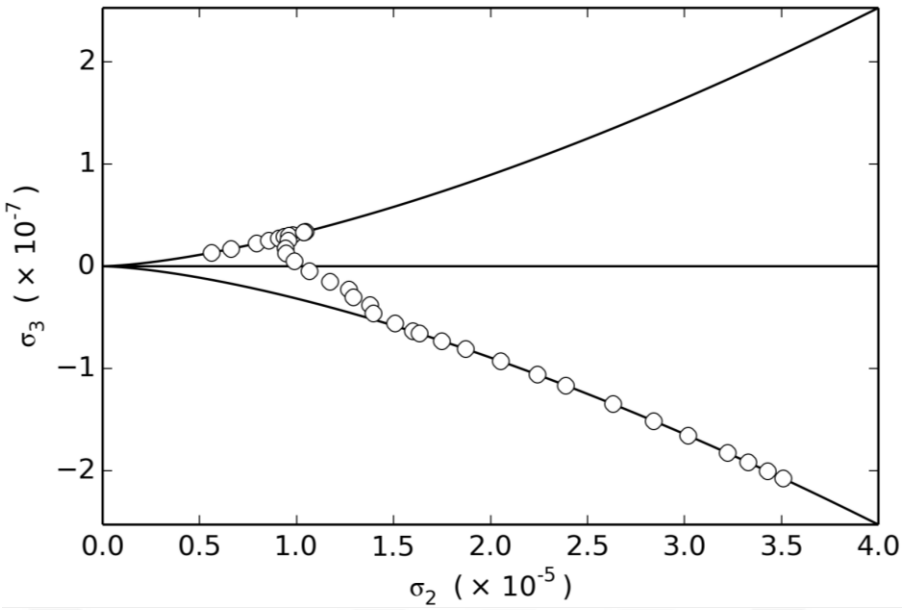

Figure 4.38. Interdependence of σ_3 and σ_2 for sample s8.

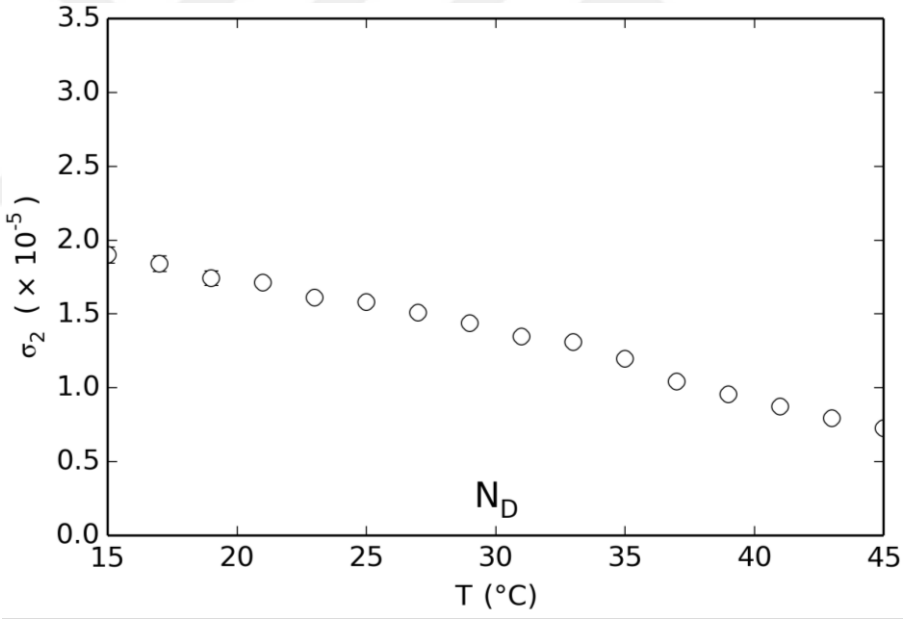

Figure 4.39. The change in the σ_2 values with temperature for sample s9.

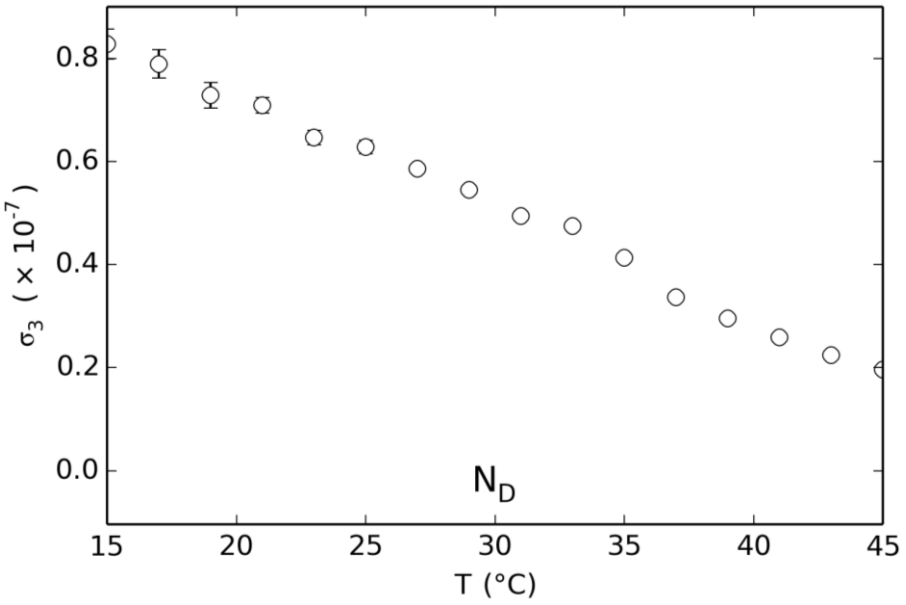

Figure 4.40. The change in the σ_3 values with temperature for sample s9.

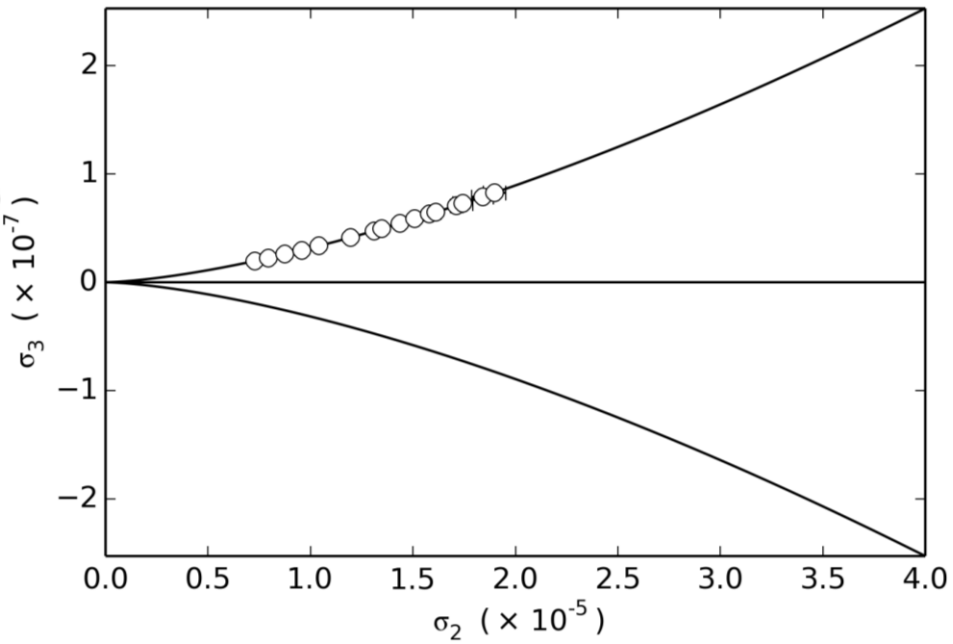

Figure 4.41. Interdependence of σ_3 and σ_2 for sample s9.

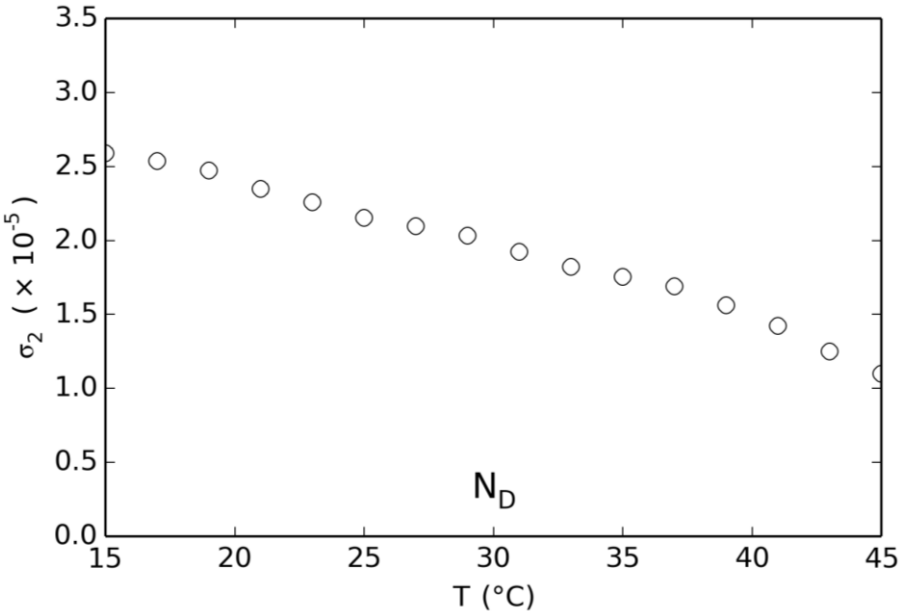

Figure 4.42. The change in the σ_2 values with temperature for sample s10.

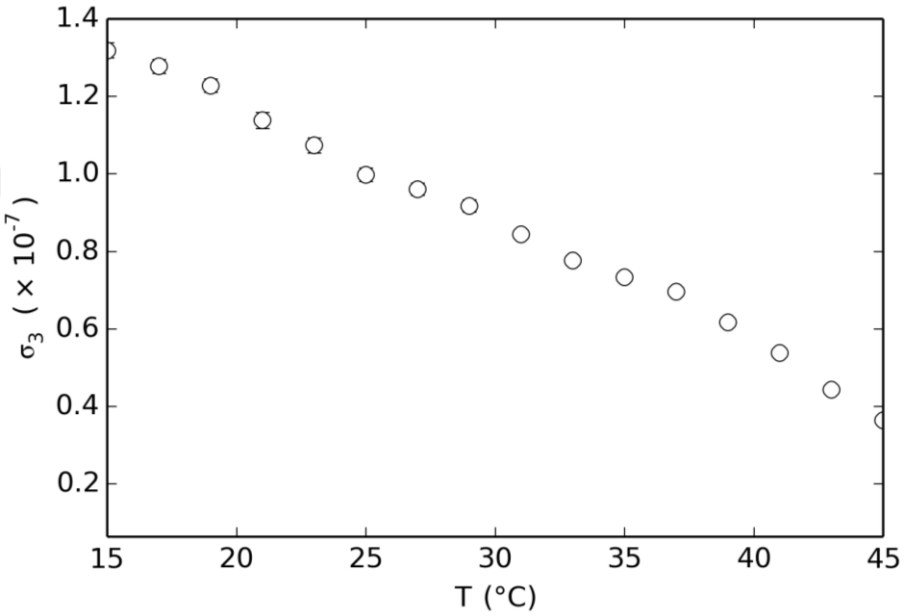

Figure 4.43. The change in the σ_3 values with temperature for sample s10.

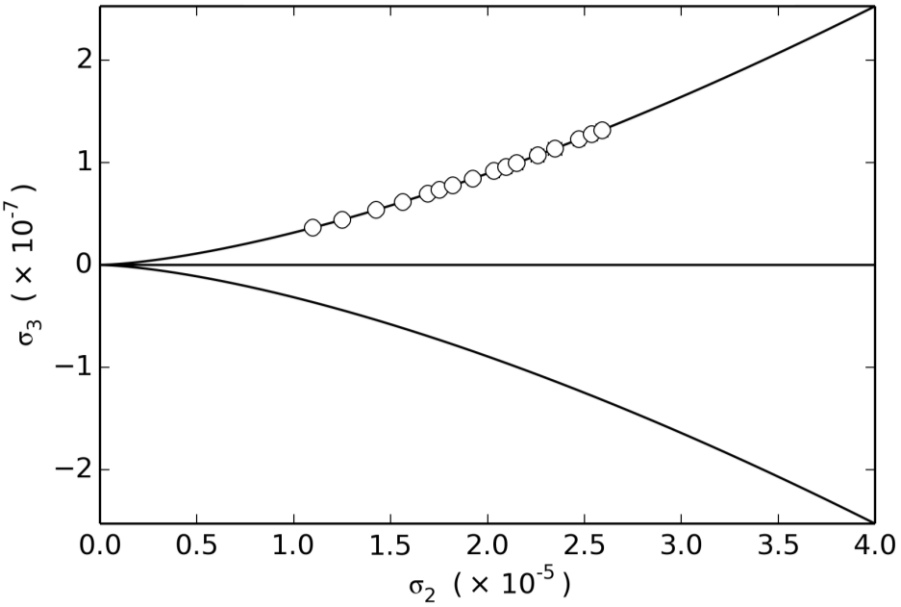

Figure 4.44. Interdependence of σ_3 and σ_2 for sample s10.

4.2 Interpretation of Small-Angle X-ray Scattering (SAXS) Data

SAXS is a very useful method to evaluate some micelle structural parameters of the lyotropic nematic phases. Considering the IBM model, the basic units of the three lyotropic nematic phases are anisometric micelles with orthorhombic or biaxial symmetry (Galerne & Liébert, 1985). Being as the simplest three-dimensional shape with orthorhombic symmetry, it was supposed an average shape of a rectangular parallelepiped for the micelles in the three nematic phases. Details of this approximated model are presented in (Akpinar et al., 2020) and in its Supporting Information.

The SAXS aligned patterns of the nematic phases were used to evaluate the average dimensions of the available volume per micelle (A, B, C) directly from the peak positions of the nematic bands. The following structural parameters were calculated from the model-based analysis: average dimensions of the micelles core (A, B, C), the average area per polar head (a_0) and the shape anisotropy (SA).

Figures 4.45-4.55 show the 2D small-angle X-ray scattering (SAXS) patterns of samples s0-s10.

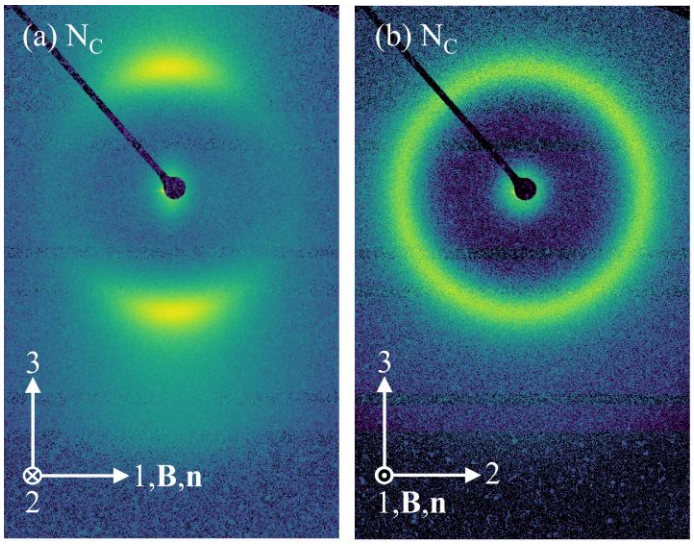

Figure 4.45. The 2D small-angle X-ray scattering (SAXS) patterns of the aligned nematic N_C phase at 40.0 °C for sample s0 at (a) the PP position and (b) the PR position. **B** and **n** are the directions of the magnetic field and nematic phase director, respectively.

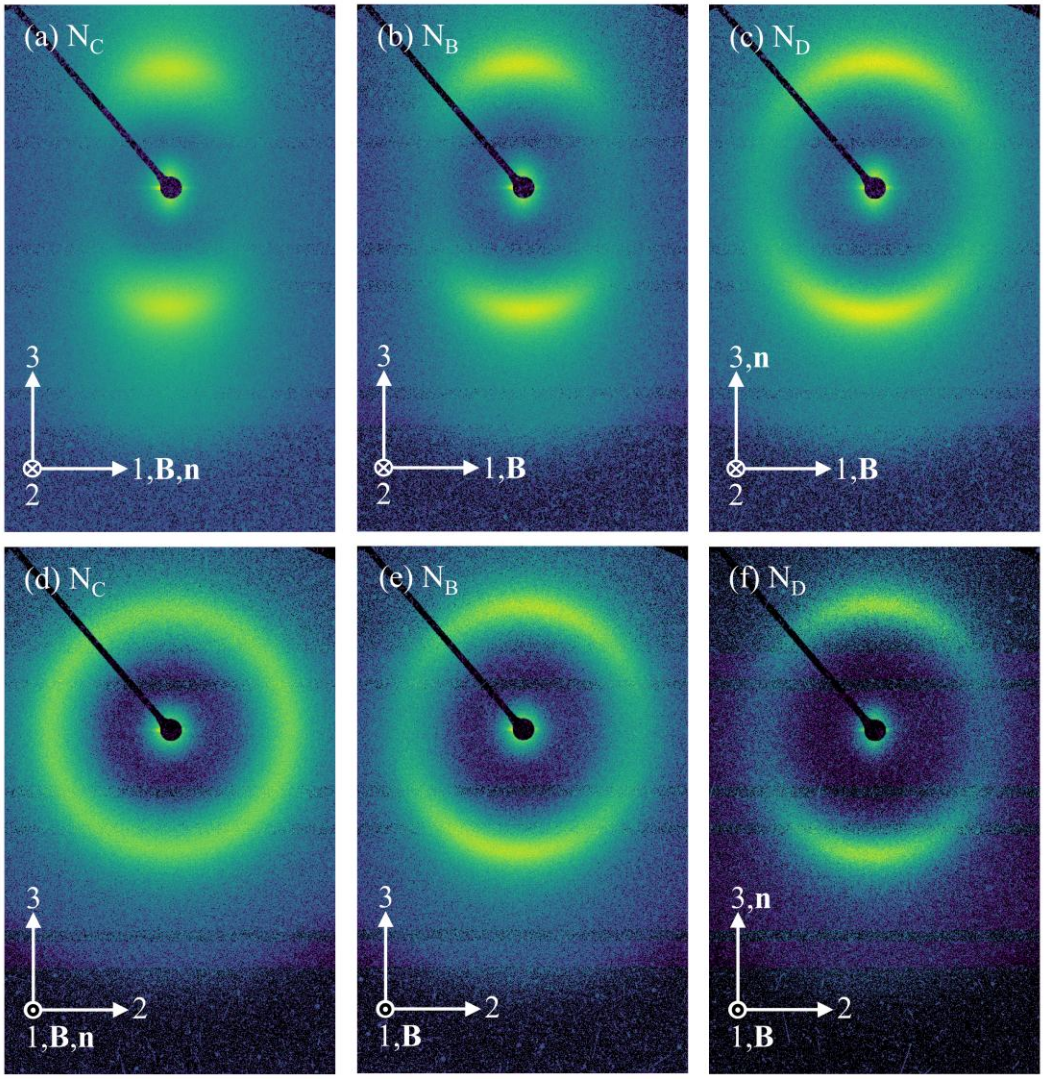

Figure 4.46. The 2D SAXS patterns of the aligned nematic N_C, N_B and N_D phases for sample s1. The patterns were measured at (a) 20.0 °C, (b) 28.0 °C, and (c) 40.0 °C, respectively, at the PP position. The patterns (d), (e) and (f) were obtained at the same temperatures at the PR position.

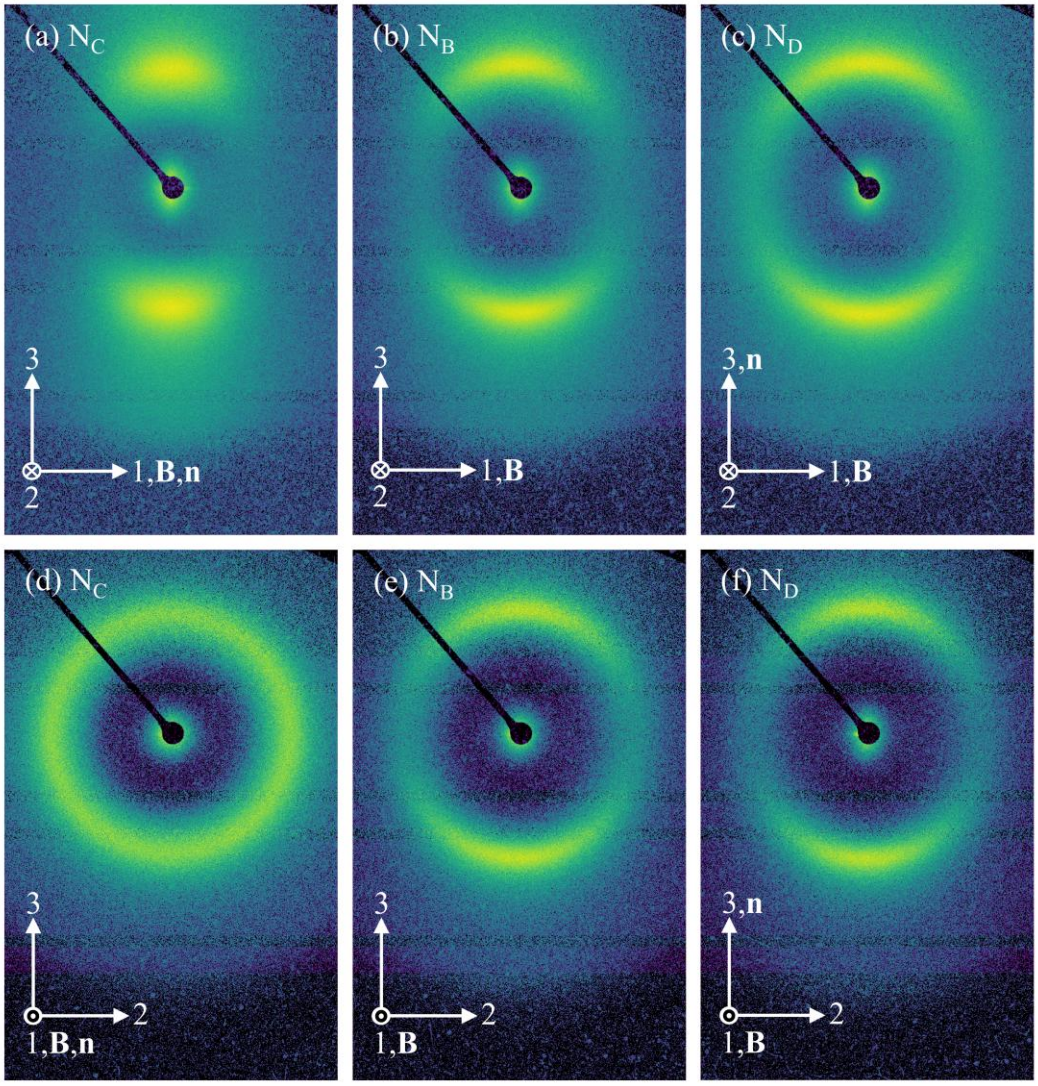

Figure 4.47. The 2D SAXS patterns of the aligned nematic N_C, N_B and N_D phases for sample s2. The patterns were measured at (a) 20.0 °C, (b) 31.0 °C, and (c) 40.0 °C, respectively, at the PP position. The patterns (d), (e) and (f) were obtained at the same temperatures at the PR position.

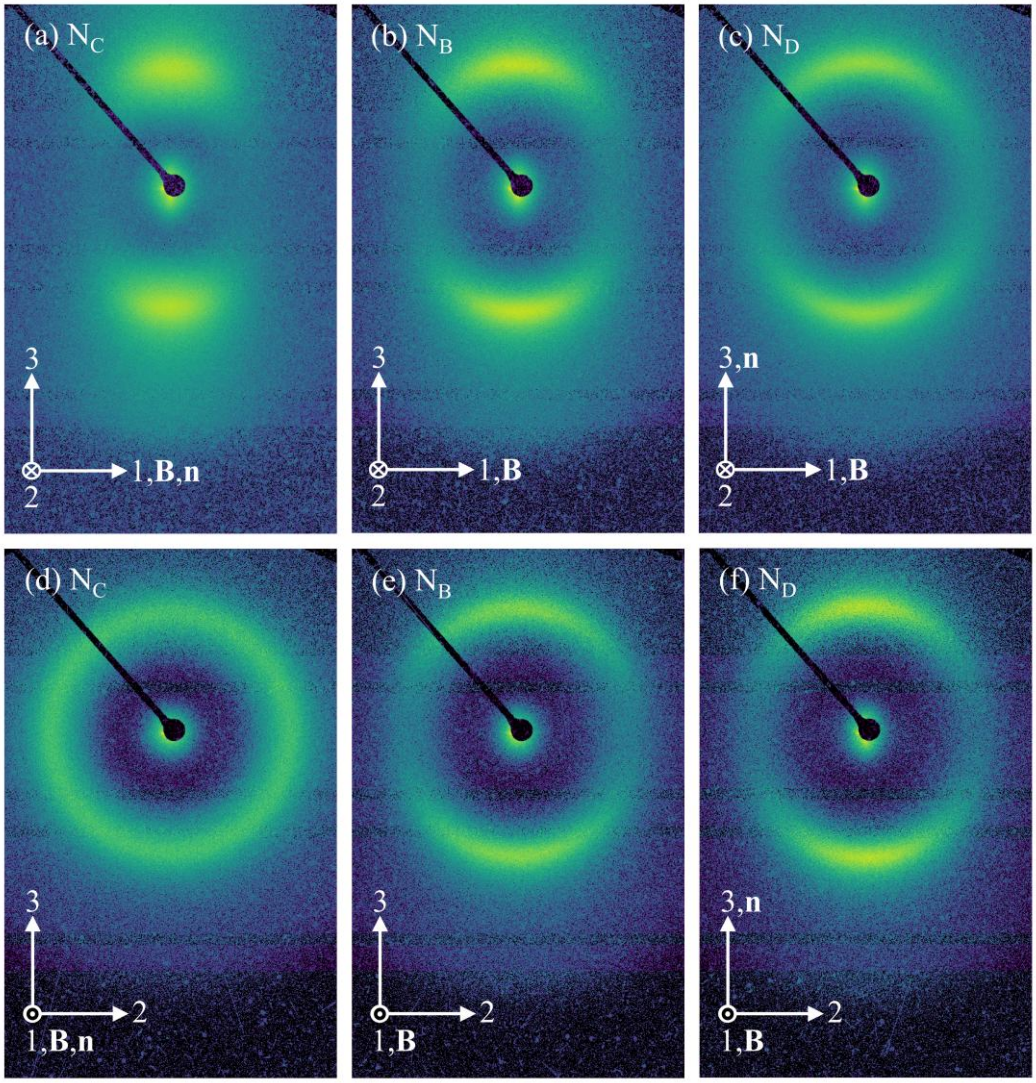

Figure 4.48. The 2D SAXS patterns of the aligned nematic N_C, N_B and N_D phases for sample s3. The patterns were measured at (a) 20.0 °C, (b) 29.0 °C, and (c) 40.0 °C, respectively, at the PP position. The patterns (d), (e) and (f) were obtained at the same temperatures at the PR position.

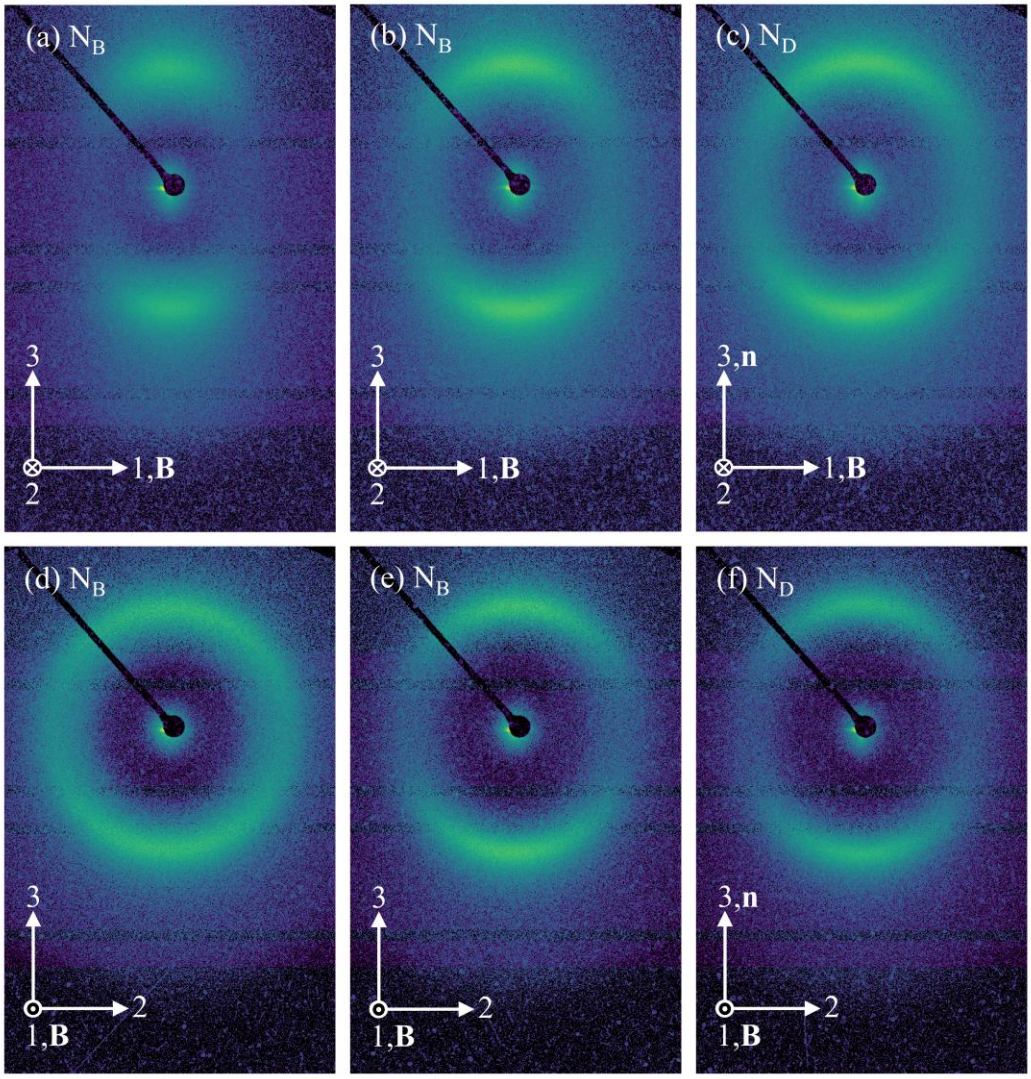

Figure 4.49. The SAXS patterns of the aligned nematic N_B, N_B and N_D phases for sample s4. The patterns were measured at (a) 18.0 °C, (b) 27.0 °C, and (c) 40.0 °C, respectively, at the PP position. The patterns (d), (e) and (f) were obtained at the same temperatures at the PR position.

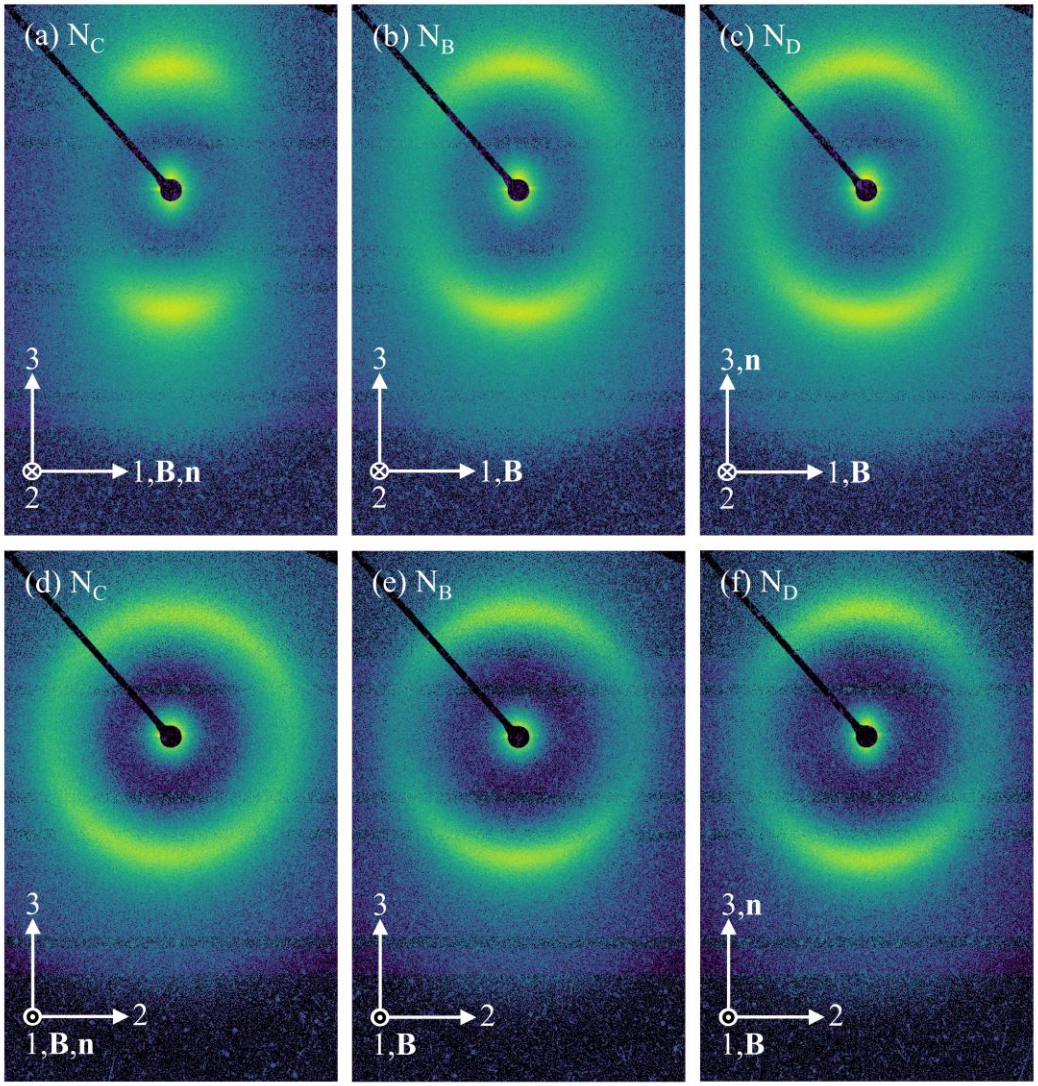

Figure 4.50. The SAXS patterns of the aligned nematic N_C, N_B and N_D phases for sample s5. The patterns were measured at (a) 18.0 °C, (b) 28.0 °C, and (c) 40.0 °C, respectively, at the PP position. The patterns (d), (e) and (f) were obtained at the same temperatures at the PR position.

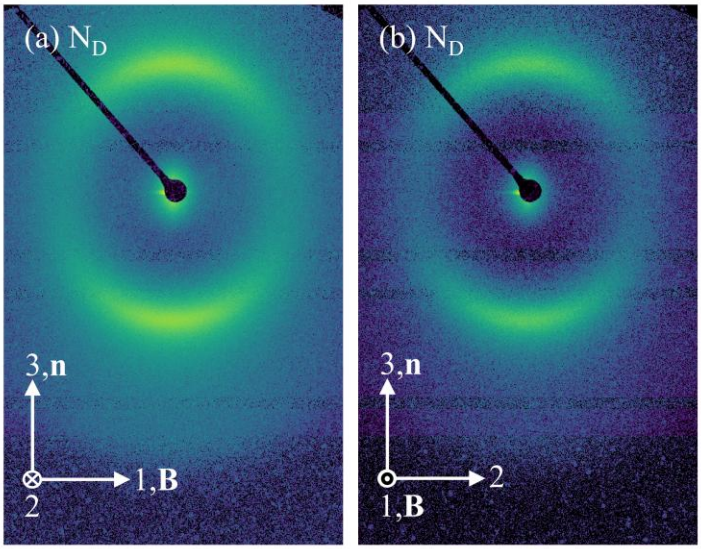

Figure 4.51. The SAXS patterns of the aligned nematic N_D phase at 40.0 °C for sample s6 at (a) the PP position and (b) the PR position.

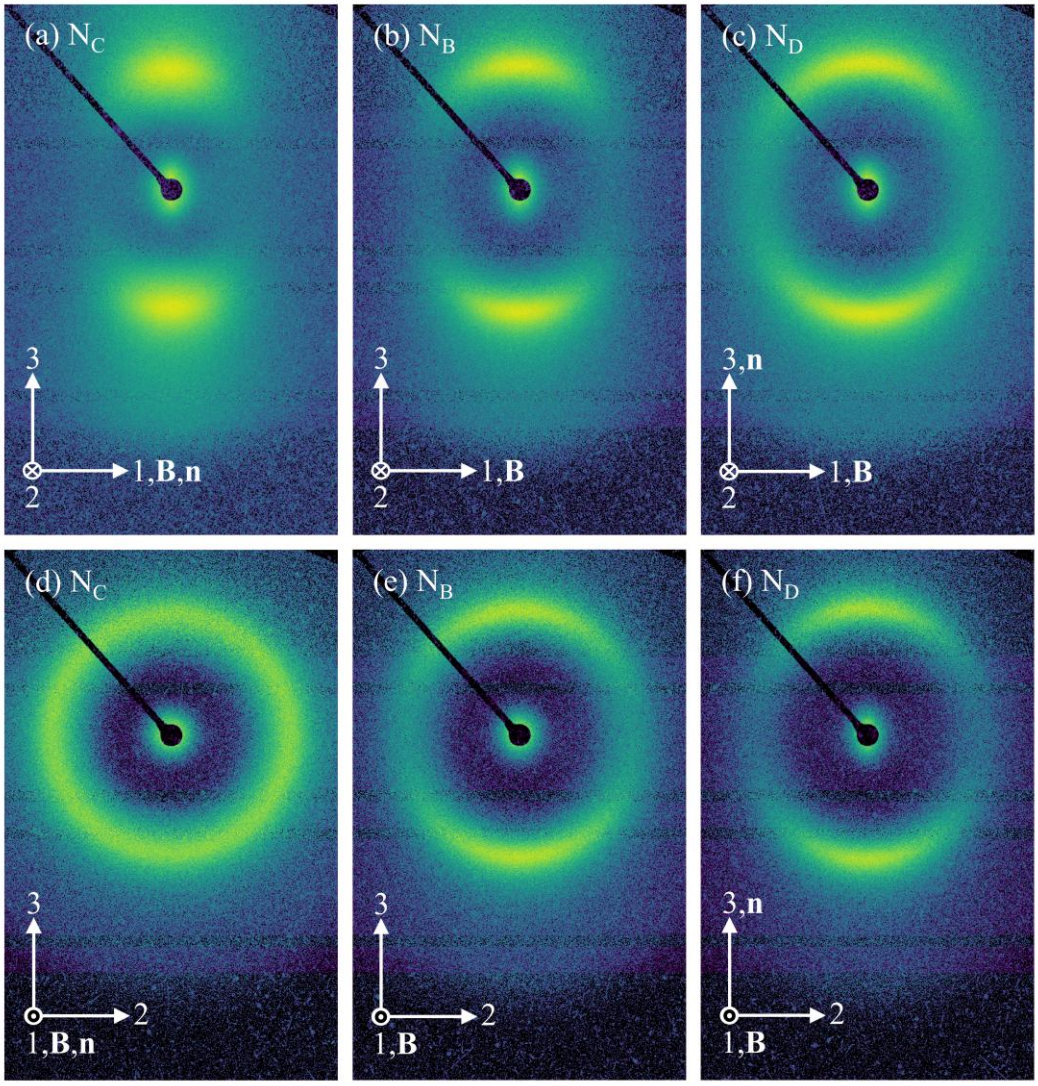

Figure 4.52. The 2D SAXS patterns of the aligned nematic N_C, N_B and N_D phases for sample s7. The patterns were measured at (a) 20.0 °C, (b) 29.0 °C, and (c) 40.0 °C, respectively, at the PP position. The patterns (d), (e) and (f) were obtained at the same temperatures at the PR position.

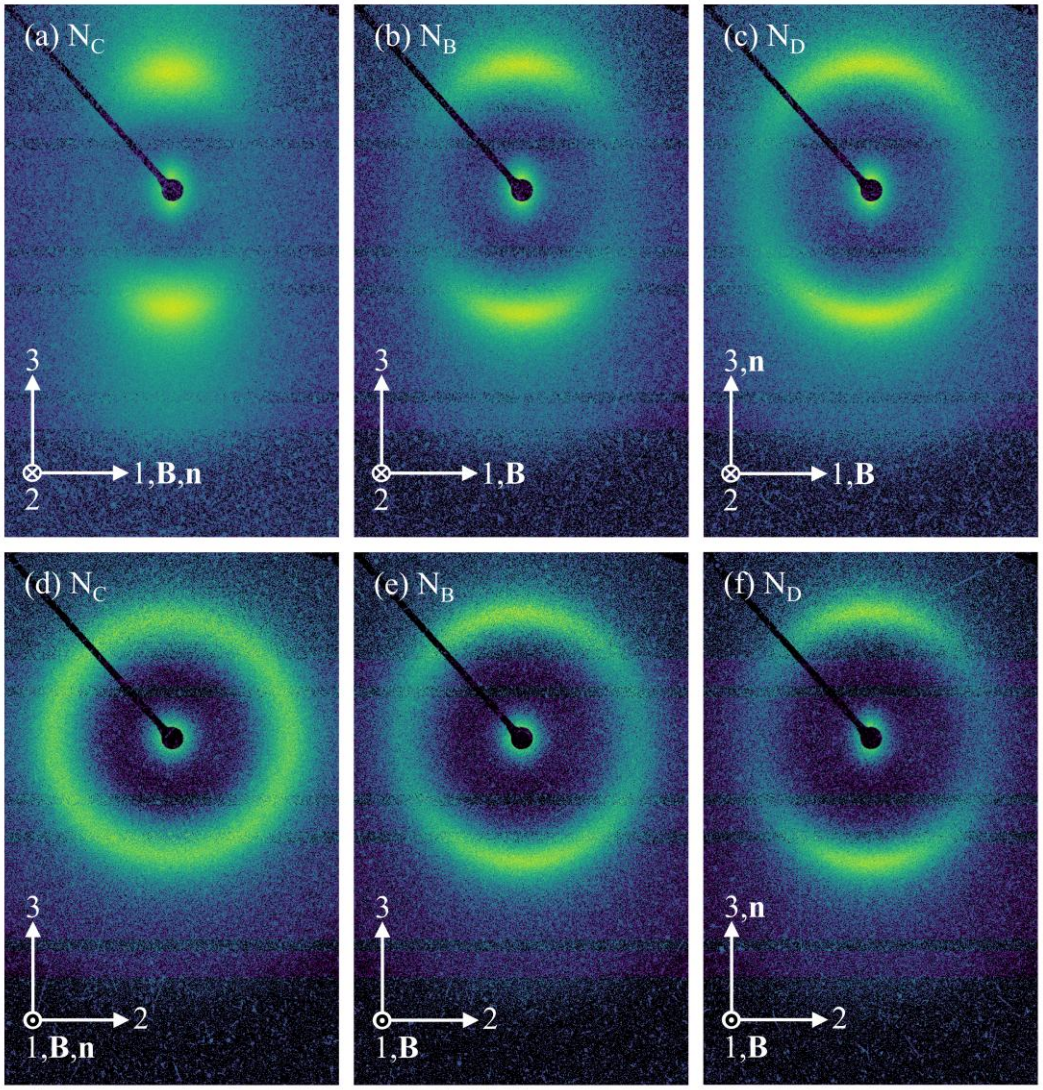

Figure 4.53. The 2D SAXS patterns of the aligned nematic N_C, N_B and N_D phases for sample s8. The patterns were measured at (a) 20.0 °C, (b) 33.0 °C, and (c) 40.0 °C, respectively, at the PP position. The patterns (d), (e) and (f) were obtained at the same temperatures at the PR position.

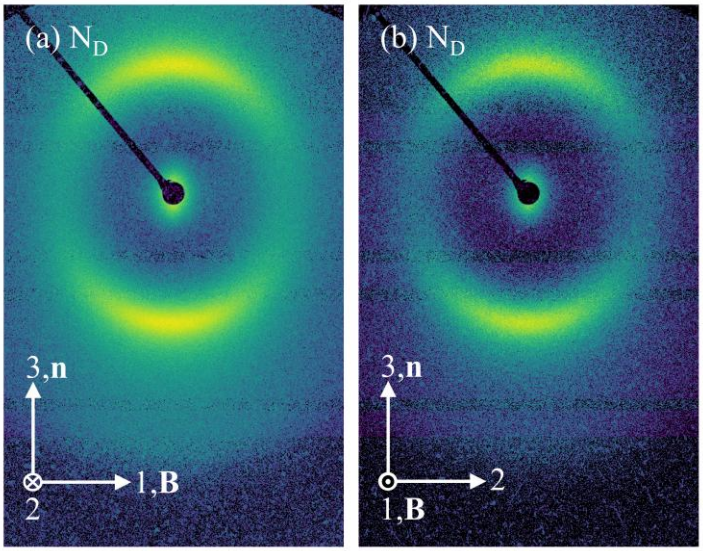

Figure 4.54. The 2D SAXS patterns of the aligned nematic N_D phase at 40.0 °C for sample s9 at (a) the PP position and (b) the PR position.

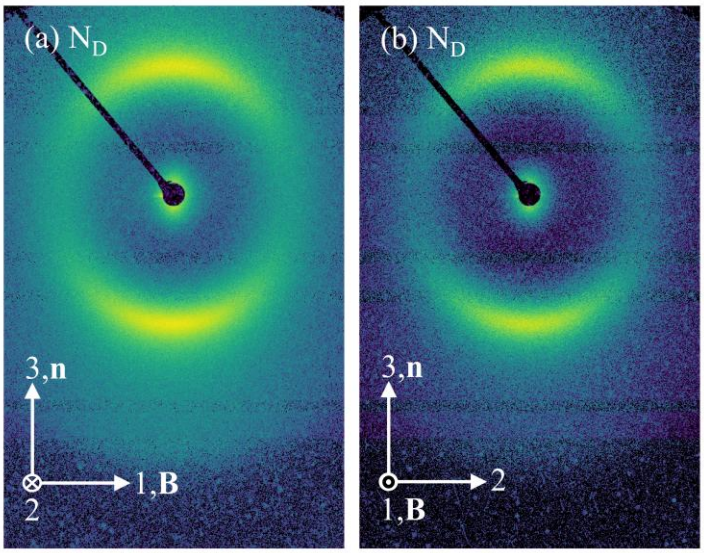

Figure 4.55. The 2D SAXS patterns of the aligned nematic N_D phase at 40.0 °C for sample s10 at (a) the PP position and (b) the PR position.

The SAXS patterns verified the existence of three nematic phases at specified temperatures. They are, in general, in good agreement with the laser conoscopy and polarized optical microscopy results. From the SAXS measurements, we evaluated some micellar parameters: micelle's core average micelle dimensions (A, B, C), micelle shape anisotropy (SA) and the average area per surfactant head group at micelle surfaces (a_0), Figure 4.56-4.58 (Akpinar et al. 2020). The SA values is calculated according to the following equation;

$$SA = \left\{ \frac{[(A+B)/2] - C}{[(A+B)/2]} \right\} \tag{4.1}$$

The SA is a measure of the average thickness of the micelle bilayer C relative to the average of the other two dimensions A and B of the micelle's core. The bilayer thickness is related to the lengths of the surfactant's alkyl chain and it varies very small variations with temperature and composition of the mixture. Therefore, it can be said that the SA gives information about the relative growth of the micelle in the directions perpendicular to the amphiphiles' bilayer direction. The micellar parameters for the samples are given in Tables 4.2.

Table 4.2. Micelle's core average dimensions (A, B, C), shape anisotropies and average area per surfactant head group at micelle surfaces of the samples.

Sample	Micelle's core average dimensions			SA	a_0/Å^2
	A/Å	B/Å	C/Å		
s1	41.8±0.7	32.5±0.5	29.4±0.5	0.209±0.015	57±1
s2	42.0±0.8	32.5±0.5	29.3±0.5	0.212±0.018	57±1
s3	41.1±1.0	34.0±0.7	29.1±0.7	0.224±0.022	57±2
s4	42.4±1.0	33.4±0.7	29.1±0.6	0.231±0.020	57±2
s5	38.7±0.7	32.5±0.5	29.7±0.4	0.165±0.016	58±1
s6	41.4±0.7	33.0±0.5	29.3±0.5	0.212±0.016	57±1
s7	39.1±0.6	33.1±0.4	29.5±0.4	0.184±0.013	58±1
s8	39.0±1.8	33.4±1.2	29.5±1.2	0.186±0.040	58±3
s9	38.8±1.5	34.2±1.1	28.9±1.0	0.208±0.034	58±3
s10	40.0±1.1	33.9±1.8	29.0±0.7	0.215±0.024	57±2

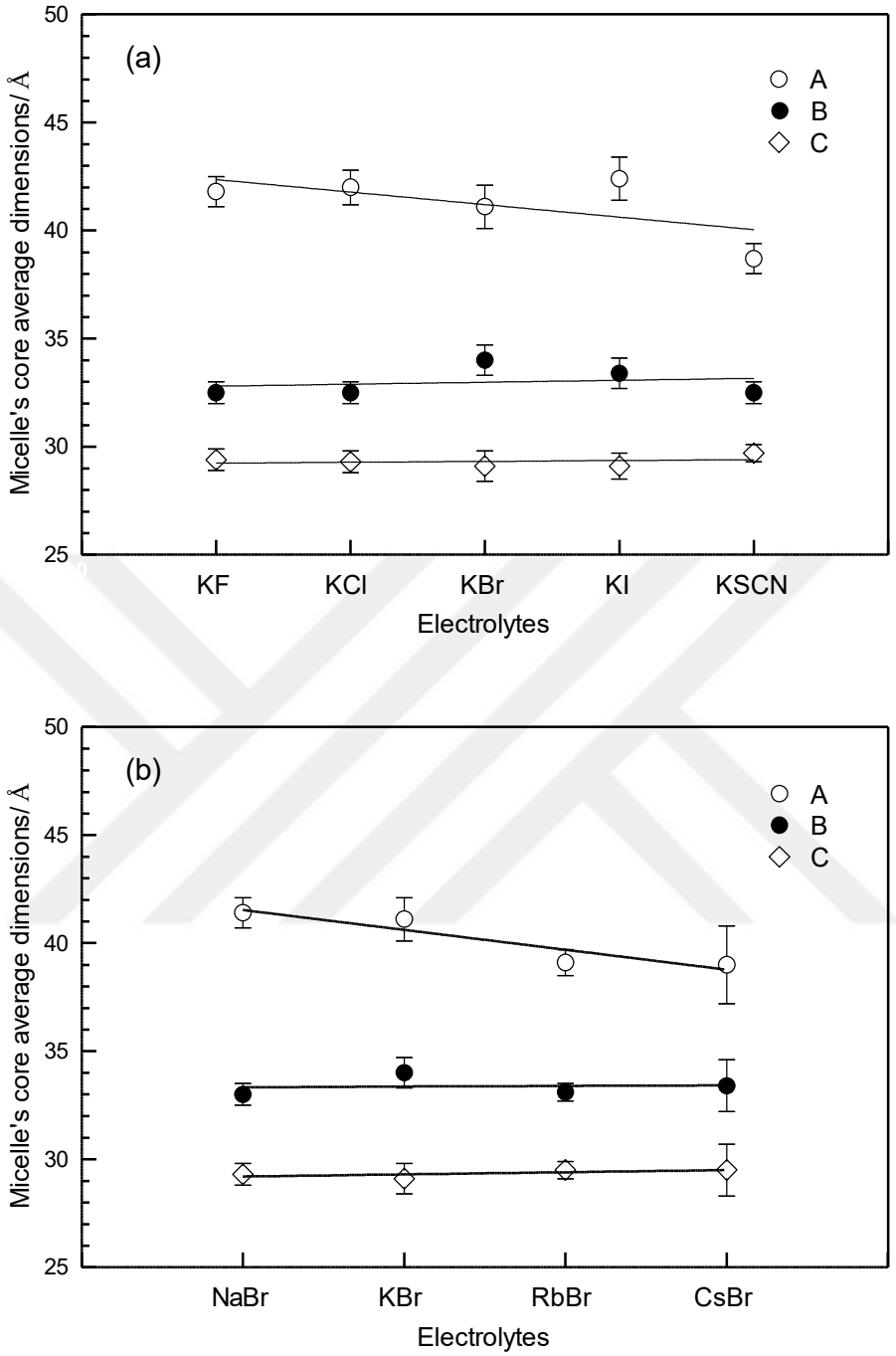

Figure 4.56. Change in the micelle's core average dimensions (A, B, and C) with Hofmeister series ions: (a) anions located in the Gouy-Chapman layer and/or intermicellar region, and (b) cations bound to the micelle surfaces in the stern layer.

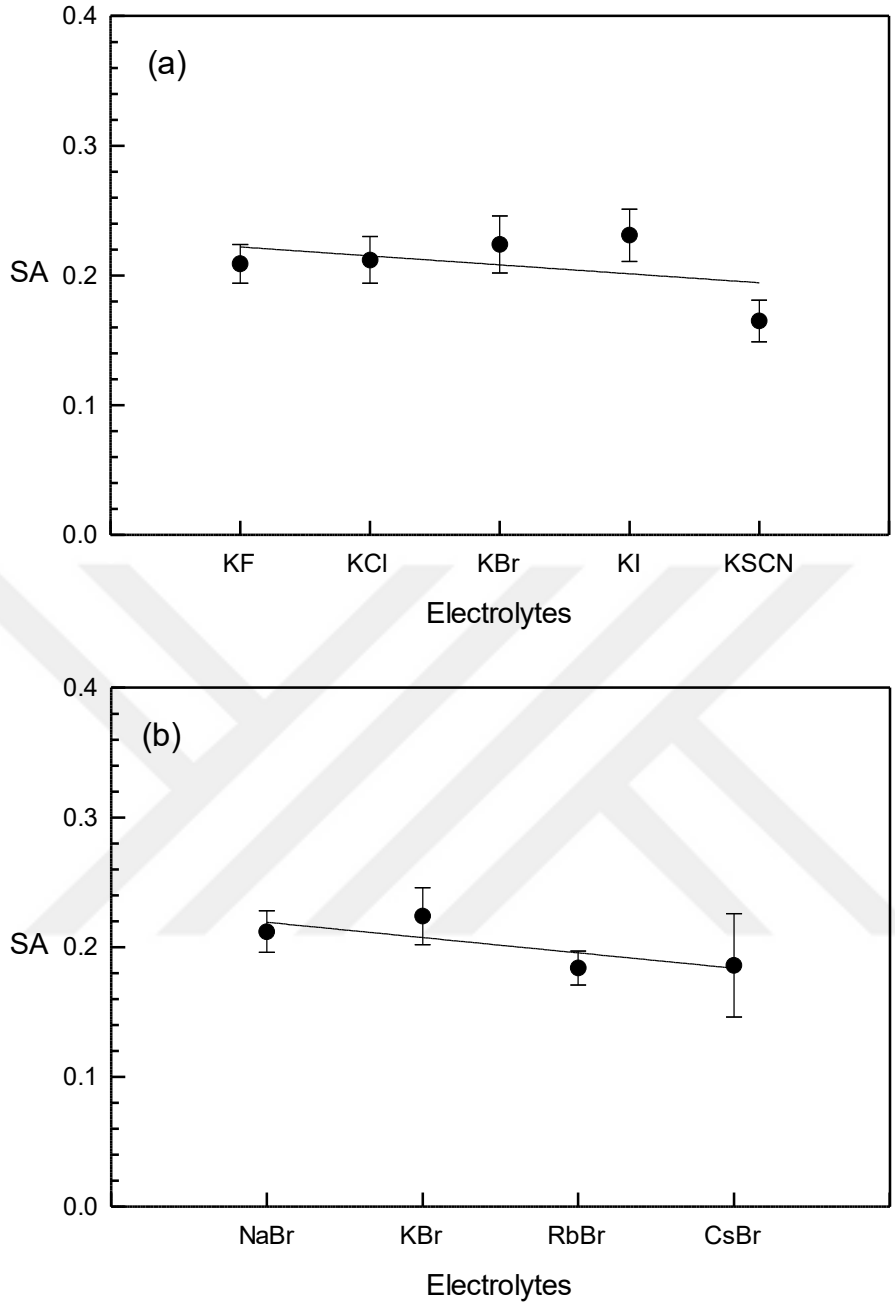

Figure 4.57. Relationship between the micelle shape anisotropy and Hofmeister series ions: (a) anions located in the Gouy-Chapman layer and/or intermicellar region, and (b) cations bound to the micelle surfaces in the stern layer.

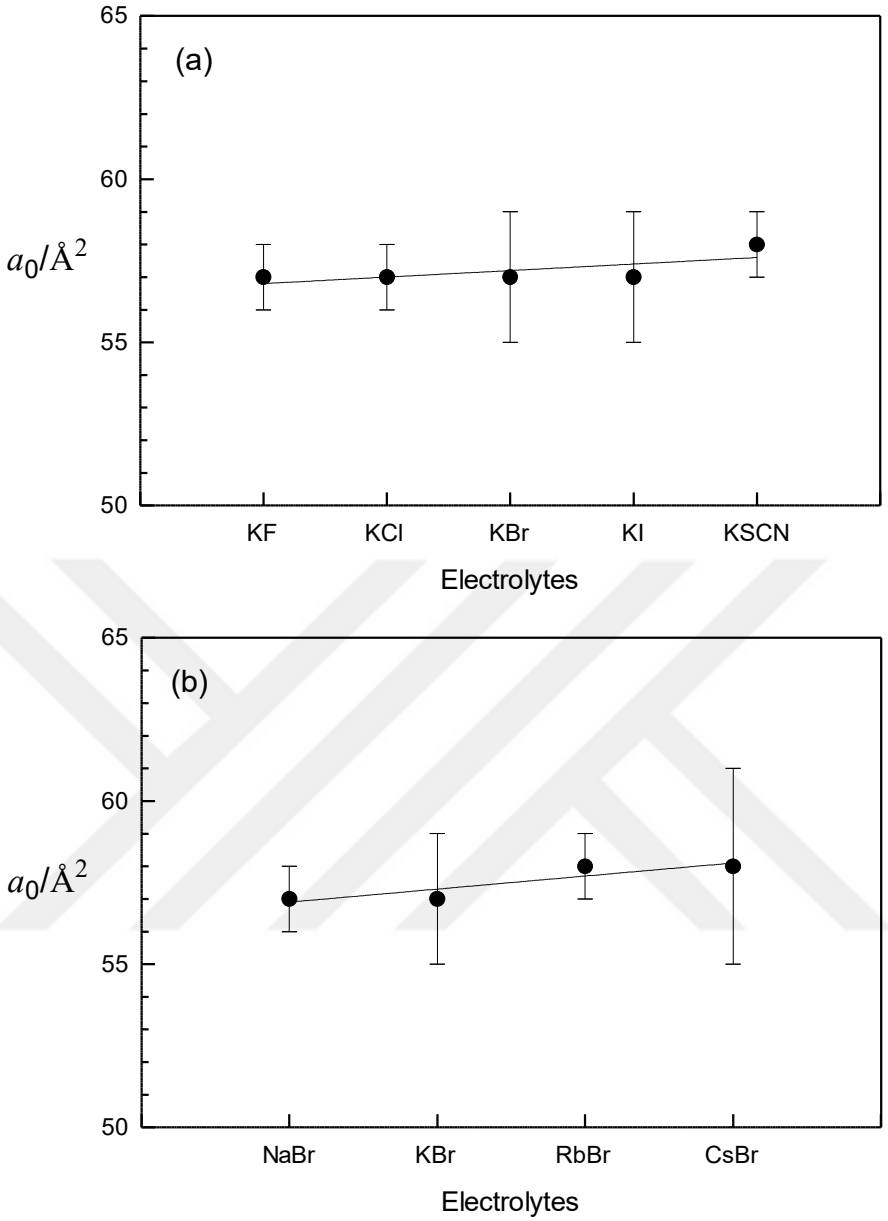

Figure 4.58. Effect of the Hofmeister (a) anions located in the Gouy-Chapman layer and/or intermicellar region, and (b) cations bound to the micelle surfaces on the average area per surfactant head group at micelle surfaces in the stern layer.

The SAXS results summarized in Table 4.2 are graphically illustrated in Figures 4.56-4.58. The micelle dimension A decreases going from F^- to SCN^- (from strongly kosmotropic to strongly chaotropic ion). However, other dimensions (B and C) increase going from F^- to SCN^-. The decrease in the dimension A is more dominant than that in the dimensions B and C. The micelle shape anisotropy SA

(the average area per surfactant head group at the micelle surface, a_0) also decreases (increases) from F^- to SCN^-. Considering the meaning of the SA, the relative micelle growth in the $A \times B$ plane decreases with respect to the amphiphiles' bilayer direction. Exactly similar trends on the micelle dimensions, SA, and a_0 were observed for the cations (from strongly kosmotropic Na^+ to strongly chaotropic Cs^+). These results show that the ions, which remain in the Gouy-Chapman layer of the electrical double layer and/or in the aqueous bulk solution (or the intermicellar region), similar to the effect of the ions located at the micelle surfaces, in the stern layer affect the micellization of the surfactants, micelle surface curvature, and the formation of different lyotropic nematic phases by modifying orientational fluctuations (considering the IBM model of the nematic phases). Thus, the interactions in the Gouy-Chapman layer and in the intermicellar region (aqueous bulk solutions) are also important to stabilize different lyotropic nematic phases.

5. CONCLUSION

In this thesis, it is aimed to investigate the effect of the Hofmeister ions present in the intermicellar region and/or Gouy-Chapman layer of the electrical double layer on the formation of different lyotropic nematic phases in the lyotropic mixture of KDD/electrolyte/DeOH/water. The physicochemical properties of lyotropic nematic phases were studied via polarized optical microscopy, laser conoscopy, and Small-angle X-ray Scattering. The results are in good agreement with each other and also with the literature. For a better understanding of the role of those ions, we also studied the effect of the ions located at the micelle surfaces (in the Stern layer). The results obtained from both regions (micelle surfaces and intermicellar region) are compared and it can be concluded that the ions present in the intermicellar region also affect the formation of lyotropic nematic phases as well as the ions located at the micelle surfaces. In other words, we have shown for the first time that the interactions between ionic species in the Gouy-Chapman layer and/or in the intermicellar region play a crucial role in the formation of the lyotropic nematic phases. The effect of these interactions comes from the kosmotropic and chaotropic nature of the ions, and the extent of the effects of the ions follows the Hofmeister series of the ions.

In summary, this thesis revealed that the ions having the same electrical charge with the surfactant head groups cannot be located at the micelle surfaces, but they play an important role in controlling the properties of surfactant-based lyotropic liquid crystals, especially the formation of the biaxial nematic phases. From this respect, researchers should consider the kosmotropic or chaotropic properties of both cations and anions of electrolytes to obtained different nematic phases, especially biaxial nematic ones.

6. REFERENCES

Akpinar, E., Reis, D., & Neto, A. M. F. (2012a). Effect of alkyl chain length of alcohols on nematic uniaxial-to-biaxial phase transitions in a potassium laurate/alcohol/K_2SO_4/water lyotropic mixture. *Liquid crystals, 39*(7), 881-888.

Akpinar, E., Reis, D., & Figueiredo Neto, A. M. (2012b). Lyotropic mixture made of potassium laurate/1-undecnol/K_2SO_4/water presenting high birefringences and large biaxial nematic phase domain: A laser conoscopy study. *Eur. Phys. J. R, 35*(50). http://doi.org/10.1140/epje/i2012-12050-9

Akpinar, E., Reis, D., & Figueiredo Neto, A. M. (2014). Anomalous behavior in the crossover between the neagtive and positive biaxial nematic mesophases in a lyotropic liquid crystal. *ChemPhysChem, 15*(7), 1463-1469. http://doi.org/10.1002/cphc.201301103

Akpinar, E., Reis, D., & Neto, A. M. F. (2015). Effect of Hofmeister anions on the existence of biaxial nematic phase in lyotropic mixtures of dodecyltrimethylammonium bromide/sodium salt/1-dodecanol/water. *Liquid Crystals, 42*(7), 973-981. https://doi.org/10.1080/02678292.2015.1011717

Akpinar, E., Otluoglu, K., Turkmen, M., Canioz, C., Reis, D., & Figueiredo Neto, A. M. (2016a). Effect of the presence of strong and weak electrolytes on the existence of uniaxial and biaxial nematic phases in lyotropic mixtures. *Liquid crystals, 43*(11), 1693-1708.

Akpinar, E., Turkmen, M., Canioz, C., & et al. (2016b). Role of kosmotrope-chaotrope interactions at micelle surfaces on the stabilization of lyotropic nematic phases. *Eur. Phys. J. E, 39,* 107. https://doi.org/10.1140/epje/i2016-16107-5

Akpinar, E., Canioz, C., Turkmen, M., Reis, D., & Figueiredo Neto, A. M. (2017). Effect of the surfactant alkyl chain length on the stabilization of lyotropic nematic phases. *Liquid Crystals, 45*(2), 219-229.

Akpinar, E., Figueiredo Neto, A. M. (2019). Experimental conditions for the stabilization of the lyotropic biaxial nematic mesophase. *Crystals, 9*(3), 158.

Akpinar, E., Guner, E., Demir-Ordu, O., & Figueiredo Neto, A. M. (2019). Effect of head-group size of some tetradecylalkylammonium bromide surfactants on obtaining the lyotropic biaxial nematic phase. *Eur. Phys. J. E, 42,* 44.

Akpinar, E., Topcu, G., Reis, D., & Figueiredo Neto, A. M. (2020). Effect of the anionic azo dye Sunset Yellow in lyotropic mixtures with unixial and biaxial nematic phases. *Journal of Molecular Liquids, 318,* 114010. http://doi.org/10.1016/j.molliq.2020.114010

Akpinar, E., Uygur, N., Demir Ordu, O., Reis, D., & Martins Figueiredo Neto, A. (2021). Effect of the head-group size dependence of the dye- surfactant interactions on the lyotropic uniaxial to biaxial nematic phase transitions. *Journal of Molecular Liquids, 332,* 115842. https://doi.org/10.1016/j.molliq.2021.115842

Akpinar, E., Tabak, M., Reis, D., & Figueiredo Neto, A. M. (2023). Properties of the uniaxial and biaxial nematic phases of the dodecyltrimethylammonium bromide/1-dodecanol/water lyotropic mixture including azo dye and drug molecules. *Phase Transitions, 97*(1-2), 66-86. https://doi.org/10.1080/01411594.2023.2284162

Akpinar, E., Okuyan, B., Reis, D., Uygur, N., & Figueiredo Neto, A. M. (2025). Investigation of the relation between surfactant head group size and formation of different types of lyotropic structures in two surfactants/dye systems. Journal of Molecular Liquids, 417, 126589. https://doi.org/10.1016/j.molliq.2024.126589

Alarfaj, N. A., & El-Tohamy, M.F. (2015). Applications of micelle enhancement in luminescence-based analysis. *Luminescence, 30,* 3-11.

Amaral, L. Q., Pimentel, C. A., Tavares, M. R., & Vanin, J. A. (1979). Study of a magnetically oriented lyotropic mesophases. *Journal of Chemial physics, 71,* 2940-2945.

Amaral, L. Q., & Tavares, M. R. (1980). On the possible formation of macromicelles in a lyomesophase. *Mol. Cryst. Liq. Cryst. Lett., 56,* 203-208.

Aswal, V. K., & Goyal, P. S. (2000). Counterions in the growth of ionic micelles in aqueous electrolyte solutions: A small-angle neutron scattering study. *Physical Review E, 61,* 2947-2953.

Bahadur, B. (Ed.). (1990). *Liquid Crystals: Applications and uses* (Vols. 1-3). World Scientific.

Bartolino, R., Chiaranza, T., Meuti, M., & Compagnoni, R. (1982). Uniaxial and biaxial lyotropic nematic liquid crystals. *Pyhsical Review A, 26,* 1116-1119.

Bates, M. A., & Luckhurst, G. R. (n.d.). Computer simulation studies of anisotropic systems. In pierre-Gilles de Gennes & J. Prost, *The physics of liquid crystals* (2nd ed.). Oxford University Press.

Bisoyi, H. K., & Li, Q. (2011). Light-driven liquid crystalline materials: From photo-induced phase transitions and property changes to applications. *Chemical Reviews, 116*(3), 1505-1631.

Buwalda, R. T., & Engberts, J. B. F. N. (2001). Aggregation of dicationic surfactants with methyl orange in aqueous solution. *Langmuir, 17*(4), 1054-1059.

Chakraborty, T., Chakrabort, I., & Ghosh, S. (2011). The methods of determination of critical micellar concentrations of amphiphilic systems in aqueous medium. *Arabian Journal of Chemistry, 4(3),* 265-270.

Charvolin, J., Levelut, A. M., & Samulski, E. T. (1979). Lyotropic nematics: Molecular aggregation and susceptibilies. *Journal de Physique Lettres, 40,* 587-592.

Collings, P. J., & Hird, M. (1997). *Introduction to liquid crystals: chemistry and physics.* Taylor & Francis.

Collings, P. J. (2002). *Liquid crystals: Nature's delicate phase of matter* (2nd ed., Chap. 1, p. 7). Princeton University Press.

Collins, K. D. (1997). Charge density-dependent strength of hydration and biological structure. *Biopysical Journal, 72,* 65-76.

Collins, K. D. (2004). Ions from the Hofmeister series and osmolytes: Effects on proteins in solution and in the crystaliztion process. *Methods, 34,* 300-311.

Collins, K. D., Neilson, G. W., & Enderby, J. E. (2007). Ions in water: Characterizating the forces that control chemical processes and biological structure. *Biophysical Chemistry, 128,* 95-104.

Conway, B. E. (1981). *Ionic hydration in chemistry and biophysics* (1st ed.). Elsevier Scientific Publishing Company.

Das, D., Roy, S., Mitra, R. N., Dasgupta, A., & Das, P. K. (2005). Head-group size or hydrophilicity of surfactants: The major regulator lipase activity in cationic water-in-oil microemulsions. *Chemistry – A European Journal, 11,* 4881-4889.

Dawin, U. C., Lagerwall, J. P. F., & Giesselmann, F. (2009). Electrolyte effects on the stability of nematic and lamellar lyotropic liquid crystal phases: Colligative and ion-specific aspects. *Journal of Physical Chemistry b, 113,* 11420.

De Gennes, P.-G., & Prost, J. (1993). *The physics of liquid crystals* (2nd ed.). Clarendon Press.

De Gennes, P.-G., & Prost, J. (1995). *The physics of liquid crystals* (2nd ed.). Oxford University Press.

Demissie, H., & Duraisamy, R. (2016). Effects of electrolytes on the surface and micellar characteristics of sodium dodecyl sulphate surfactant solution. *Journal of Scientific and Innovative Research, 5*(6), 208-214.

Dierking, I., & Martins Figueiredo Neto, A. (2020). Novel trends in lyotropic liquid crytsals. *Crystals, 10*(7), 604.

Faergemand, M., & Krog, N. (2003). Using emulsifiers to improve food texture. In Texture in food. Volume 1: Semi-solid foods (pp.216-250). Woodhead Publishing Ltd.

Fairhurst, C. E., Fuller, S., Gray, J., Holmes, M. C., & Tiddy, G. J. T. (1998). Lyotropic surfactant liquid crystals. In D. Demus, J. Goodby, G. W. Gray, H.-W. Spiess, & V. Vill (Eds.), *Handbook of liquid crystals* (1st ed.). Wiley-VCH.

Figueirinhas, J. L., et al. (2005). A unifying picture of lyotropic biaxial nematic phases. *Liquid Crystals, 32*(8), 1079-1086.

Filho, A. M., Laverde, A., & Fujiwara, F. Y. (2003). Observation of two biaxial nematic mesophases in the tetradecyltrimethylammonium bromide/decanol/water system. *Langmuir, 19,* 1127-1132.

Forrest, B. J., Reeves, L. W., & Robinson, C. J. (1981). Transition in the sign of the diamagnetic anisotropy of a lyotropic mesophase without a phae change: Type O disk micelle systems. *Journal of Physical Chemistry, 85,* 3244-3247.

Freiser, M. J. (1970). Ordered states of a nematic liquid. *Physical Review Letters, 24*(20), 1041-1043. https://doi.org/10.1103/PhysRevLett.24.1041

Galerne, Y., & Marcerou, J. P. (1983). Orientation-induced ordering in liquid crystals. Physical Review Letters, 51(23), 2109–2112.

Galerne, Y., & Liebert, L. (1985). Zigzag disclinations in biaxial nematic liquid crystals. *Physical Review Letters, 55,* 2449-2451.

Galerne, Y., & Marcerou, J. P. (1985). Determination of the elastic constants of a nematic by transient director deformation. Journal de Physique, 46(4), 589–598.

Galerne, Y., Neto, A. M. F., & Liebert, L. (1987). Microscopic structure of the uniaxial and biaxial lyotropic nematics. *Journal of Chemical Physics, 87,* 1851-1856.

Galindo, A., Haslam, A. J., Varga, S., Jackson, G., Vanakaras, A. G., Photinos, D. J., & Dunmur, D. A. (2003). The phase behavior of a binary mixture of rodlike and disclike mesogens: Monte Carlo simulation, theory, and experiment. *Journal of ChemicalPhysics, 119,* 5216-5225.

Goodby, J. W. (2005). Microscopy applications: Liquid crystals. In P. Worsfold, A. Townshend, & C. Poole (Eds.), *Encyclopedia of analytical science* (2nd ed., pp. 74-84). Elsevier.

Goodby, J, W. (2014). Materials and phase structures of calamitic and discotic liquid crystals. In J. Chen, W. Cranton, & M. Fihn (Eds.), *Handbook of visual display technology* (pp. n/a). Springer.

Guo, C., Wang, J., Cao, F., Lee, R. J., & Zhai, G. (2010). Lyotropic liquid crystal systems in drug delivery. *Drug Discovery Today, 15*(23), 1032-1040.

Hendrikx, Y., Charvolin, J., & Rawiso, M. (1986). *Physical Review B: Condensed Matter and Materials Physics, 33,* 3534-3537.

Ho, C. C., Hoetz, R. J., & El-Aasser, M. S. (1991). A biaxial lyotropic nematic phase in dilute solutions of sodium lauryl sulfate-1-hexadecanol-water. *Langmuir, 7,* 630-635.

Holmes, M. C., Leaver, M. S., & Smith, A. M. (1995). Nematic and disrupted lamellar phases in cesium pentadecafluorooctanoate/2H_2O: A small angle scattering study. *Langmuir, 11,* 356-365.

Israelachvili, J. N. (1991). *Intermolecular and surface forces* (2nd ed.). Academic Press.

Jin, X., Yang, W., Gao, X., Zhao, J.-Q., Li, Z., & Jiang, J. (2020). Modeling the unfrozen water content of frozen soil based on the absorption effect of clay surfaces. *Water Resources Research, 56*(12), e2020WR027482. https://doi.org/10.1029/2020WR027482

Kim, Y., -K. Cukrov, G., Vita, F., Scharrer, E., Samulski, E. T., Francescangeli, O., et al. (2016a). Search for microscopic and macroscopic biaxiality in the cybotactic nematic phase of new oxadiazole bent-core mesogens. *Physical Reviews E, 93*(6), 062701.

Kim, Y.-K., Senyuk, B., Shin, S.-T., Kohlmeier, A., Mehl, G. H., & Lavrentovich, O. D. (n.d.) (2016b). Surface alignment, anchoring transitions, optical properties, and topological defects in the thermotropic nematic phase of an organo-siloxane tetrapodes.

Kooji, F. M., & Lekkerkerker, H. N. W. (2000). Liquid-crystal phases formed in mixed suspensions of rod- and platelike colloids. *Langmuir, 16,* 10144-10149.

Kooji, F. M., Vogel, M., & Lekkerkerker, H. N. W. (2000). Phase behavior of a mixture of platelike colloids and nonadsorbing polymer. *Physical Review E, 62,* 5397.

Kurilov, A. D., Chekulaev, I. S., Irani, S. M. S., Parashchuk, N. S., Bezruchenko, V. S., Belyaev, V. V., & Chausov, D. N. (2021). Diamagnetic anisotropy and rotational viscosity of 6CHBT nematic liquid crystal. *Journal of Physics: Conference Series, 2056*, 012029. https://doi.org/10.1088/1742-6596/2056/1/012029.

Lawson, K. D., & Flautt, T. J. (1967). Magnetically oriented lyotropic liquid crystalline phases. *Journal of the American Chemical Society, 89*(21), 5489-5491.

Leaver, M. S., & Holmes, M. C. (1993). A small angle neutron scattering study of the lamellar and nematic phases of caesium pentadecafluorooctanoate (CsPFO)/2H_2O and CsPFO/CsCl/2H_2O. *Journal de Physique II, 3,* 105-120.

Lei, X., Liu, B., Di, C., Wei, Z., Deng, P., Chen, Z. (2025). Molecular interactions of surfactants with othwr chemicals in chemical flooding processes. A comprehensive review on molecular dynamics simulation studies. *Advances in Colloid and Interface Science, 341,* 103498.

Leontidis, E. (2002). Hofmeister anion effects on surfactant self-assembly and the formation of mesoporous solids. *Current Opinion in Colloid & Interface Science*, *7(1-2)*, 81-91.

Mao, L., Li, G., Zhang, B., Wen, K., Wang, C., Cai, Q., Zhao, X., Guo, Z., & Zhang, S. (2024). Functional hydrogels for aqueous zinc-based batteries: Progress and perspectives. *Advanced Materials, 36*, 2416345. https://doi.org/10.1002/adma.202416345

Marcus, Y. (1985). *Ion Solvation* (1st ed.). John Wiley and Sons.

Martin, A . N., Sinko, P. J., & Singh, Y. (2011). *Martin's physical pharmacy and pharmaceutical sciences: Physical chemical and biopharmaceutical principles in the pharmaceutical sciences* (6th ed.). Lippincott Williams & Wilkins.

Mohan, S., Kato, E., Drennen, J. K., & Anderson, C. A. (2019). Refractive index measurement of pharmaceutical solids: A review of measurement methods and pharmaceutical applications. *Journal of Pharmaceutical Sciences, 108*(11), 3478-3495.

Moriera, L., & Firoozabadi, A. (2010). Molecular thermodynamic modeling of specific ion effects on micellization of ionic surfactants. *Langmuir, 26,* 15177-15191. https://doi.org/10.1021/la102536y

Mozrzymas, A. (2019). On the head group effect on critical micelle concentration of cationic surfactants using molecular connectivity indices and atomic partial charges. *Journal of Solution Chemistry, 48,* 875-890.

Nasrin, L., Kabir, E., & Rahman, M. (2016). External magnetic field-dependent tricritical points of uniaxial-to-biaxial nematic transition. *Phase Transitions, 89*(2), 193–201.

Neto, A. M. F., Galerne, Y., Levelut, A. M. & Liebert, L, (1985a). Pseudolamellar ordering in uniaxial and biaxial lyotropic nematics – A synchrotron X-ray diffraction experiment. *Journal de Physique Lettres, 46,* 409-505.

Neto, A. M. F., Liebert, L., & Galerne, Y. (1985b). *Journal of Physical Chemistry, 89,* 3737-3739.

Neto, A. M. F., & Salinas, S. R. A. (2005). *The physics of lyotropic liquid crystals: Phase transitions and structural properties* (1st ed.). Oxford University Press.

Neto, A. M. F., & Galerne, Y. (2015). Biaxial nematic liquid crystals, theory, simulation, and experiment. In G. R. Luckhurst & T. J. Sluckin (Eds.), *Lyotropic systems* (Vol. 11, pp. 285-304). Wiley.

Oelschlaeger, C., Suwita, P., & Willenbacher, N. (2010). Effect of counterion binding efficiency on structure and dynamics of wormlike micelles. *Langmuir, 26*(9), 7045–7053.

Oliveira, E. A., Liebert, L., & Figueiredo Neto, A. M. (1989). A new soap/detergent/water lyotropic liquid crystal with a biaxial nematic phase. *Liquid Crystals, 5*(11), 1669–1675.

Park, S.-J., & Seo, M. -K. (2011). Chapter 1 – intermolecular force. In S.-J. Park & M.-K. Seo (Eds.), *Interface science and technology* (Vol. 18, pp. 1-57). Elsevier.

Quing, A., Zhao, Y., & Zhang, Z. (2024). Introduction to liquid crystals. *In Microwaves, millimeter wave and terahertz liquid crystlas: Preparation, characterization ans applications* (Chap. 1, p. 25). Springer Nature.

Quist, P. O. (1995). First order transitions to a lyotropic biaxial nematic. *Liquid Crystals, 18*(4), 623–629. https://doi.org/10.1080/02678299508036666

Radley, K., & Reeves, L. W. (1975). Studies of ternary nematic phases by nuclear magnetic resonance. Alkali metal decyl sulfates/decanol/D_2O. *Canadian Journal of Chemistry, 53,* 2998-3004.

Radley, K., & Reeves, L. W. (1976). Effect of counterion substitution on the type and nature of nematic lyotropic phases from nuclear magnetic resonance studies. *The Journal of Physical Chemistry, 80*(2), 174–182. https://doi.org/10.1021/j100543a018

Radley, K., &Saupe, A. (1978). The structure of lyotropic nematic decylammoniumchloride and bromide systems by PMR of monomethyltin complexes and by microscopic studies. *Molecular Crystals and Liquid Crystals, 44,* 227-235.

Samulski, E. T. (2010). Meta-cybotaxis and nematic biaxiality. *Liquid Crystals, 37*(6-7), 669-678.

Santos, O. R., Braga, W. S., Luders, D. D., Sampaio, A. R., Kimura, N. M., Simões, M., et al. (2021). Optical characterization of biaxial nematic between uniaxial nematic lyotropic phases. *Phase Transitions, 94*(6-8), 546-555.

Schnee, V. P., & Palmer, C. P. (2008). Cationic surfactants for micellar electrokinetic chromatography: 1. Characterization of selectivity using the linear solvation energy relationship model. *Electrophoresis, 29,* 767-776.

Sein, A., & Engberts, J. B. F. N. (1995). Micelle to lamellar aggregate transition of an anionic surfactant in dilute aqueous solution induced by alkali metal chloride and tetraalkylammonium chloride salts. *Langmuir, 11,* 455-465.

Shih, C. S., & Alben, R. (1972). Molecular theory of smetic-A ordering in nematic liquid crystals. *The Journal of Chemical Physics, 57*(7), 3055-3062. https://doi.org/10.1063/1.1678675

Stannarius, R. (2014). Diamagnetic properties of nematic liquid crystals. In *Handbook of liquid crystals* (Vol. 3, Part II, Chap. 7). Wiley.

Stroobants, A., & Lekkerkerker, H. N. W. (1984). Liquid crystal phase transitions in a solution of rodlike and disklike particles. *The Journal of Physical Chemistry, 88*(18), 3669–3674. https://doi.org/10.1021/j150660a058

Ugochukwu, C. U. (2019). Chapter 9 – Characteristics of clay minerals relevant to bioremediation of environmental contaminated systems. IM M. Mercurio, B. Sarkar, & A. Langella (Eds.), *Modified clay and zeolite nanocomposite materials* (pp. 219-242). Elsevier.

Varga, S., Galindo, A., & Jackson, G. (2002). Phase behavior of symmetric rod-plate mixtures revisited: Biaxiality versus demixing. *Journal of Chemical Physics, 117,* 10412.

Vasilevskaya, A. S., Kitaeva, E. L., & Sonin, A. S. (1990). Optically biaxial mesophases in lyotropic nematics. *Russian Journal of Physical Chemistry, 64*, 599–601.

Vlachy, N., Jagoda-Cwiklik, B., Vácha, R., Touraud, D., Jungwirth, P., Kunz, W. (2009). Hofmeister series and specific interactions of charged headgroups with aqueous ions. *Advances in Colloid and Interface Science*, 146, 42-47.

Wensink, H. H., Vroege, G. J., & Lekkerkerker, H. N. W. (2002). Biaxial versus uniaxial nematic stability in asymmetric rod-plate mixtures. *Pyhsical Review E, 66,* 041704.

Xu, K., Zeng, G. -M., Huang, J. H., Wu, J.-Y., Fang, Y. Y., Huang, G., Li, J., Xi, B., & Liu, H. (2007). Removal of Cd^{2+} from synthetic wastewater using micellar enhanced ultrafiltration with hollow fiber membrane. *Colloids and Surfaces A: Physicochemical and Engineering Aspects, 294*(1-3), 140-146.

Yadav, T., Tikariha, D., Lakra, J., Satnami, M. L., Tiwari, A. K., Saha, S. K., & Ghosh, K. K. (2015). Solubilization of polycyclic aromatic hydrocarbons in structurally different gemini and monomeric surfactants: A comparative study. *Journal of Molecular Liquids, 204,* 216-221.

Yang, J. W., Lee, Y. J., Park, J. Y., Kim, S. J., & Lee, J. Y. (2005). Application of APG and Calfax 16L-35 on surfactant enhanced electrokinetic removal of phenanthrene from kaolinite. *Engineering Geology, 77,* 243-255.

Yang, S., & Lee, J.-H. (2016). Optical simulation of viewing angle property of biaxial nematic bent-core liquid crystal. *Journal of the Optical Society of Korea, 20*(4), 510-514.

Yeagle, P. L. (2016). Chapter 7 -Structures of lipid assemblies. In P. L. Yeagle (Ed.), *The membranes of cells* (3rd ed., pp. 115-154). Academic Press.

Yu, L. J., & Saupe, A. 1980a. Liquid crystalline phases of the sodium decylsulfate/decanol/water system: Nematic-nematic and cholesteric-cholesteric phase transitions. *Journal of the American Chemical Society, 102,* 4879-4883.

Yu, L. J., & Saupe, A. 1980b. Observation of a biaxial nematic phase in potassium laurate-1-decanol-water mixtures. *Physical Review Letters, 45,* 1000-1003.

Zografopoulos, D. C., Ferraro, A., & Beccherelli, R. (2019). Liquid-crystal high-frequency microwave technology: Materials and characterisation. *Advanced Materials Technologies, 4*(12), 1800447. https://doi.org/10.1002/admt.201800447